Investigation of Airflow and Heat Transfer in Earth-to-Air Heat Exchangers

Jian Zhang

A Thesis

In the Department

of

Building, Civil, and Environmental Engineering

Presented in Partial Fulfillment of the Requirements

For the Degree of Doctor of Philosophy (Building Engineering) at

Concordia University

Montreal, Quebec, Canada

April 2009

Your file Votre référence
ISBN: 978-0-494-63439-4
Our file Notre référence
ISBN: 978-0-494-63439-4

ABSTRACT

Investigation of Airflow and Heat Transfer in Earth-to-Air Heat Exchangers

Jian Zhang, Ph.D.
Concordia University, 2009

An Earth-to-Air Heat Exchanger (ETAHE) uses the massive thermal storage capacity of the ground to dampen ambient air temperature oscillations by delivering outdoor air to the indoors through a horizontally buried duct. Owing to their low airflow resistance, large cross-sectional area ETAHEs have been found more energy efficient than the conventional small duct ETAHEs, especially when integrated in hybrid ventilated buildings. However, the lack of available methods for determining the surface heat convection has made accurate energy simulation and design difficult.

A field investigation in a large ETAHE was carried out at beginning of this research. Detailed airflow and heat transfer data were collected to analyze the heat convection process and to verify computational fluid dynamics (CFD) simulations. In the CFD model, a two-layer turbulence model was used to ensure accuracy in resolving flow information in the near-wall region. The modeling method was verified by comparing its results with measured data. The results indicated that the entrance and buoyancy effects in ETAHEs caused surface heat convection distribution to be highly non-uniform, and its intensity is significantly higher than that in conventional small duct ETAHEs. Using the CFD model, sensitivity of heat convection intensity to various design parameters was analyzed, and six parameters were identified as being influential. A large number of CFD simulations were then performed to find mathematical relations between the design parameters and local heat convection rate. Based on these cases, an Artificial Neural Network based Heat Convection (ANN-HC) algorithm was developed. It predicts local

Nusselt numbers on ETAHE surfaces, and the results are in good agreement with CFD predictions. A thermal simulation model of ETAHEs was developed to solve three-dimensional unsteady conductive heat transfer in the ground surrounding ETAHEs, and the ANN-HC algorithm is coupled with the model to provide local heat convection boundary conditions at duct surfaces. A case study showed that the new model can properly simulate the interactions between an ETAHE and its environment, and the results are more accurate than the existing simulation models. It will be a useful tool for designers to predict and analyze ETAHE performance in order to obtain optimal design solutions.

ACKNOWLEDGEMENTS

I would like to express my sincere thanks to my thesis supervisor Dr. Fariborz Haghighat for his thorough guidance, generous support, and constant encouragement throughout this research.

The field measurements in this research were carried out with generous help from Dr. Per Olaf Tjelflaat, Dr. Bjørn Jenssen Wachenfeldt, and Mr. Dao Van Pham from Norwegian University of Science and Technology. Technical communications with members of the IEA-ECBCS Annex 44 project, e.g. Dr. Qingyan Chen of Purdue University, Dr. Tor Helge Dokka of SINTEF, Dr. Per Heiselberg of Aalborg University, Dr. Inger Andresen of SINTEF, Dr. Marco Perin of Politecnico di Torino, were great benefits to this research. Experimental data received from Dr. Daniel E. Fisher and Dr. Jeffrey Spitler of Oklahoma State University is sincerely appreciated. Many thanks are also due to my colleagues and friends at Concordia University, especially Dr. Wahid S. Ghaly, Dr. Liang Zhou, Dr. Qian Mao, Dr. Karava Panagiota, Dr. Shuangxi Xie, and all members of our research group for their instructive technical discussions and spiritual encouragements.

Financial assistance from Natural Sciences and Engineering Research Council of Canada (NSERC) and Concordia University is gratefully acknowledged.

Finally, from the bottom of my heart, I thank my wife, Jingwei Zhuge, and my parents for their patience, understanding, encouragement, and love. I could not have completed this dissertation without them.

TABLE OF CONTENTS

LIST OF FIGURES

LIST OF TABLES

NOMENCLATURE

Acronyms:

ANN	Artificial Neural Network
ANN-HC	Artificial Neural Network based Heat Convection
CFD	Computational Fluid Dynamics
CHTC	Convective Heat Transfer Coefficient
ETAHE	Earth-to-Air Heat Exchanger

Equation Variables:

A_c	duct cross-sectional area, m^2
$A_{element}$	duct surface element's area, m^2
A_{ETAHE}	ETAHE duct surface area, m^2
A_{in}	inlet opening area, m^2
A_s	amplitude of daily mean ground surface temperature in a year, °C
A_μ	constant
c_l	constant
$c_{p,air}$	air specific heat capacity, $J/(kg \cdot °C)$
$c_{p,s}$	soil specific heat capacity, $J/(kg \cdot °C)$
C_μ	constant
D	distance of the first grid from the wall, m
D_h	hydraulic diameter, m
f	friction factor
g_i , g	gravity acceleration in x_i direction, m/s^2

Gr_{D_h}	Grashof number based on hydraulic diameter
h	convective heat transfer coefficient (CHTC) or film coefficient, $W/(m^2 \cdot °C)$
h_0	coefficient of heat transfer by long-wave radiation and convection, $W/(m^2 \cdot °C)$
h_x	local convective heat transfer coefficient, $W/(m^2 \cdot °C)$
H	duct height, m
I	turbulence intensity
I_{in}	inlet turbulence intensity
I_t	total solar radiation incident on a surface, W/m^2
k	thermal conductivity, $W/(m \cdot °C)$, or turbulent kinetic energy, m^2/m^2
k_s	soil thermal conductivity, $W/(m \cdot °C)$
l	turbulence length scale, m
l_μ	turbulence length scale, m
L	duct length, m
L_{en}	characteristic length, m
Nu_{avg}	area-weighted local average Nusselt number
Nu_x	local Nusselt number
Nu	Nusselt number
Pr	Prandtl number
Pr_t	turbulent Prandtl number
p	pressure, Pa
q''_x	local heat flux, W/m^2

q''	heat flux, W/m^2
$\dot{q}_{element}$	duct surface element's heat flow rate, W
Q	volumetric airflow rate, m^3/s
Re	Reynolds number
Re_{D_h}	Reynolds number based on duct hydraulic diameter
Re_y	turbulent Reynolds number
Ri	Richardson number
t	time, day
T_s	ground temperature, °C
t_0	a phase constant since the beginning of the year of the lowest average ground surface temperature, day
T_1	temperature of air at the first grid next to the surface, °C
T_{air}	air temperature, °C
T_e	sol-air temperature, °C
T_m	fluid bulk mean temperature, also referred to as the "mixing cup" or "flow average" temperature, °C
T_{surf}	surface temperature, °C
$T_{s,m}$	annual mean ground temperature, °C
T	fluid temperature, °C
T_{out}	outlet air temperature, °C
T_{in}	inlet air temperature, °C
$T_{surf,x}$	average surface temperature over a cross section, °C

T_∞	reference fluid temperature, °C
u	velocity, m/s
u_i , u_j	velocity along coordinate axes (i and j = 1, 2, 3), m/s
u_m	mean velocity, m/s
U	bulk velocity in duct, m/s
V_{en}	volume of enclosure, m^3
$\vec{V}$	velocity vector
W	duct width, m
W_{in}	duct inlet width, m
W_{out}	duct outlet width, m
x	distance along x coordinate axis, m
x_i, x_j	distance along coordinate axes (i and j = 1, 2, 3), m
$\frac{x}{L}$	distance to ETAHE inlet relative to duct length
y	perpendicular distance of a grid from the nearest surface, m, or distance along y coordinate axis, m
z	ground depth, m, or distance along z coordinate axis, m
α	surface absorptance for solar radiation
α_s	soil thermal diffusivity, m^2/day
α_{air}	air thermal diffusivity, m^2/s
β	thermal expansion coefficient of air, $(°C)^{-1}$
ε	hemispherical emittance of surface, or turbulent kinetic energy dissipation rate

ΔR	the difference between long-wave radiation incident on surface from sky and surrounding W/m^2
ΔT	temperature difference, °C
ρ	density, kg/m^3
ρ_s	soil density, kg/m^3
λ	thermal conductivity, $W/(m \cdot °C)$
μ	dynamic viscosity, kg/(m·s)
μ_t	turbulent viscosity, kg/(m·s)
ν	kinematic viscosity, m^2/s

Chapter 1 Introduction

1.1 Background

The sustainable development of humankind depends on efficient energy exploitation and environmental protection. According to the International Energy Agency – Energy Conservation in Building and Community Systems (IEA-ECBCS 2002), approximately one third of total energy consumption in European and North American countries was spent on space heating, cooling, lighting, and appliance operation in non-industrial buildings. These buildings account for the largest share of CO_2 emissions compared to other CO_2 sources. To diminish the threat of global warming and energy depletion, research into building energy efficiency over the last decade has been undertaken to improve building service systems and specific construction components in order to create technologies and solutions (Heiselberg 2004). At the service system level, new concepts, such as low exergy heating/cooling and hybrid ventilation systems, have been developed. At the component level, Environmentally Responsive Elements have been introduced to improve buildings' energy efficiency, for example, the double skin façade, earth coupling system, and phase changing material. "Environmentally Responsive Elements are defined as building construction elements which are actively used for the transfer and/or storage of heat, light, water and air to maintain an appropriate balance between optimum interior conditions and environmental performance" (Heiselberg 2004). It is believed future energy saving potential will be from rational integration of technologies from the two levels, i.e. the system level and the component level. This would allow buildings to be designed under whole building concepts to achieve an optimized performance. The challenges are to understand, simulate, predict

and optimize the dynamic interaction between service systems and Responsive Building Elements. To this end, IEA-ECBCS initiated an international research project, Annex 44 Integrating Environmentally Responsive Elements in Buildings. The research in this dissertation is conducted under the framework of Annex 44, and it is focused on the integration of Earth-to-Air Heat Exchangers (ETAHEs) with hybrid ventilation systems.

1.2 Thermal Energy Storage of Ground

Thermal energy storage is known as a flexible heating and/or cooling technique to dampen diurnal and seasonal peak energy demands of buildings. Among various thermal storage media, the ground is the most favorable one for buildings due to its massive capacity and availability. Relatively stable ground temperatures have made it an effective heat source, sink, and storage medium used in some building energy conservation measures. Ground thermal storage applications for space heating and cooling can be classified into three categories: 1) the direct method, which conditions indoor environment by increasing direct contact of buildings with the ground; 2) the indirect method, which preheats or pre-cools ventilation air using the thermal storage capacity of the ground before delivering the air to indoor; and 3) the isolated method, which uses a heat carrier medium, such as ground water or coolant, to exchange energy between the ground and the indoor environment.

1.3 Principle of Earth-to-Air Heat Exchangers

An Earth-to-Air Heat Exchanger (ETAHE) is a typical environmental responsive element following the indirect method. It ventilates air to the indoor space through one or several horizontally buried ducts. In this way, the ground large thermal storage capacity and relatively stable temperatures are used to preheat or pre-cool the air, resulting in

energy savings. Figure 1.1 is a schematic of an ETAHE. For most residential and commercial buildings with desired indoor temperatures from 20°C to 25°C, ETAHEs are primarily used for cooling purposes since the corresponding ground temperatures are normally below this range for the whole year. ETAHEs can also be used for winter pre-heating when the outdoor air temperature is lower than that of the ground, but additional heating systems may be required.

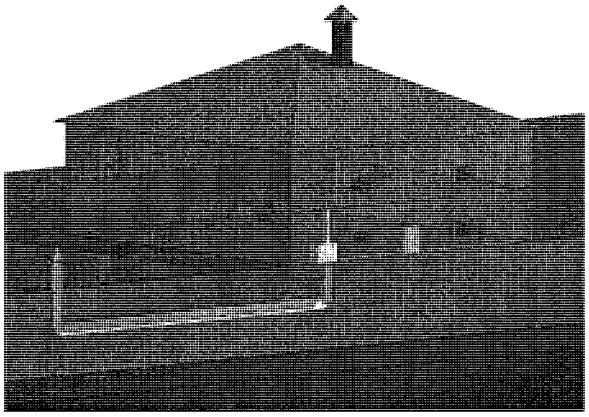

Figure 1.1: Building with an Earth-to-Air Heat Exchanger

The working principle of cooling air with ventilated underground spaces has been known since ancient times (Bahadori 1978); however, in the past, applications were very rare due to uncertainties in airflow driving forces. Since mechanical ventilation systems became widespread, a large number of ETAHE systems have been built in residential and commercial buildings, as well as in greenhouses and livestock houses. ETAHEs can also be applied to a wide range of climates with large temperature differences between summer and winter as well as between day and night. In literature, names such as Earth Cooling Tube, Ground Coupled Air System, Cool-Tube in-Earth Heat Exchanger, Earth Air Tunnel, Earth Contact Cooling Tube, Earth Tube Heat Exchanger, Buried Pipe

Cooling System, Underground Solar Airheater, Earth Air-Pipes System, Air-Soil Heat Exchanger, Embedded Duct, Earth Channel, and Hypocaust are used as all alternatives to ETAHEs. The name, Earth-to-Air Heat Exchanger, is adopted in this thesis because it is commonly used in the industry and it represents the principle of the technology without limiting its physical configurations.

ETAHEs' performance is highly dependent on its design and operation, especially the airflow rate. Integration of ETAHEs with building service functions is critical for the success of the design. Most existing ETAHEs are installed in mechanically ventilated buildings, in which fans provide the required driving force for the airflow. In such systems, an ETAHE can be a single duct or multiple parallel ducts made of prefabricated metal, PVC, or concrete pipes with diameters at a magnitude of 10 cm.

In the case of the parallel pipe systems, the distance between the pipes should be kept approximately 1.0 meter from each other in order to minimize the thermal interaction. Greater spacing was not found to bring extra benefits (Zimmermann and Remund 2001). The size of an ETAHE depends on the designed airflow rate and the available space. A maximum air velocity of 2 m/s is normally recommended for smaller systems, and larger systems can be designed for air velocity up to 5 m/s. Due to the high velocity and small duct size, a large amount of energy has to be spent on the mechanical ventilation systems to deliver the required airflow rate through the ETAHEs.

1.4 Integration of ETAHEs and Hybrid Ventilation

In recent years, there has been a trend of improving the energy efficiency of mechanical ventilation systems. A hybrid ventilation concept, which alternatively or simultaneously uses mechanical and natural airflow driving forces, has been implemented

in many building designs (Heiselberg 2002). It is based on the reduction of pressure drop in the ductwork by increasing its cross-sectional area so that natural airflow driving forces, such as buoyancy and wind, can be used to reduce fan energy consumption. Hybrid ventilation is a promising system concept, and its implementation imposes some special requirements on the building design. When ETAHEs are integrated in hybrid ventilation, the duct cross-sectional areas should be much larger than those of the conventional ducts used in mechanical ventilation systems. Schild (2001) investigated 17 hybrid ventilated buildings in Norway; and among them 12 buildings were designed with ETAHEs. Their duct hydraulic diameters were all around 1.5 meters. It has been found that large cross-sectional area ducts are more suitable than that in the conventional small ones when they need to be integrated in hybrid ventilation systems. However, this change in the ductwork size causes the heat transfer process in ETAHEs to become more complicated than the conventional ones. The integration of ETAHE and hybrid ventilation is regarded as a new approach to improve building energy efficiency (Heiselberg 2004) but the lack of available methods for determining heat convection at the duct surfaces has made accurate energy simulation and proper system design overly difficult.

1.5 Research Objectives

Earth-to-Air Heat Exchangers and hybrid ventilation are the representative technologies of Environmentally Responsive Elements and building service systems, respectively. To integrate them under the whole building design concepts, one needs proper tools to accurately simulate their performance and then to be able to achieve optimal design and control solutions. Therefore, the objectives of this research are

- To review the state-of-the-art of ETAHEs
- To study the airflow and heat transfer processes in large cross-sectional area ETAHEs
- To develop a method to predict convective heat transfer in ETAHEs, and
- To develop a thermal model to simulate the energy performance of ETAHEs

1.6 Thesis Organization

Following the introduction in Chapter 1, Chapter 2 summarizes the state-of-the-art review of ETAHE design and information related to the current research methodology. Chapter 3 starts with a field investigation of an ETAHE and then a numerical experimental method is developed using Computational Fluid Dynamics technique. The method is verified by comparing its results to experimental measurements. Using the CFD model as a tool, Chapter 4 identifies the influential design parameters that determine heat convection inside ETAHEs, and then an Artificial Neural Network technique is used to develop an algorithm to predict local heat convection in ETAHEs. Chapter 5 introduces a new thermal simulation model of ETAHEs. It solves three-dimensional transient heat conduction in the ground surrounding an ETAHE. The developed algorithm in Chapter 4 is coupled with this thermal simulation model. A case study is used to demonstrate the use of the thermal model, and the results show its advantages over existing ETAHE simulation models. In Chapter 6, conclusions from this research are summarized along with suggestions for future work.

Chapter 2 State-of-the-Art Review of ETAHEs

2.1 Introduction

A general description of ETAHEs has been addressed in the previous chapter. A change in ETAHE design, i.e. from small diameter circular pipes to large cross-sectional area ducts, has been implemented in actual projects. The incentive for the change is to reduce the energy cost for delivering the air through ETAHEs but it is believed that the change may have also created some difficulties in designing and evaluating the ETAHEs. To this end, a literature review was conducted to identify this discrepancy in the current knowledge of ETAHEs and to raise awareness of the need for designing large cross-sectional area ETAHEs.

2.2 Heat Transfer in the Earth

From ground surface to a hundred-meter depth, heat transfer processes take place in various forms. At the ground surface, heat transfer is caused by short/long wave radiation, evapotranspiration, and convection. Conduction is the main form of heat transfer in the ground except for regions with water movements. Although other forms also take place (such as latent heat transfer through evaporation and condensation, and sensible heat transfer by moisture transfer), engineering practices usually use an effective soil thermal conductivity to take them into consideration. Geothermal energy from the layers below the crust (the mantle and core) flows up like a constant heat source, but it is negligible when analyzing the heat flows in a shallow region, e.g. depth less than 20 meters (Rybach and Sanner 2000).

2.3 Ground Temperature Distribution

When analyzing the natural heat flow in the shallow ground, one can simplify the ground as semi-infinite media and describe the heat conduction using Fourier's law as shown in Equation 2.1. Ground surface temperature records can be used to solve this equation but their availability is very limited due to the lack of field measurements. Similar to ambient air temperatures, daily average ground surface temperatures follow a sinusoid variation with time, and their yearly amplitude is about equal to that of the ambient air. Such information can also help to solve Equation 2.1 and to obtain an undisturbed ground temperature at depth z and at time t as shown in Equation 2.2 (Labs 1979).

$$\rho_s c_{p,s} \frac{\partial T_s}{\partial t} = \frac{\partial}{\partial z}\left(k_s \frac{dT_s}{dz}\right) \tag{2.1}$$

$$T_s(z,t) = T_{s,m} - A_s \cdot exp\left[-z\left(\frac{\pi}{365\alpha_s}\right)^{0.5}\right] cos\left\{\frac{2\pi}{365}\left[t - t_0 - \frac{z}{2}\left(\frac{365}{\pi\alpha_s}\right)^{0.5}\right]\right\} \tag{2.2}$$

Where

ρ_s is the soil density, kg/m^3

$c_{p,s}$ is the soil specific heat capacity, $J/(kg \cdot °C)$

t is the time, day

z is the ground depth, m

k_s is the soil thermal conductivity, $W/(m \cdot °C)$

$T_{s,m}$ is the annual mean ground temperature, °C

T_s is the ground temperature, °C

A_s is the amplitude of daily mean ground surface temperature in a year, °C

t_0 is a phase constant since the beginning of the year of the lowest average ground surface temperature, day, and

α_s is the soil thermal diffusivity, m^2/day

Figure 2.1 and Figure 2.2 show typical ground temperature profiles as a function of time and depths. As far as ground temperatures are concerned, an ETAHE should ideally be installed as deep as possible to prevent temperature variations. However, the excavation cost for laying an ETAHE very deep may not be economical. In existing applications, ETAHEs are usually buried 1-4 m below the ground surface.

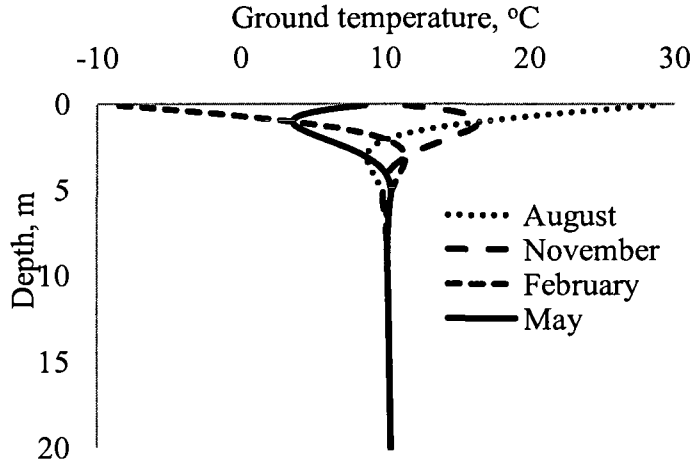

Figure 2.1: Typical ground temperature profiles at different seasons

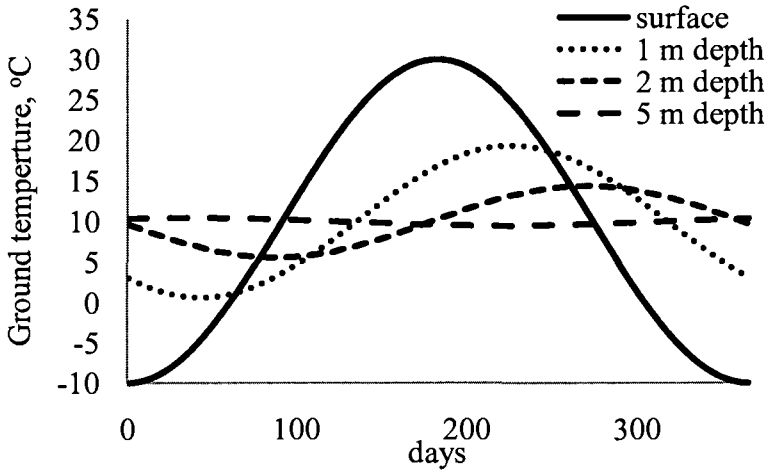

Figure 2.2: Typical annual ground temperature variations at different depths

2.4 Heat Transfer in ETAHEs

According to Figure 2.2, in summer, the soil temperatures below a two-meter depth are close to the annual mean ambient air temperature, and as air passes through an ETAHE, convective heat transfer takes place between the air and duct surfaces. The air's enthalpy and dry bulb temperature decrease along the flow direction. If the duct is long enough and the duct surfaces are cooler than the dew point temperature, condensation may take place. When no other cooling device is used, the air conditioning processes can be expressed as shown in Figure 2.3. From point 1, the ambient air condition, to point 2 the air is cooled with a constant humidity ratio. Depending on the duct cross-sectional size and air speed, relative humidity (RH) distribution at a cross-section could affect the condensation condition. If the cross-sectional size is small and the air velocity is large, the RH would be close to uniform and point 2 would be on the 100% RH curve. However, if the air RH at the cross section has a large variation, the boundary layer air would condense first even thought the average air condition has not reached saturation. Point 3 is determined by the duct surface temperature. If the duct length is infinite, the cooling and dehumidification process will happen as from Point 2 to Point 3. However, in practice Point 3' will be the ETAHE outlet air condition. The air temperature may increase slightly to reach Point 4 due to heat gain during distribution. Finally, the indoor loads change the air condition from Point 4 to 5. It should be noted that for the process from point 2 to 3, two assumptions are made. The first one is that the duct is long enough so that the air has become saturated. Due to space limitations, the duct lengths are dependent on projects. The second assumption is that the duct surface temperature is not much elevated by the warm air, and then Point 3 is determined based on an undisturbed

ground temperature. However, in practice, the heat transfer between the air and the duct surface is a dynamic process. When the air is cooled, the duct wall temperatures are warmed up. Therefore the cooling performance of an ETAHE is mainly determined by the dry cooling process from Point 1 to 2, and as such it is the focus of the current research.

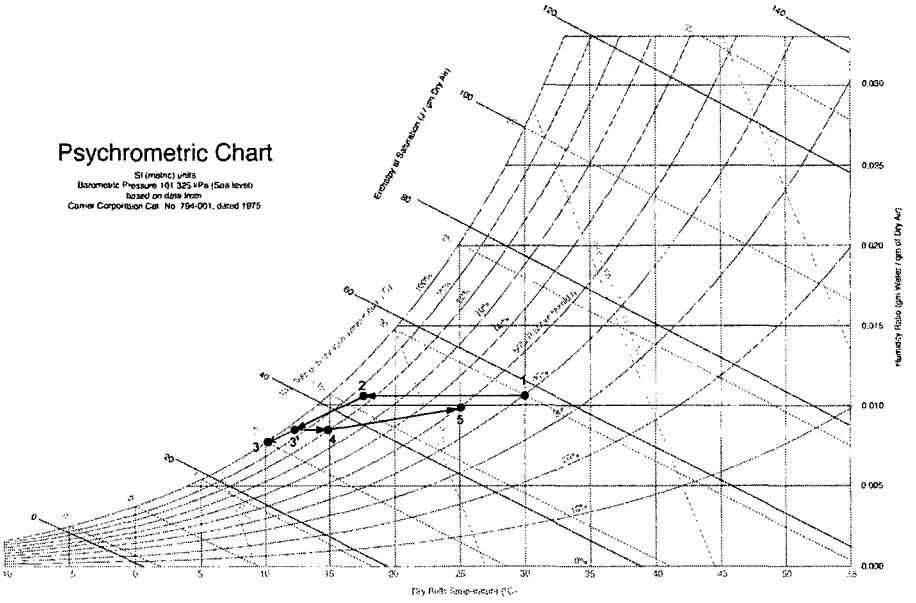

Figure 2.3: The cooling processes of ETAHEs in Psychrometric chart, 1: outdoor air condition; 2: transition condition (condensation starts); 3: duct surface condition; 3': ETAHE outlet air condition; 4: room supply air condition; 5: room air condition (Mu 1982)

Since the annual mean temperature of the ground is lower than indoor thermal comfort temperatures, ETAHEs are primarily used for cooling purposes. However, when the outdoor air temperature is very low in winter, it is also beneficial to preheat the supply outdoor air using ETAHEs. The air conditioning processes are shown in Figure 2.4. Point 1 is the outdoor air condition. After it passes through the buried duct, the air

temperature increases and its humidity ratio remains the same. From Point 2 to 3, a heating unit further elevates the supply air temperature. Then the supply air is mixed with the return air (Point 5) to reach an appropriate supply air condition: Point 4. The heating load is removed by the supply air from Point 4 to 5. ETAHE performance in winter is mainly determined at the process from Point 1 to 2. This process may also happen during the summer as night ventilation to cool down the ETAHE surfaces and to recharge its cooling capacity.

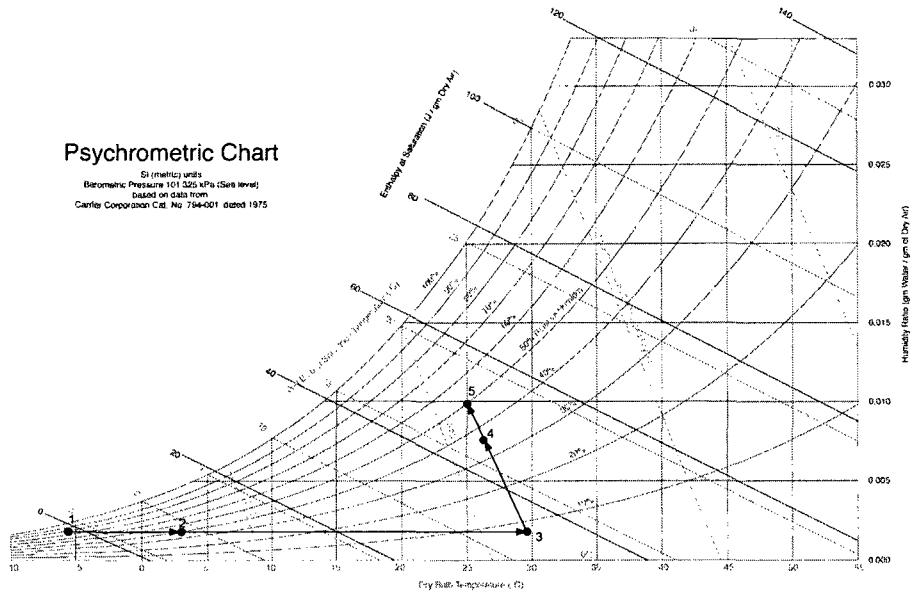

Figure 2.4: The heating processes of ETAHEs in Psychrometric chart. 1: outdoor air condition; 2: ETAHE outlet air condition; 3: air condition after secondary heating; 4: mixing air condition; 5: return duct air condition (Mu 1982)

As addressed in Figure 2.3 and Figure 2.4, changes in air conditions from 1 to 2 are due to sensible heat exchange and they are the dominant processes determining ETAHE performance. The heat transfer is in the form of convection, and its intensity is

significantly dependent on the airflow rate, pattern, and temperature differences between the air and the duct surfaces.

2.5 Energy Cost for Mechanical Fans

An ETAHE is not a completely passive system, and in most applications it requires energy for air circulation. To enhance heat convection one may think of having longer pipes, enlarging their surface area and roughness, or creating turbulence, etc. However, these measures also result in more energy cost for air circulation. In addition, the energy dissipation of mechanical fans may increase the air temperature.

2.6 Classification of ETAHEs

According to the system configuration, ETAHEs can be classified as open-loop and closed-loop systems. Figure 1.1 shows an open-loop system, which delivers fresh air to the indoors by locating its inlet outdoors. A closed-loop system circulates return air through the ETAHE. The latter one is usually used in greenhouses, livestock houses and buildings with separate outdoor air supply. The major benefit of open-loop systems is to provide a path for the outdoor air intake. However, concerns for insect ingress and noise transmission need to be taken into account at the design stage.

In terms of integration with ventilation systems, pressure drops through the ETAHEs determine if they are suitable for mechanical or hybrid ventilation systems. The former one is the conventional design. To reduce the required fan energy, the large cross-sectional duct system can be adopted. Although the difference between the two systems appears to be their sizes, their design, operation, and simulation may be greatly different from each other.

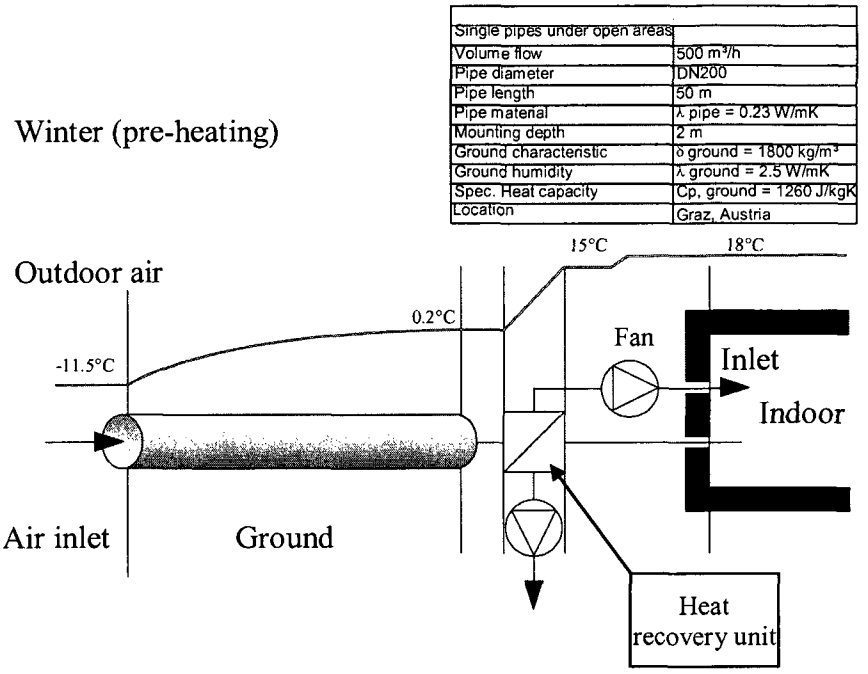

Figure 2.5: ETAHE with heat recovery during the winter operation. (Fink et al. 2002)

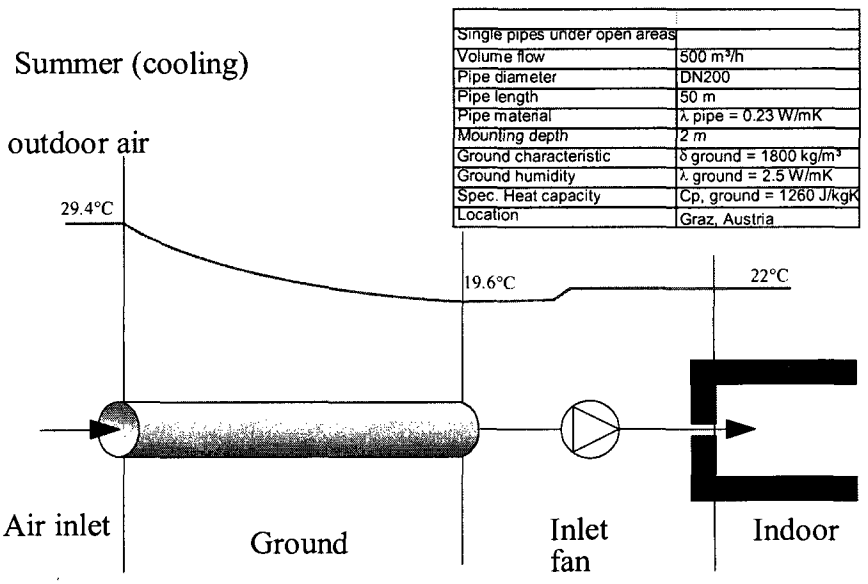

Figure 2.6: ETAHE with heat recovery during the summer operation. (Fink et al. 2002)

Based on functionality, ETAHEs may be categorized into heating and cooling systems. When an ETAHE is used for winter pre-heating, it is usually coupled with a heat

recovery unit or other heating devices to prevent icing. Figure 2.5 shows an example of such an application (ETAHE and heat recovery system). In summer, a properly designed ETAHE system may fully satisfy the building's cooling load. Figure 2.6 shows an example of the temperature progression of the inlet air when the ETAHE is operated during cooling seasons. When the ETAHE cooling capacity is not enough, the remaining load can be provided by other measures, such as static cooling surfaces (e.g. radiant cooling ceilings or cooled slab). Cooling possibilities for ETAHEs are: natural night ventilation, mechanical night ventilation, and component cooling (Fink et al. 2002).

2.7 Design and Analysis Methods for ETAHEs

The energy saving potential of an ETAHE has attracted many studies to develop design and analysis methods for ETAHEs. Santamouris and Asimakopoulos (1996) presented a calculation chart for predicting the outlet air temperature given an ETAHE's length, diameter, depth, air velocity and inlet air temperature. Their method is based on simplified statistical analysis and regression techniques so its accuracy and features are limited.

A computer simulation program, WKM was also developed to size ETAHEs with the following claimed features (http://www.igjzh.com/huber/wkm/wkm.htm):

- Yearly simulation of the ground system with heat recovery and bypass,
- Weather data can easily be integrated,
- Collective ducts and funnels are considered,
- Calculation of pressure drop in the ground,
- Type of pipe and ground characteristics are suggested,
- Influence of basement is taken into account,

- Excel interface for input and output, and
- Ventilation method and airflow rates are selectable.

The Division of Building Physics and Solar Energy, University of Siegen, Germany, developed a software program, GAEA (Graphische Auslegung von Erdwärme Austauschern) for the design of ETAHEs (Benkert et al. 1997 and Benkert and Heidt 1998). This software is based on the calculation of heat exchange in the soil, the buried pipes and the air in the system. An optimization routine presents a choice of possible layout variations and their assessment concerning heat gains and economics. A validation study of GAEA was published by Heidt and Benkert (2000).

Under the framework of the IEA-ECBCS Annex 28, an early ETAHE design guide for different weather conditions and locations was developed by Zimmermann and Remund (2001) using few design charts and tables. In an EU project, a design tool was developed under the guidance of AEE Gleisdorf and Fraunhofer ISE by 15 engineering companies (Reise 2001).

De Paepe and Janssens (2003) developed a one-dimensional analytical method, which can be used to analyze the influences of ETAHE design parameters on its thermo-hydraulic performance. A relationship between a specific pressure drop and the thermal effectiveness was derived. This was used to formulate a design method which can be used to determine an ETAHE's characteristic dimensions. The desired design is defined as a system with optimal thermal effectiveness as well as an acceptable pressure loss. The choice of the characteristic size thus becomes independent of the soil and climatological conditions. This method is claimed to allow designers to choose a proper configuration for an ETAHE with an optimal performance.

Hollmuller and Lachal (1998) developed an ETAHE model compatible with the TRNSYS environment. The model is based on energy and mass balance within underground ducts taking into account the sensible as well as latent heat exchanges between air and ducts, frictional losses, diffusion into surrounding soil, as well as water infiltration and flow along the ducts. Heat gain from fan motors can also be taken into account. Direction of the airflow can be controlled (stratification in case of heat storage) and flexible geometry allows for non-homogenous soils and diverse boundary conditions.

2.8 Design Guide and Recommendations

Many applications have also demonstrated ETAHEs' practical value. In order to promote the application further, its advantages should be highlighted in order to attract more attention from building owners and designers. The advantages include:

- The general availability of the ground makes ETAHEs applicable to most buildings to reduce the energy of active heating and cooling systems,
- In several climatic contexts, the use of appropriately sized ETAHE systems may avoid the use of other mechanical systems,
- ETAHEs can reduce green house gas (GHG) emissions,
- ETAHEs can improve indoor thermal comfort,
- Appropriate exploitation of moisture transfer between air and soil may provide moisture control for the supply air,
- ETAHE ducts have a filtration effect (a concentration reduction of airborne particle, spores and bacteria after passing through the ETAHE),
- Sometime ETAHEs are cheaper and easier to construct than active cooling systems,

- Maintenance and operation costs for ETAHEs are low compared to other air conditioning methods,
- ETAHEs have a long lifespan,
- The outlet air from ETAHEs can be further treated by other traditional air handling units, and
- The general availability of pipe materials makes ETAHE systems easy to be replicated anywhere.

ETAHE technology has proven to be applicable for a wide range of climates and various types of buildings, such as livestock houses, greenhouses, residential and commercial buildings. For buildings with moderate cooling load, properly sized ETAHE systems may become alternatives to traditional mechanical heating and cooling systems. Significant energy savings and corresponding reduction of green house gas emission will attract greater use of ETAHE. Hybrid ventilation systems have very good potential for being integrated with ETAHE. When an ETAHE needs to be integrated into a hybrid ventilated building, the pressure loss through the duct is a critical issue. Large cross-sectional area ducts are favored for the integration. Buildings with the following favorable factors are potential users of ETAHEs:

- moderate cooling loads,
- low ground temperatures,
- large daily outdoor air temperature swings,
- relatively low requirements for indoor environment, and
- a displacement ventilation system.

From a general point of view, the most significant issues that have to be carefully considered when designing and operating an ETAHE system are:

- The airflow rate through an ETAHE needs to satisfy the airflow requirement of the building, assuming the ETAHE is the only air inlet for the building,
- It is desirable to maximize the heat transfer rate between air and duct wall while also minimizing airflow resistance,
- For buildings with displacement ventilation, the air exit temperature from ETAHEs should always be below that of the room air,
- Condensation and moisture infiltration on the ETAHE duct wall should be avoided,
- The hygrothermal properties of the soil need to be considered in the site selection,
- The buried ducts should be anticorrosive and structurally stable,
- An ETAHE provides a path between outdoors and indoors. Safety, insect entrance, and noise transmission should be taken into account,
- The long term operation of an ETAHE with a high heating or cooling load may exhaust its capacity. System recharge methods need to be decided in system control design, and
- Ducts should be accessible for inspection and cleaning.

2.9 Experimental Procedure to Assess the ETAHE Performance

An ETAHE's performance is directly related to airflow rate and temperature difference between duct surface and inlet air. There is no standard experimental procedure for evaluating its performance. Usually, the following parameters involved in the heat transfer processes are monitored:

- Sensible and latent heat changes of airflow,
- Airflow rate,
- Pressure drop through an ETAHE, and
- Soil temperature distribution.

In the case of large cross-sectional ducts, the experimental setup needs to take into account the possible non-uniform distributions of air velocity, air temperature, or surface temperature. It should be noted that conductive heat flow within the soil is a slow process. It may take a few months for the soil temperature to be established after an ETAHE starts working. The process is always dynamic since ambient temperatures change hourly, daily and seasonally: the soil temperature varies as well. Therefore, long-term monitoring is needed to evaluate the performance. Some examples of detailed experimental procedures can be found from studies reported by Tzaferis et al. (1992), Hollmuller (2002), Kumar et al. (2003a), Pfafferott (2003), Burton (2004), Wachenfeldt (2003), and Ghosal et al. (2004).

2.10 Examples of Existing Applications

Three buildings with ETAHEs are reviewed in this section. The first one is a conventional mechanically ventilated building and the other two are hybrid ventilated. The review is focused on the ETAHEs' configurations, operations, and performance.

2.10.1 The Schwerzenbacherhof Building, Zurich, Switzerland

The Schwerzenbacherhof building is a commercial building near Zurich, Switzerland, with a heating energy consumption of 144 MJ/m^2 per year for 8050 m^2 of heated surface area. It was a major case study in the IEA-ECBCS Annex 28 (Low Energy Cooling) (Zimmermann and Remund 2001, Liddament 2000, and Zimmermann 1995 and

Hollmuller 2002). Figure 2.7 shows the building with the ETAHE's inlet. There are two paths for the building to intake outdoor air: it can either pass through the ETAHE system under the building, or directly go to air handling units, as shown in Figure 2.8.

Figure 2.7: The Schwerzenbacherhof Building

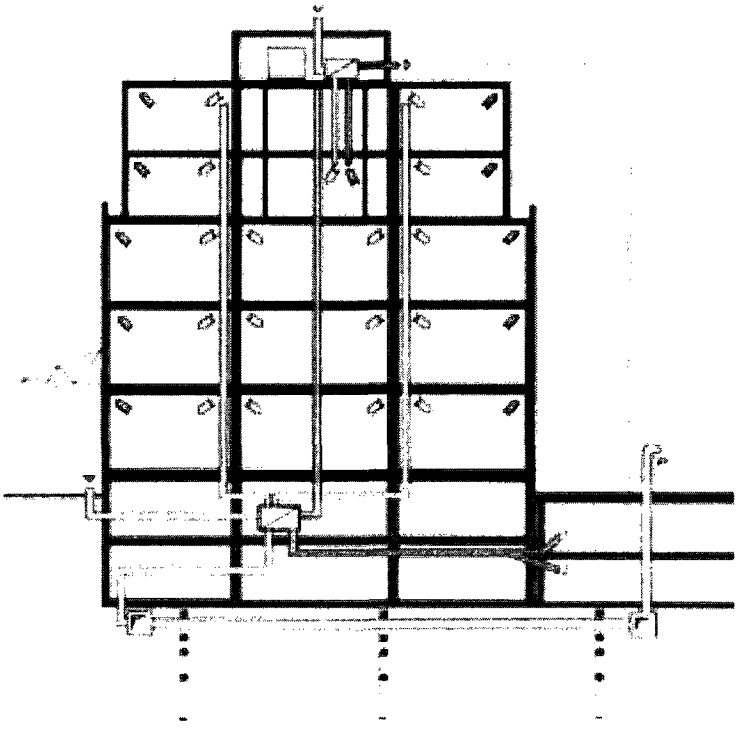

Figure 2.8: Schematic of the Schwerzenbacherhof building ventilation system (Hollmuller 2002)

2.10.1.1 Component Description

The ETAHE is 6 m beneath the ground surface and 75 cm below the building's unheated second basement. The system consists of 43 parallel high-density polyethylene pipes with a one percent inclination (Figure 2.9). Each pipe has a length of 23 m, and a diameter of 23 cm and the mean axial distance between two pipes is 116 cm. Two large concrete ducts, before and after the pipe system distribute and collect the air. Drainage to sewage is provided in the intake-side concrete duct (Figure 2.9 right). A varying airflow rate during office hours (12,000 m^3/h in winter and 18,000 m^3/h in summer) is maintained by two fans in the system (Figure 2.10).

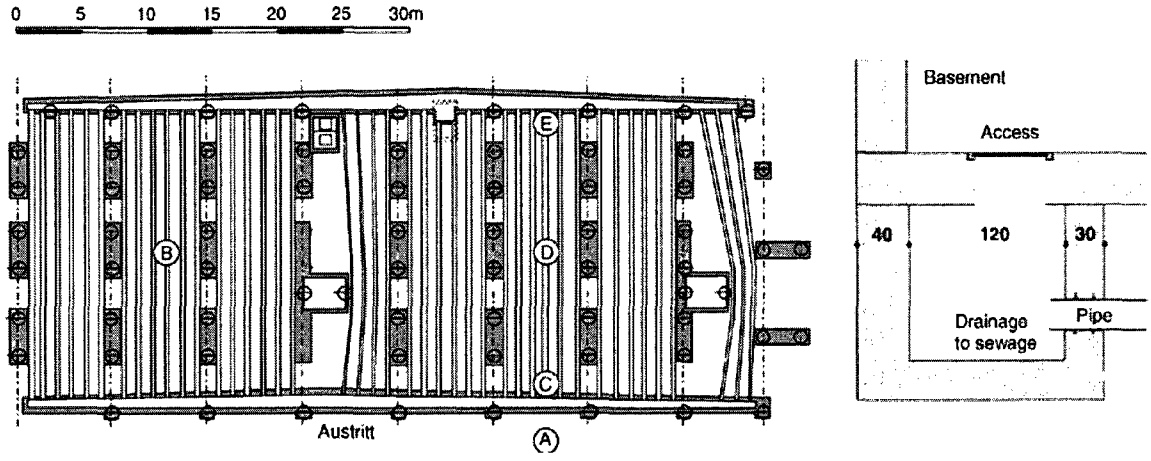

Figure 2.9: General layout and construction detail of the ETAHE system in the Schwerzenbacherhof building (Hollmuller 2002)

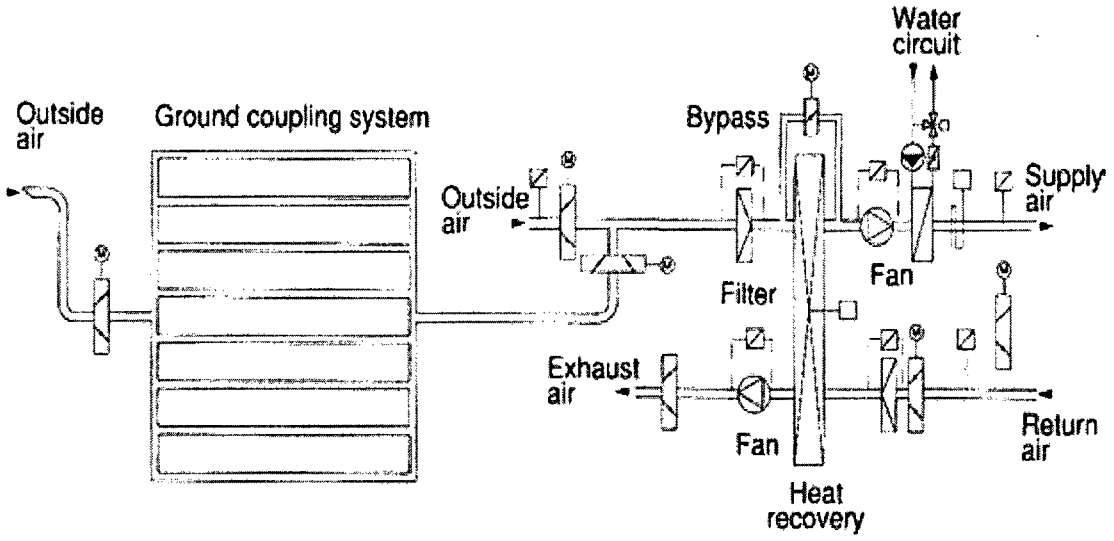

Figure 2.10: The Schwerzenbacherhof building - Ventilation system's components (Hollmuller 2002)

2.10.1.2 Control Strategy

The ETAHE system is activated in summer when the outdoor air temperature exceeds 22°C. The air is cooled down as it passes through the pipes, and then it is directly supplied to the rooms. When the outdoor temperature is lower than 22°C, the air bypasses the ETAHE and is taken in directly from outside. This normally happens at night-time. The ETAHE provides about 1/3 of total cooling, and the rest is provided by night cooling of the thermal mass. Thus the ETAHE is only a supplement (mainly during the daytime) when night cooling is insufficient.

In winter, when the ambient temperature falls below 7°C, the ETAHE starts to be used to provide preheating. Then the outlet air from ETAHE passes through the heat recovery unit, which transfers heat from the exhaust air to the air from the ETAHE. The use of the ETAHE during winter time also helps to cool the ground for the next summer and to prevent freezing of the heat recovery unit.

2.10.1.3 Measured Performance

The Schwerzenbacherhof building was selected as a case study to investigate the performance of ETAHE as a low energy cooling measure in the IEA-ECBCS Annex 28 project (Liddament 2000). A one year monitoring program was conducted. The monitored parameters from the ETAHE system were:

- Upper soil temperature (75 cm above the pipe bed),
- Lower soil temperature (600 cm beneath the pipe bed),
- Inlet/outlet air temperatures and humidity.

From this monitoring program, Liddament (2000) reported the following performance conclusions:

- The measured heating demand was 150 kW at -8°C. Without the ETAHE, the estimated load would be 240 kW. The ETAHE itself can meet a peak demand of 60 kW,
- The measured heating energy consumption was 144 MJ/m^2 per year which is well below the Swiss Standard, at the time, of 240 MJ/m^2 per year,
- The measured electrical current to operate the ventilation system was 23 MJ/m^2 per year which, again, was well below a conventional requirement of 90 MJ/m^2 per year, and
- The maximum cooling rate was 54 kW at an outdoor supply temperature of 32°C. Comfort cooling was achieved at all times.

2.10.2 The Mediå School, Grong, Norway

The Mediå School is a 1001 m^2 one-floor building located in Grong, Norway. It was one of the case studies in the IEA-ECBCS Annex 35, Control Strategies for Hybrid

Ventilation in New and Retrofitted Office Buildings (HybVent). It was investigated by Tjelflaat (2000a and 2000b) and Wachenfeldt (2003) and Jeong and Haghighat (2003). The building's layout and the ventilation system schematic are shown in Figure 2.11 and Figure 2.12, respectively.

2.10.2.1 Component Description

A triangular cross-sectional vertical inlet duct, which is located north of the building and on a 35° slope, is the air intake for the ETAHE, as shown in Figure 2.13. The height from the tower's top to its base is approximately 6 m. On each side of the tower there is an opening, which is covered by a metal shield to protect it from rain. Behind the shield each opening is equipped with a one way damper allowing air entrance when pressure in the tower is lower than outside.

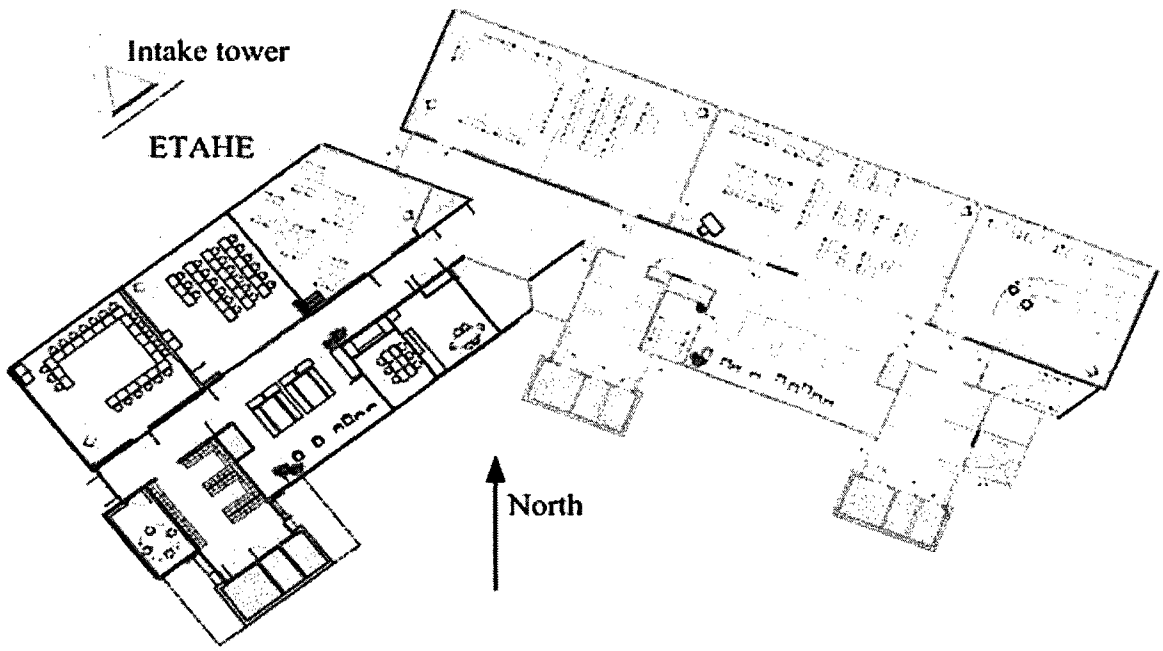

Figure 2.11: The Mediå School building layout (Tjelflaat 2002b)

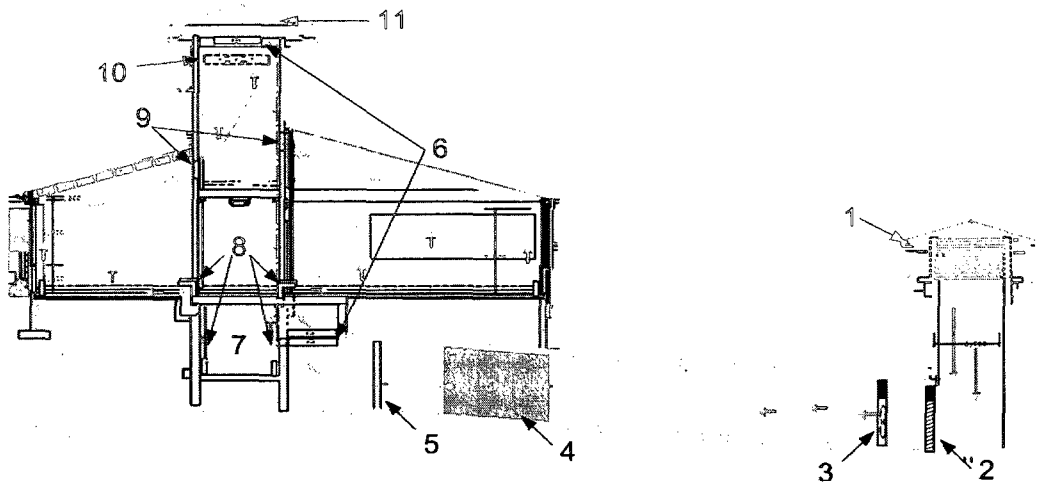

Figure 2.12: Air flow paths and location of components. 1: triangular intake tower with openings and vents; 2: damper; 3: supply fan; 4: sound absorber; 5: filters; 6: heat exchangers for supply air preheating using run-round heat recovery via a circulating water-glycol mixture as well as additional reheating; 7: air distribution duct; 8: units for noise attenuation plus openings and grilles for supply of ventilation air to the classrooms; 9: dampers for extracting exhaust ventilation air from the classrooms; 10: exhaust fan; 11: triangular roof tower with exhaust vents (Tjelflaat 2002a)

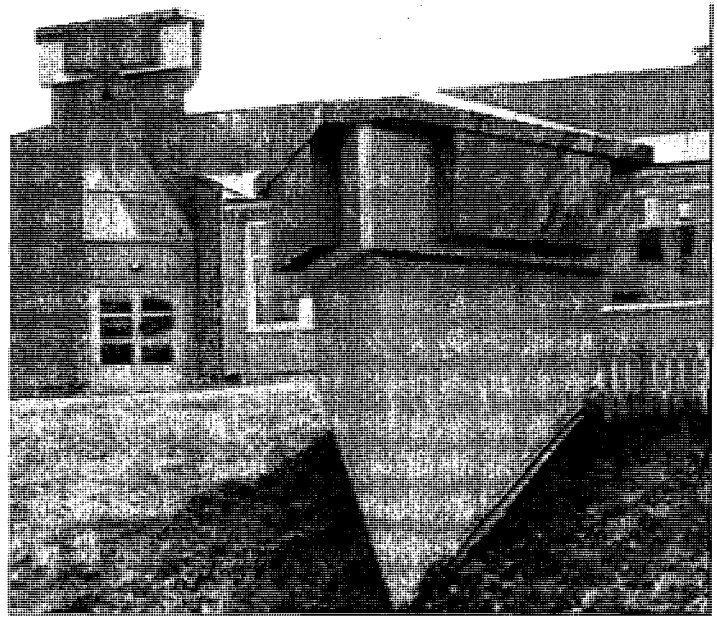

Figure 2.13: ETAHE's intake tower of the Mediå School

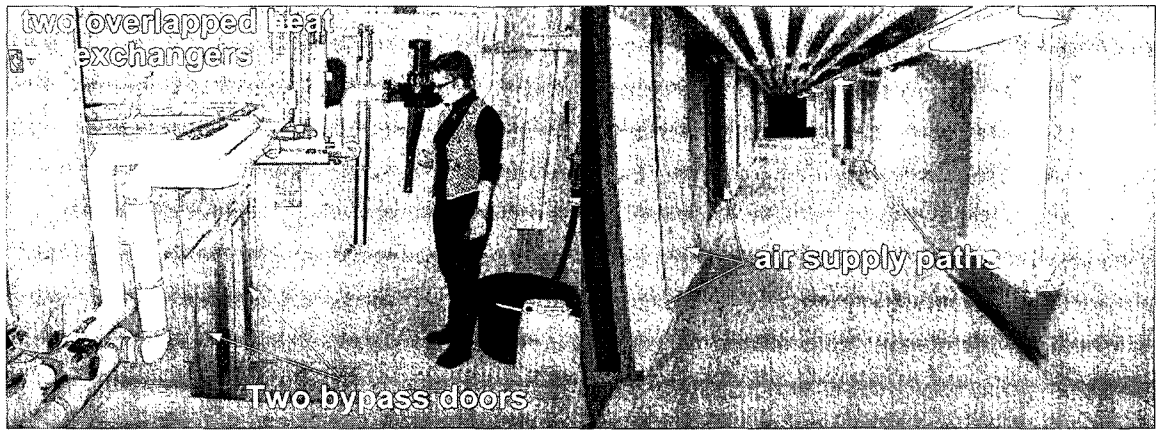

Figure 2.14: Air distribution duct of the Mediå School (Left shows heat exchangers and bypass doors. Right shows the distribution duct and supply air paths) (Tjelflaat 2002a)

After passing through the intake tower, air enters a horizontal 1.5 m wide and 2 m high concrete intake duct whose ceiling is approximately 1.5 m below the ground surface (refer to Figure 2.12). A damper is installed at the beginning of the duct. A frequency-controlled variable-speed propeller fan with a diameter of 1.4 m is located 1.5 m away from the damper on the leeward side. Its operation is interlinked with the damper opening position. A noise absorber is located 6.3 m from the fan. Six fine filter blocks are installed at the end of the duct. The total distance from the damper to the filters is 11.1 m. The duct has a 5% incline to the inlet direction to allow improved dust deposition and drainage. Drainage is located at the base of the air intake tower. After leaving the intake duct, the air vertically passes through two overlapped horizontal heat exchangers (see Figure 2.14 left) and enters a 2.2 m wide and 2 m high horizontal air distribution duct. This duct has two branches which are below the building's corridor. The air from the intake duct can also bypass the heat exchangers by flowing through two bypass doors beside the heat exchangers. Figure 2.14 (right) shows the distribution duct with the air

supply paths attached on the walls and connected to the ground level classrooms. These paths suppress sound transmission between rooms.

2.10.2.2 Control Strategy

The HVAC system is monitored and controlled by a centralized supervisory Building Energy Management System (BEMS) with CO_2 and temperature sensors located in the classrooms. The ETAHE preheats air in winter. The temperature set point in the distribution duct is 19°C. This is ensured by the two heat exchangers at the end of the air intake duct. In summer, The building does not have a mechanical cooling system, and the ETAHE is the only component for cooling purposes. When the CO_2 level is over the limit, the BEMS opens the damper between the classroom and the attic. The displacement ventilation driven by the buoyancy and wind forces is the first choice to satisfy the ventilation requirements. When natural driving forces are insufficient, the frequency controlled supply and exhaust fans are activated. The ventilation is primarily controlled by the differences between the classrooms' CO_2 levels and their set point. However, when the room temperature exceeds a set value of 24°C the ventilation airflow rate is increased to avoid further temperature rise. When the two heat exchangers are not needed, the bypass doors can be manually opened to reduce the pressure loss.

2.10.2.3 Measured Performance

The cooling effects of the ETAHE in a typical summer week were investigated by Tjelflaat (2000b) by monitoring the inlet and outlet air temperatures, as shown in Figure 2.15. The maximum temperature reduction was about 8°C. A rough estimation, based on an efficient ETAHE surface area of 200 m^2 and an airflow rate of 1.1 m^2/s, gave an average heat transfer rate of 12 kW.

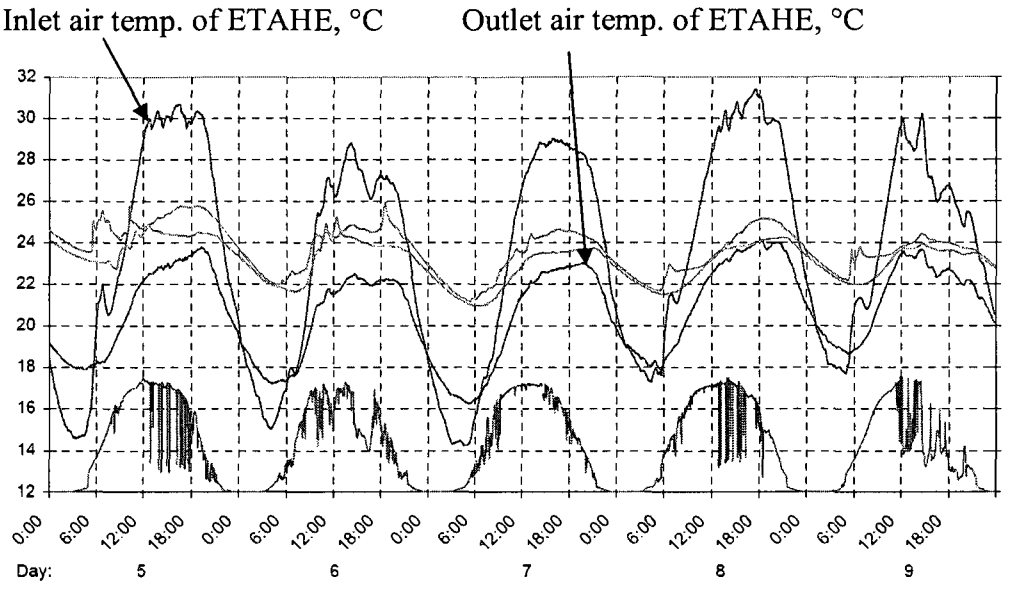

Figure 2.15: Air temperature developments during an extremely hot period 5-9 June 2002 (Tjelflaat 2000b)

2.10.3 The Jaer School, Oslo, Norway

The Jaer primary school is an 850 m^2 two-storey heavy weight building near Oslo, Norway. It was another case study of IEA-ECBCS Annex 35. The schematic of the building ventilation system is shown in Figure 2.16 and Figure 2.17.

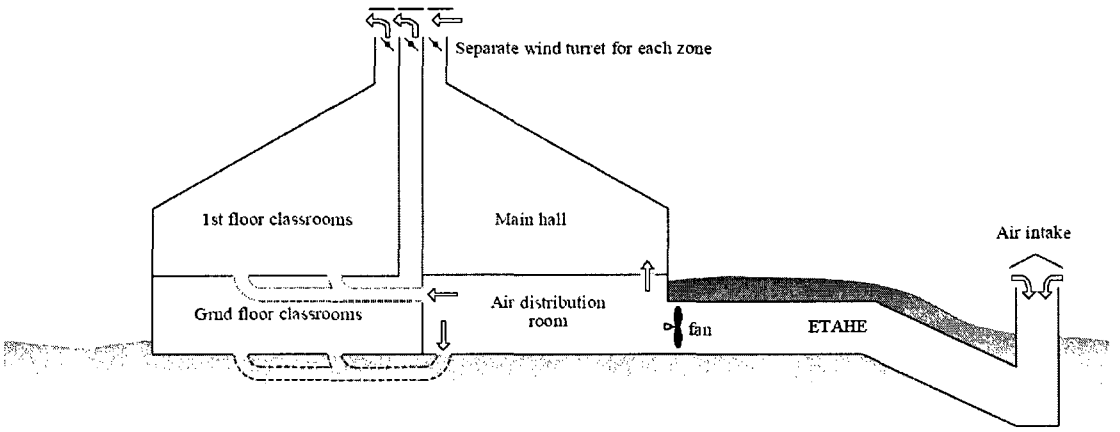

Figure 2.16: Schematic cross section of the Jaer School showing air flow paths and components (Schild 2002)

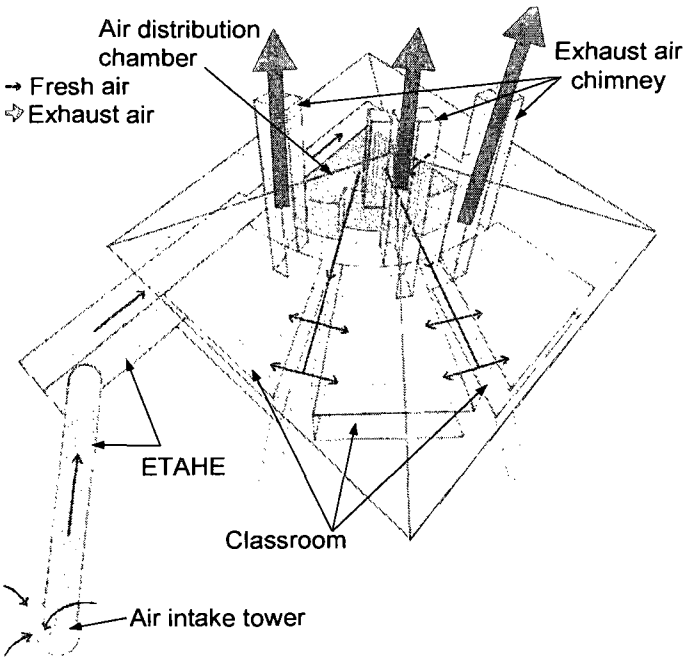

Figure 2.17: 3D schematic of the Jaer School ventilation system (Schild 2002)

2.10.3.1 Component Description

The ETAHE's air intake tower, about 2 m height from the ground surface, is located outside the building. To minimize the pressure drop, the air intake louvers are open without any rain and snow shielding. A frost-protected drain is provided on the base of the tower (see Figure 2.18).

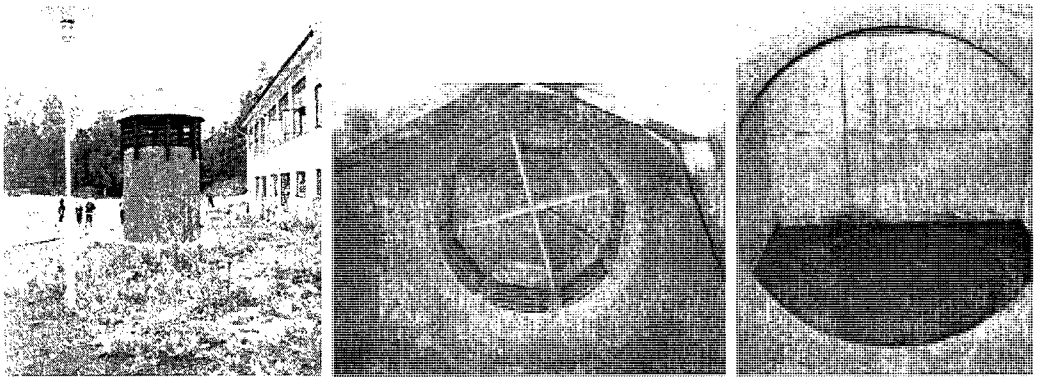

Figure 2.18: Air intake tower of the Jaer School (Left: outside, Middle: inside looking up, Right: inside horizontally into base of the tower from the horizontal duct.) (Schild 2002)

The ETAHE consists of two parts: a prefabricated concrete pipe (20 m length and 1.6 m diameter) and a rectangular cast-in-place concrete duct (35 m length, 2 m width, and 3 m height) with a total surface area of about 450 m^2. At the end of the rectangular duct, there are two possible parallel paths through which outdoor air can enter the air distribution chamber. One is to pass through a speed controlled fan and the other is through a preheat unit as shown in Figure 2.19: the selection of airflow path is made by a Building Energy Management System.

From the distribution chamber, the air is then delivered to various rooms at the floor level through plastic subterranean ducts. The hybrid ventilation concept is mainly implemented in the rooms by exploiting buoyancy forces. Furthermore, a wind-assisted exhaust tower on top of the building helps to improve the wind driven effect. When these natural forces are not enough to keep necessary airflow rates, the mechanical fan is activated to a proper speed.

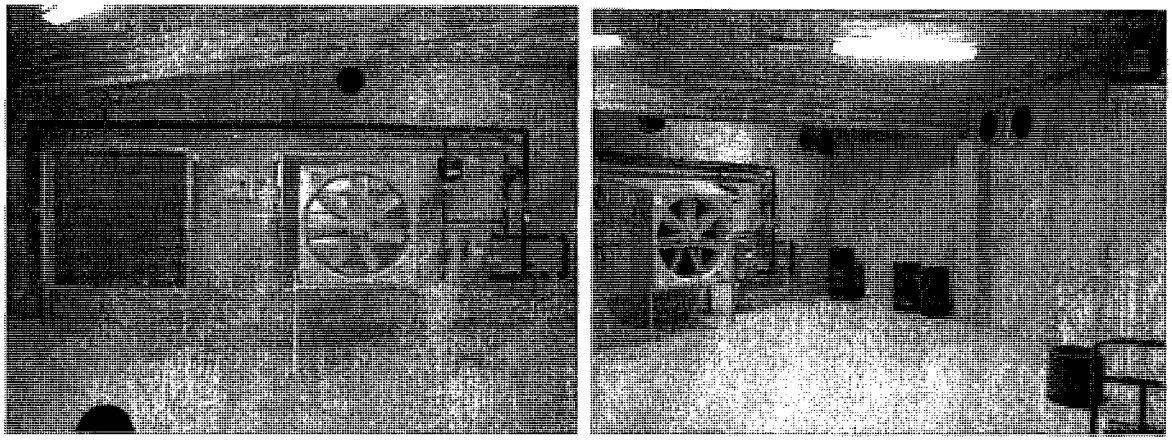

Figure 2.19: The air distribution room, showing the preheat unit (left) and fan, as well as the plastic subterranean ducts leading to the various rooms (Schild 2002)

2.10.3.2 Control Strategy

The whole HVAC system is monitored and controlled by a centralized supervisory Building Energy Management System. There are 4 main operation modes, depending on two bimodal parameters: (1) Preheating needed; (2) Preheating not needed though cooling possibly needed; (A) Day, and (B) Night. There is night-time ventilation for pre-cooling in summer. When the CO_2 level or temperature in a room rises above set-point values, the damper at the roof outlet opens gradually. If the CO_2 concentration level remains above the set-point, then the fan is started. The axial fan at the end of the ETAHE is frequency-controlled to maintain constant over-pressure in the culvert. Since the pressure drop through the ventilation system is very small, the stack effect alone in the building has always been enough to satisfy the indoor air quality requirement. The fan is only used when additional cooling is needed. When the supply air needs to be heated, the BEMS controls the ratio of fresh air to pass the preheat unit.

2.10.3.3 Measured Performance

The monitored inlet and outlet air temperatures in the Jaer School ETAHE system are reported by Schild (2001). The ambient temperature oscillation was clearly dampened as shown in Figure 2.20.

2.11 ETAHE Simulation Studies

The energy saving potential of ETAHE has attracted many simulation studies since the 1980s. The main efforts have been made on the development of the simulation methods. Since the performance of large cross-sectional ETAHEs has not been well studied, simulation methods were developed based on the working principles of the conventional small pipe systems. As noted earlier, the major difference between large

cross-sectional duct systems and small ones is the complexity of the heat transfer processes. All the modeling methods reviewed here assume simple convective heat transfer.

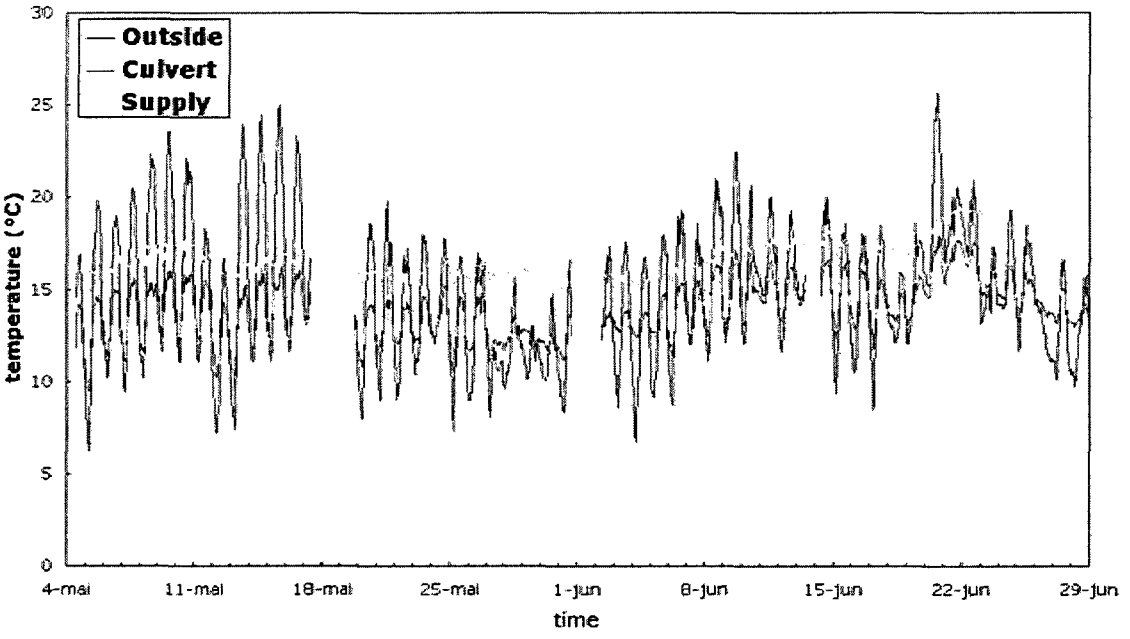

Figure 2.20: Measured air temperatures of the Jaer School ETAHE system. "Culvert" line is the ETAHE outlet air, "outside" is the ambient air, and "supply" is the air after the preheat unit (Schild 2001)

By assuming an undisturbed temperature of the earth surface in contact with the ETAHE pipe, Athienitis et al. (2005), De Paepe and Janssens (2003) and Al-Ajmi et al. (2006) used an analytical relationship to calculate variation of air temperature along the pipe length. However, this is a very simplistic approach and it does not account for heat transfer in the soil and other physical phenomena in ETAHEs.

Sawheny and Mahajan (1994), Sodha et al. (1994), Sodha et al. (1985) and Krarti and Kreider (1996) proposed a steady-state analytical model to determine the annual

heating and cooling potential of an underground air pipe system, while soil temperature was assumed as the mean annual temperature.

Several authors have presented theoretical studies based on numerical techniques to investigate the performance of ETAHE systems, for example, Chen et al. 1984, Schiller 1982, Levit et al. 1989, Elmer and Schiller 1981, Santamouris and Lefas 1986, Sodha et al. 1984, Rondriguez et al. 1988, Shukla et al. 2006, and Seroa da Motta and Young 1985. All these models assumed the soil surrounding an ETAHE to be undisturbed and homogeneous with a constant temperature, the value of which is obtained from an undisturbed soil temperature algorithm. The models are based on the principle of dividing a pipe into a number of control volumes. A heat balance relationship is applied to every control volume as shown in Figure 2.21. Using the exit air temperature from the first control volume as the inlet air temperature of the next control volume, the exit temperature for that volume was calculated. Continuing this process from one volume to the next, the temperature of air at the outlet of the ETAHE duct was calculated.

All the aforementioned models have simplified dynamic heat transfer in the soil with steady soil temperatures. Although they are easy to handle, dynamic processes in the soil are neglected. According to a soil temperature model developed by Bansal et al. (1983), soil properties and surface conditions can greatly influence ETAHE thermal performance. Mihalakakou et al. (1996) also concluded that earth surface conditions might be a significant controllable factor for the improvement of ETAHE performance. The thermal analysis of soil surrounding ETAHEs requires the solution of a three-dimensional heat conduction equation with appropriate boundary conditions. Matching

the solution on all edges and corners makes the solution of such problems very difficult. Different authors have made different assumptions for solving these equations.

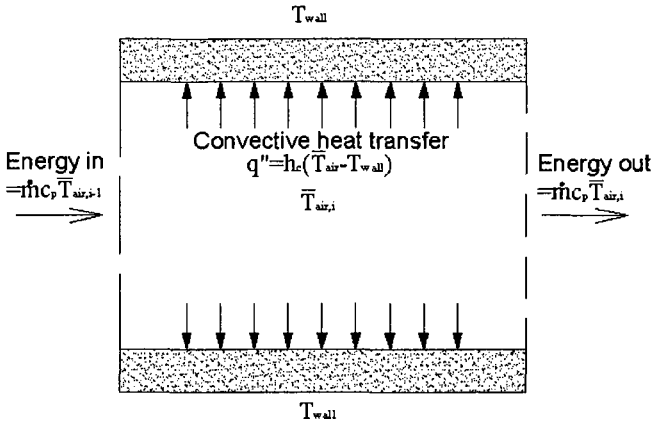

Figure 2.21: Heat convection between ETAHE walls and air

Goswami and Dhaliwal (1985), Goswami and Ileslamlou (1990), and Arzano and Goswami (1996) reported the development of a model, which assumes that heat transfer in the soil only happens in the radial direction and the radius of the affected cylinder of earth is finite. In regions outside of the cylinder, soil temperatures are undisturbed.

A Model developed by Mihalakakou et al. (1994a) considers that the energy transfer inside the soil is driven by simultaneous heat and moisture transfer gradients along both axial and radial directions. By superimposing the heat transfer from more than one duct, Mihalakakou et al. (1994b) modified the previous model so that it is capable of simulating multiple-pipe ETAHEs. The authors defined the difference between inlet and outlet air temperatures as the ETAHE's energy potential. Using this definition, the systems' sensitivity to duct length, duct radius, soil depth, and distance between adjacent ducts was analyzed. Jacovides and Mihalakakou (1995) used the same model to simulate an ETAHE buried under a building foundation. Kumar et al. (2003a and 2003b) used it

again and defined the ETAHE energy potential as the daily or monthly integration of the convective heat flux between the air and the ETAHE walls. They adopted this energy potential to conduct a parametric study to evaluate the importance of design parameters.

Bojic et al. (1997) developed a method to solve the heat transfer in the soil by horizontally dividing the earth into a number of parallel layers, each having a uniform temperature. Heat transfer among the soil layers is solved using energy balance equations for each soil layer. Bojic et al. (1999) modified the method by dividing the earth layers into smaller control volumes.

Wagner et al. (2000) and Beisel (1999) developed a model to simulate the performance of ETAHEs by solving the unsteady conductive heat transfer problems in their specially discretized simulation domain. They used cylindrical control volume close to the ducts and Cartesian control volume far away from the ducts. The modeling was conducted with the simulation tool, SMILE.

Mihalakakou et al. (2003) developed a simulation tool using an Artificial Neural Network model. They used the validated numerical model developed by Mihalakakou et al. (1994a) to simulate the thermal performance of an ETAHE with a wide range of design parameters. The simulation results were used to train the neural network model. Comparison between simulation results from the neural network model and the numerical model showed good agreements.

2.12 Heat Convection in Ducts

The discussion about ETAHE working principle in the earlier section has shown the importance of heat convection in determining the performance of an ETAHE system. The goal of this section is to review the existing methods for the calculation of heat

convection. Heat transfer rate at the duct surfaces is usually calculated using Newton's law of cooling, as shown in Equation 2.3.

$$q'' = h \cdot (T_{surf} - T_{\infty}) \quad 2.3$$

Where

q'' is heat flux, W/m^2

h is the convective heat transfer coefficient (CHTC), $W/(m^2 \cdot °C)$

T_{surf} is the surface temperature, °C, and

T_{∞} is the reference fluid temperature, °C.

The CHTC, h, is a function of the flow condition, thermo-physical properties (viscosity, thermal conductivity, specific heat, density) of the fluid, and geometry and dimensions of the surface. The goals of most heat convection studies are to generalize this function. Although analytical solutions might be derivable for some special flow problems, for instance fully developed laminar flow forced convection in circular ducts; the most common method is to develop empirical correlations by using their experimental results. To analyze heat convection in a large cross-sectional area ETAHE, this section starts from comparing it to simple duct flow problems.

2.12.1 Heat Convection in Circular Pipe

According to the application of ETAHEs, the discussion scope can be narrowed down to steady-state incompressible airflow of constant property. The effects of natural convection and inlet/outlet configurations will be discussed later. In such context, turbulent duct flows can be divided into four categories: hydrodynamically developing, thermally developing, simultaneously developing, and fully developed. The last two types are of the interest to the current study. As air flows through a circular and infinitely

long duct with uniform velocity and temperature profile; the viscous forces and the temperature differences between the duct and the air cause the velocity and temperature profiles to gradually change in the axial direction. The velocity and thermal boundary layers develop simultaneously. At a certain location, both of the viscous and thermal effects completely spread across the duct cross section. From the inlet to that location is theoretically defined as the entry or entrance region; and the distance is called entry or entrance length (Lienhard and Lienhard 2005). Beyond that point, the flow is considered to be fully developed. When studying heat convection in a duct, two common thermal boundary conditions are particularly interesting, i.e. uniform wall heat flux and uniform wall temperature. Figure 2.22 shows the development of temperature profiles for the two boundary conditions, and it also shows the variations of fluid bulk temperatures and wall temperatures with the axis.

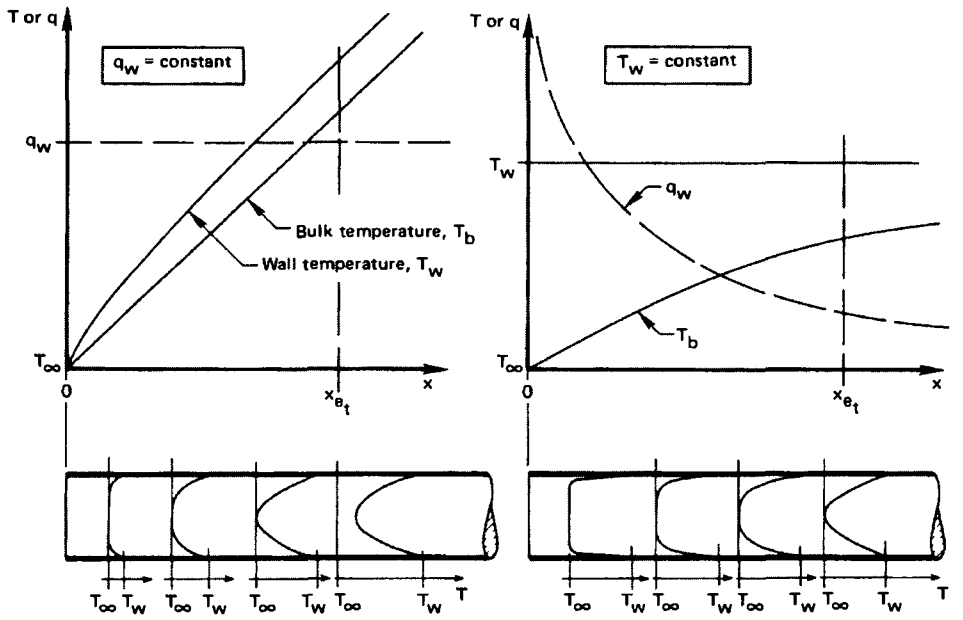

Figure 2.22 Thermal behavior of fluid flows in circular duct with a uniform wall heat flux and with a uniform wall temperature (Lienhard and Lienhard 2005)

The bulk temperature of the fluid shown in Figure 2.22 is defined by Equation 2.4. Based on this definition the local convective heat flux can be derived using Equation 2.5 and the local Nusselt numbers are accordingly defined by Equation 2.6.

$$T_m = \frac{1}{A_c \cdot u_m} \int_{A_c} u \cdot T \cdot dA_c \qquad 2.4$$

$$q''_x = h_x \cdot \left(T_{surf,x} - T_m\right) \qquad 2.5$$

$$Nu_x = \frac{h_x \cdot D_h}{k} = \frac{q''_x \cdot D_h}{k \cdot \left(T_{surf,x} - T_m\right)} \qquad 2.6$$

Where

T_m is the fluid bulk mean temperature, also referred to as the "mixing cup" or "flow average" temperature, °C

A_c is the duct cross-sectional area, m^2

u_m is the mean velocity, m/s

u is the velocity, m/s

T is the fluid temperature, °C

q''_x is the local heat flux, W/m^2

h_x is the local convective heat transfer coefficient, $W/(m^2 \cdot °C)$

Nu_x is the local Nusselt number

D_h is the hydraulic diameter, m

k is the thermal conductivity, $W/(m \cdot °C)$, and

$T_{surf,x}$ is the average surface temperature over a cross section, °C.

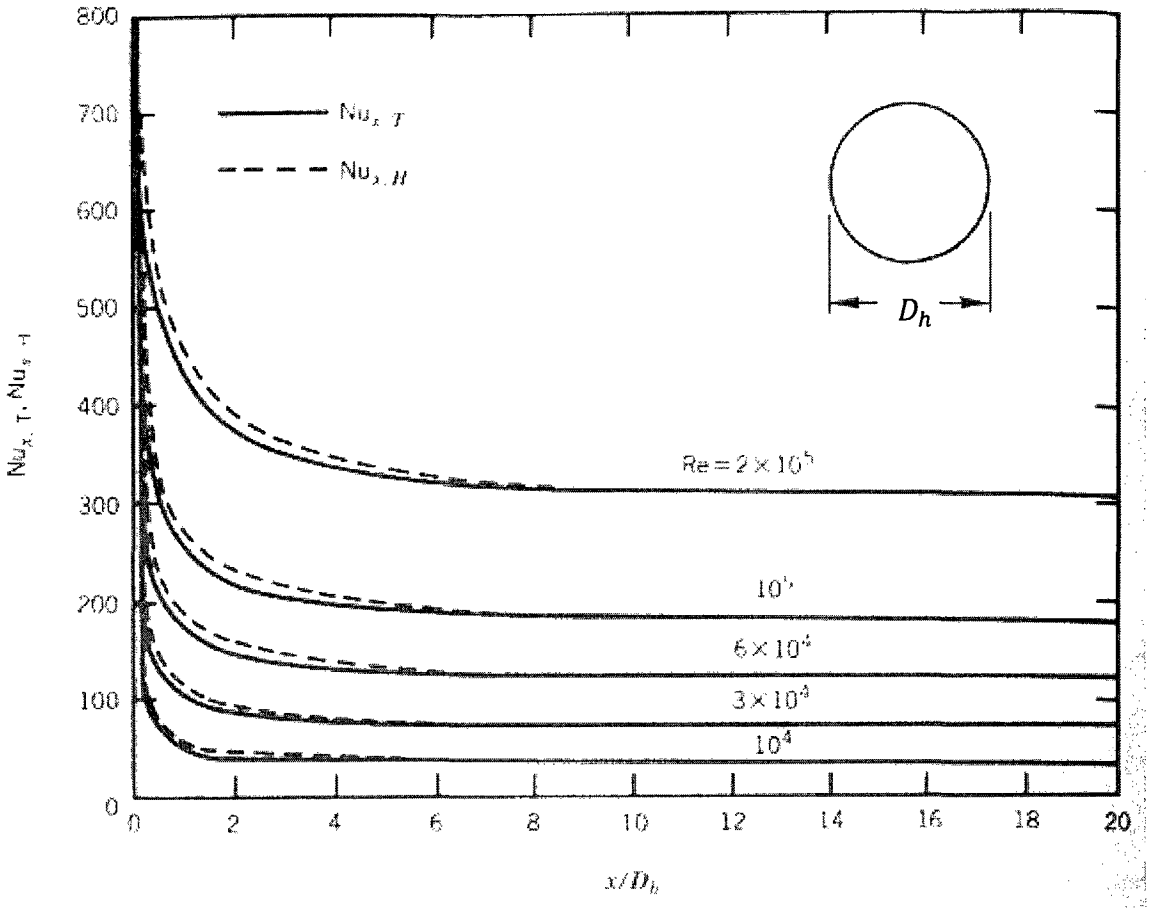

Figure 2.23: Local Nusselt numbers for simultaneously developing turbulent flow in a smooth circular duct for Pr = 0.73 (Deissler 1953)

2.12.2 Effects of Two Different Boundary Conditions

Deissler (1953) presented two local Nusselt number correlations, i.e. $Nu_{x,T}$ and $Nu_{x,H}$, for simultaneously developing turbulent flow in a smooth circular duct for Pr = 0.73 under two corresponding boundary conditions. $Nu_{x,T}$ is for a uniform wall temperature and $Nu_{x,H}$ is for a uniform wall heat flux. Figure 2.23 shows Nu numbers based on the correlations for different Reynolds numbers. According to the figure $Nu_{x,H}$ and $Nu_{x,T}$ are very close to each other for $10^4 < Re < 2 \times 10^5$.

Another study conducted by Sleicher and Tribus (1956) compared the differences between $Nu_{x,H}$ and $Nu_{x,T}$ for fluid with Pr < 0.71 as displayed in Figure 2.24. It again confirmed that the convective heat transfer coefficients are not sensitive to the two types of boundary conditions when the turbulent flow is fully developed. Therefore for fully developed turbulent airflow in circular pipes, Nu_H and Nu_T are not differentiated.

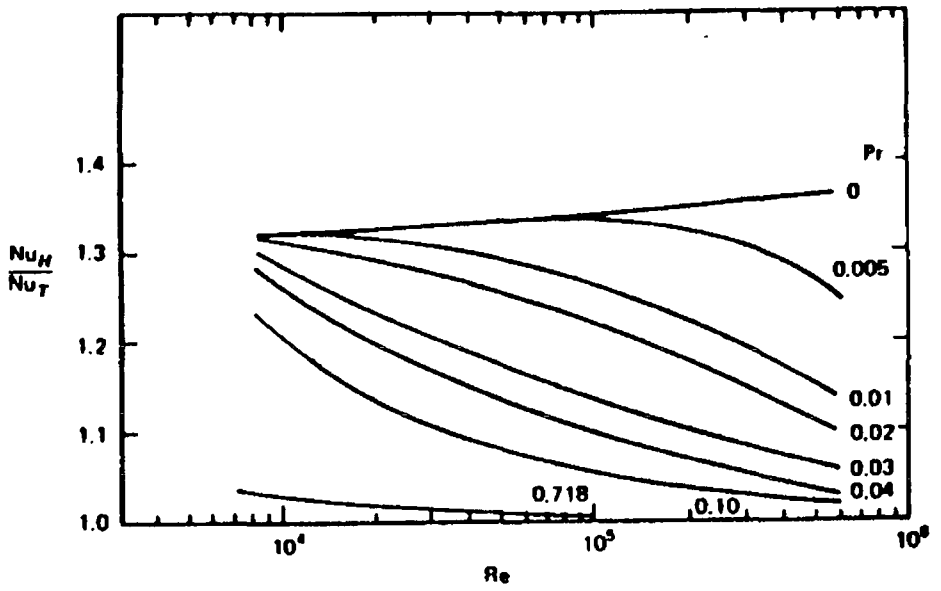

Figure 2.24: The ratio of Nu_H to Nu_T for fully developed turbulent flow in a circular duct (Sleicher and Tribus 1956)

2.12.3 Empirical Correlations of Fully Developed Turbulent Flow

As shown in Figure 2.23, for $10^4 < Re < 2 \times 10^5$, the local Nu numbers greatly decrease at the beginning of the ducts due to entrance effects. It takes up to a distance of $10D_h$ for the curves to become flat. In conventional ETAHE systems, it is typical to have buried ducts with 10 cm < D_h < 40 cm and lengths longer than 20 meters. Such sizes mean the ratios of the lengths to the hydraulic diameters are at order of magnitude of 100. Therefore, it was reasonable for most existing ETAHE simulation studies to assume

airflows are mostly fully developed and to adapt the corresponding empirical correlations to calculate the heat convection. In order to examine this assumption, eight Nu correlations used by other ETAHE simulation studies are collected in Table 2.1.

Table 2.1: List of various CHTC correlations

#	***Correlations***	***Reference***
1	$Nu = \frac{0.0036(u_m \rho D_h)^{0.8}}{k}$	*Arzano and Goswami 1996*
2	$Nu = 0.011Re^{0.96}Pr^{0.3}$	*Bojic et al. 1997 (cooling)*
3	$Nu = 4.5Re^{0.427}Pr^{0.1}$	*Bojic et al. 1997 (heating)*
4	$Nu = \frac{5.8(1 + 0.85u_m)D_h}{k}$	*Singh 1994*
5	$Nu = \frac{(f/8)(Re - 1000)Pr}{1 + 12.7\sqrt{f/8}\,(Pr^{2/3} - 1)}$	*De Paepe and Janssens 2003*
6	$Nu = 0.023Re^{0.8}Pr^{0.33}$	*Hollmuller 2003*
7	$Nu = 0.023Re^{0.8}Pr^{0.4}$	*Sodha 1994*
8	$Nu = 0.0214(Re^{0.8} - 100)Pr^{0.4}$	*Benkert et al. 1997*

Where friction factor for smooth pipes is given by:

$$f = \frac{1}{(1.82\log Re - 1.64)^2} \qquad 2.7$$

Table 2.2: Air properties and design parameters in a typical ETAHE system

Parameters	***Value***
Air conductivity	$0.0251\ W/(m \cdot °C)$
Air density	$1.164\ kg/m^3$
Air viscosity	$1.82\ E\text{-}05\ kg/(m \cdot s)$
Air specific heat capacity	$1012\ J/(kg \cdot °C)$
Duct diameter	*0.4 m*

Since the correlations were all derived for fully developed turbulent airflow, ideally, they are expected to yield similar values for the same operating condition. To examine this, a typical design of conventional ETAHE ducts in mechanical ventilation systems is used to calculate the CHTC. The duct configuration and air properties are

listed in Table 2.2. Figure 2.25 shows the comparison of the CHTC produced by different correlations (Table 2.1) as a function of Reynolds numbers.

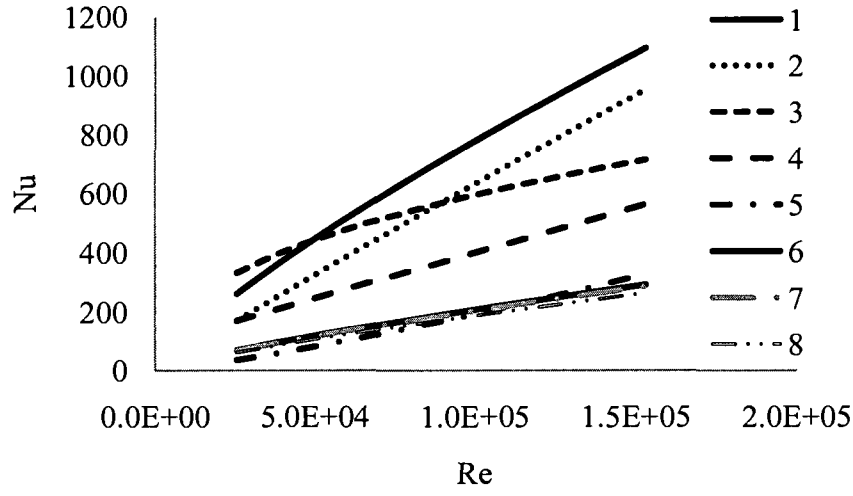

Figure 2.25: Calculated Nu based on different empirical correlations (see Table 2.1 for curve legends of the curve)

As shown in Figure 2.25, very large differences can be seen among the eight correlations. Usually, slight variation of accuracy within approximately 20 percent is expected for the empirical correlations (Burmeister 1993). This might be attributed to different experimental conditions, which were adopted to derive the correlations: for example, the surface roughness of the experimental ducts. The large discrepancies indicate that the appropriate correlation has to be selected if one uses any of the existing models to simulate the performance of an ETAHE.

2.12.4 Entrance Effects

The above discussion was presented under the assumption that the flow in ETAHE heat is mostly fully developed. It is probably acceptable for conventional ETAHE ducts with a large ratio of length to hydraulic diameter. However extensive

experimental investigations carried out by Boelter et al. (1948) and Mills (1962) indicate that the Nu_x in the entrance region is significantly sensitive to the inlet configurations. Figure 2.26 shows that L_{en} can be up to more than 30 hydraulic diameters and Nu_x can be significantly larger than Nu_∞ in the entrance region. The 90 degree elbow entrance case shown in the figure is a simplified representative of the ETAHE problem. In reality, the problem is more complicated. The ratio L/D_h of large cross-sectional ETAHEs is usually at a magnitude of 10. The ETAHE ducts are rectangular; the buoyancy force may play an important role; and Nu at ceiling, wall, and floor need to be differentiated for energy simulation purposes. Namely, the whole duct length is within the entrance length.

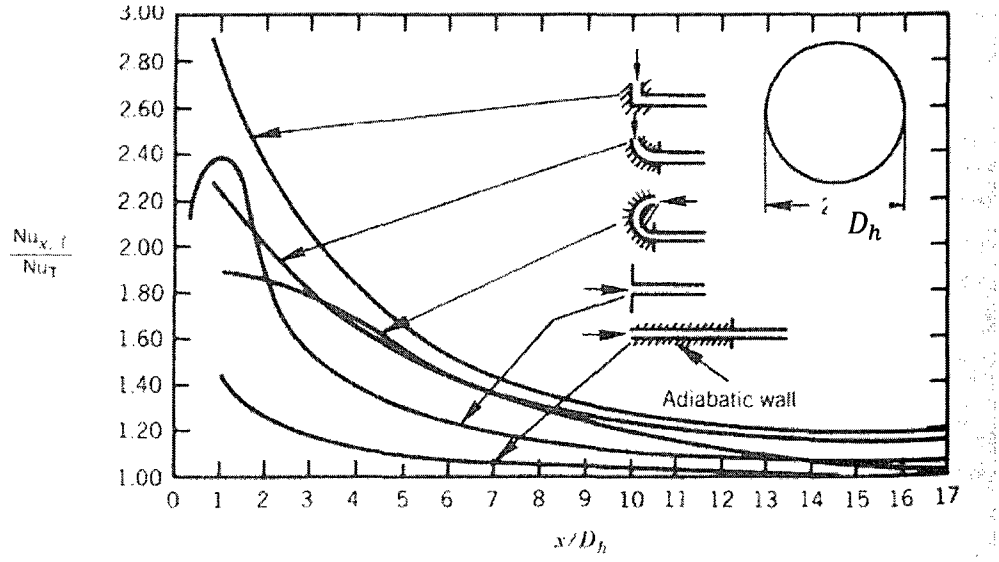

Figure 2.26: Effects of entrance configuration on normalized local Nusselt numbers of smooth circular ducts for Pr = 0.7 and Re = 5×10^4 (Boelter et al. 1948)

2.13 Summary of Literature Review

Thanks to the low pressure loss feature, large cross-sectional area Earth-to-Air Heat Exchangers have been found with better energy efficiency than the conventional

small ducts, especially when they are integrated in hybrid ventilation systems. A state-of-the-art review of ETAHEs is carried out, and it includes the working principle, classification, design and analysis methods, design guidance, and available experimental procedures for assessing the performance of ETAHEs. Several simulation methods of ETAHEs have been reviewed in this chapter; their common algorithms are to simultaneously determine the heat conduction in a soil mass around the ETAHEs and the heat convection in the ducts. Convective heat flux is used as a boundary condition for the two calculation domains at the duct and air interface. Although some differences exist among the various models, they are commonly based on assumptions that:

- The airflow in the duct is hydrodynamically and thermally fully developed at any pipe cross section,
- The duct is buried deep enough that the distance between the ground surface and the ETAHE can be considered as far-field, and
- The effect of ground temperature variation happens only at far-field and at the ETAHE burial depth and the effect is radically symmetrical.

A review on available correlations on turbulent heat convection in ducts was conducted. It shows that existing correlations may not be able to predict heat convection in large cross-sectional area ETAHEs because they are only suitable for fully developed turbulent flow and the entrance and buoyancy effects in large ETAHE ducts are not included in the correlations. The current research is focused on the large cross-sectional area ETAHEs from now on, therefore the acronym ETAHE solely refers to a large cross-sectional area ETAHE unless noted otherwise.

Chapter 3 Investigation of Convective Heat Transfer in ETAHEs

3.1 Introduction

The preceding discussion on turbulent heat convection in circular pipe provides a reference for the complexity of a large cross-sectional area ETAHE problem. Even though the turbulent heat convection in a circular duct seems to be simple, great effort has been made to predict the heat transfer rate. Therefore, a field investigation was firstly conducted at the previously mentioned Mediå School, and the results are shown in this chapter. Then a detailed numerical technique, using a Computational Fluid Dynamic method, is carried out to study the airflow and temperature distribution in large ETAHEs.

3.2 Field Investigation

There were two major purposes for conducting the site investigation: the first one was to observe airflow and heat transfer phenomena in an ETAHE under different working conditions, and the second one was to collect detailed boundary conditions and flow field data for CFD modeling validation. Since the building and ETAHE component information have been described in Section 2.10.2, in this section the site information specific to the measurement is provided. The building location is at 12°E, 65°N and 30 m above sea level. The annual mean air temperature in Grong is 4.0°C with lowest daily mean value of -5.1°C in January and highest daily mean value of 15.6°C in July. The winter design temperature is −23°C and the summer design temperature is 23°C. The test was planned to observe the cooling performance of the ETAHE system and in order to avoid the measurement uncertainties caused by the occupation, the test period was selected from June 31st to July 2nd, 2005 when the school was on summer break.

3.2.1 Experimental Design

As described in Section 2.10.2, the schematic of the ventilation system is shown in Figure 2.12. It does not have a mechanical cooling system, and the ETAHE is the only cooling component. Normally, the ventilation system is automatically controlled by the BEMS. However, if experimental data were collected in such mode, they would not be able to serve for steady-state CFD model validation. Therefore, some temporary modifications to the system were implemented as follows, and the modified ETAHE is shown in Figure 3.1.

- The measurements were performed under quasi-steady state conditions, and manual control was used to override the automatic control,
- All doors and windows were closed, and the exhaust fans in the bathrooms were deactivated,
- The classroom dampers were fully open, and the damper in front of the supply fan was removed,
- The supply fan was deactivated, and it was prevented from free rotation,
- The filters at the ETAHE duct end were replaced by polyethylene film with an 0.6 m by 1.2 m opening on the top, and two air capture hoods were installed on this opening to measure the airflow rate, and
- The exhaust fan was used as the only device to control airflow rate.

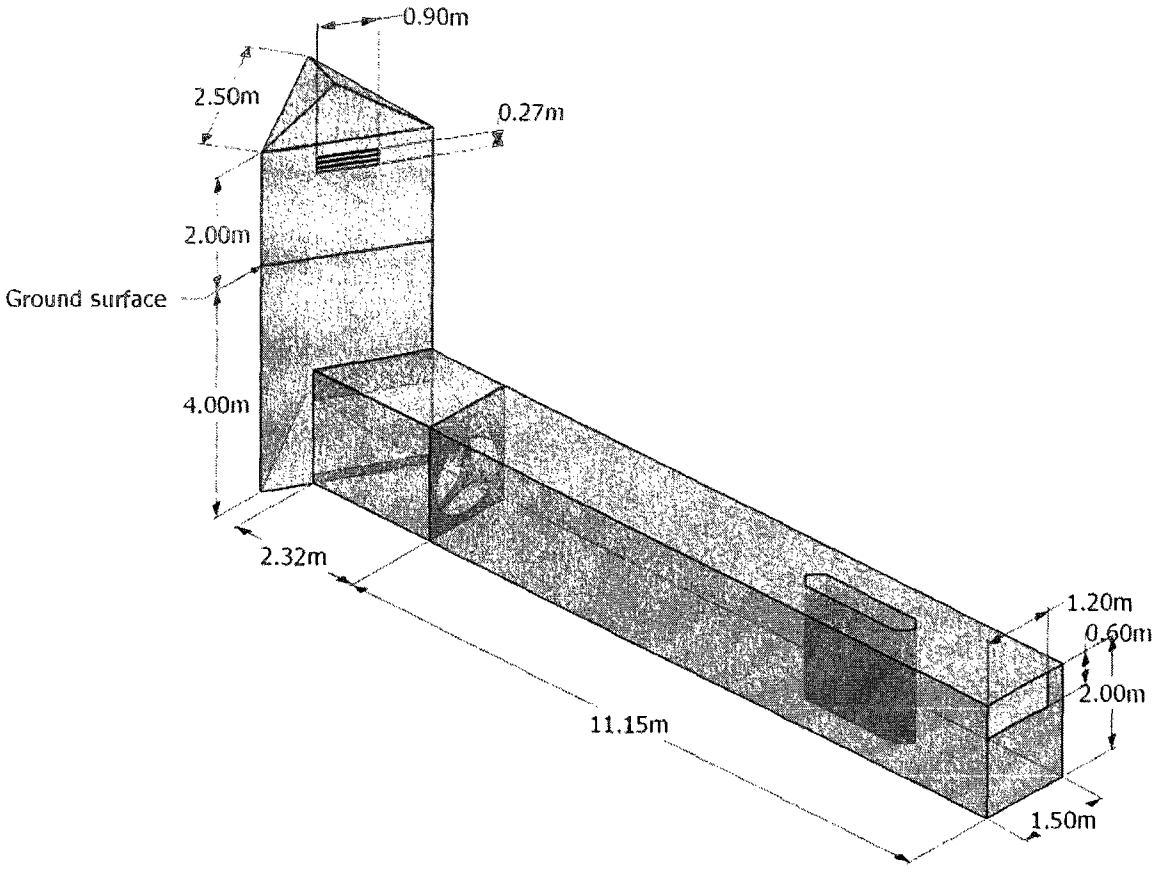

Figure 3.1: Schematic of the ETAHE in the Mediå School for the field investigation and CFD simulation

The following parameters were simultaneously measured using a 60-channel Aglient 34970A data logger and eight 8-channel Mitec AT40 data loggers:

- Duct surface temperatures using 46 thermal couples,
- Air velocities on a vertical line of the duct middle plane using seven velocity transducers,
- Air temperatures on a vertical line of the duct middle plane using 20 thermal couples,

- Air temperatures on a horizontal line of the duct middle plane using 20 thermal couples,
- Volumetric airflow rate, using two air capture hoods, and
- Inlet and outlet air temperatures using two thermal couples.

Since these parameters are needed for CFD model validation, the time period for each measurement was long enough for quasi-steady states to be reached. For each measurement, the actual time period was around one hour. The first half hour was for the heat transfer processes to reach a quasi-steady state: Data during the second half hour were used to for the time-averaging. The measurement results are shown together with the simulation data in later section.

3.2.2 Instrument Calibration

All the sensors were calibrated in the laboratory at the Norwegian University of Science and Technology. Ninety thermal couples were calibrated by submerging the thermal couples in a temperature controlled thermal bath of liquid ethanol with an accuracy of $\pm 0.01°C$. Three temperature set points were selected (i.e. 5°C, 15°C and 25°C) to cover the possible range of the later measurement. The differences between the data logger readings and the thermal bath temperature were used to calibrate the thermal couples. It was found that the accuracy of the sensor readings was about $\pm 0.5°C$. Nine velocity transducers were also previously calibrated using a wind tunnel. The results are shown in Table 3.1.

Table 3.1: Comparison of velocity transducer readings with reference velocity

Sensor #	*Reading 1, m/s*	*Accuracy*	*Reading 2, m/s*	*Accuracy*
Reference set point	*0.17*	*N/A*	*0.96*	*N/A*
Sensor 1	*0.192*	*-12.9%*	*0.916*	*4.6%*
Sensor 2	*0.136*	*20.0%*	*0.825*	*14.1%*
Sensor 3	*0.194*	*-14.1%*	*0.898*	*6.5%*
Sensor 4	*0.195*	*-14.7%*	*0.971*	*-1.1%*
Sensor 5	*0.172*	*-1.2%*	*0.87*	*9.4%*
Sensor 6	*0.144*	*15.3%*	*0.88*	*8.3%*
Sensor 7	*0.177*	*-4.1%*	*0.958*	*0.2%*
Sensor 8	*0.192*	*-12.9%*	*1.05*	*-9.4%*
Sensor 9	*0.207*	*-21.8%*	*0.974*	*-1.5%*

3.2.3 Airflow Rate Measurement

As shown in Figure 3.2 (upper-right), two air capture hoods were installed at the end of the duct to measure the airflow rate. The manufacture's manual indicated that they were calibrated with accuracy of $\pm 0.002\ m^3/s$ within a range from 0.013 to $0.972\ m^3/s$. Since the hoods' readings could not be directly logged (missing connecting cables), an indirect measurement method was developed: a velocity sensor was placed at one hood's center. Under various airflow rates, the readings of hoods and velocity sensors were simultaneously taken. The relationship between them was plotted in Figure 3.3. Using this figure, instantaneous airflow rate could be obtained by using the logged velocity transducer readings. An example of the measured airflow rates is shown in Figure 3.4 to illustrate its stability.

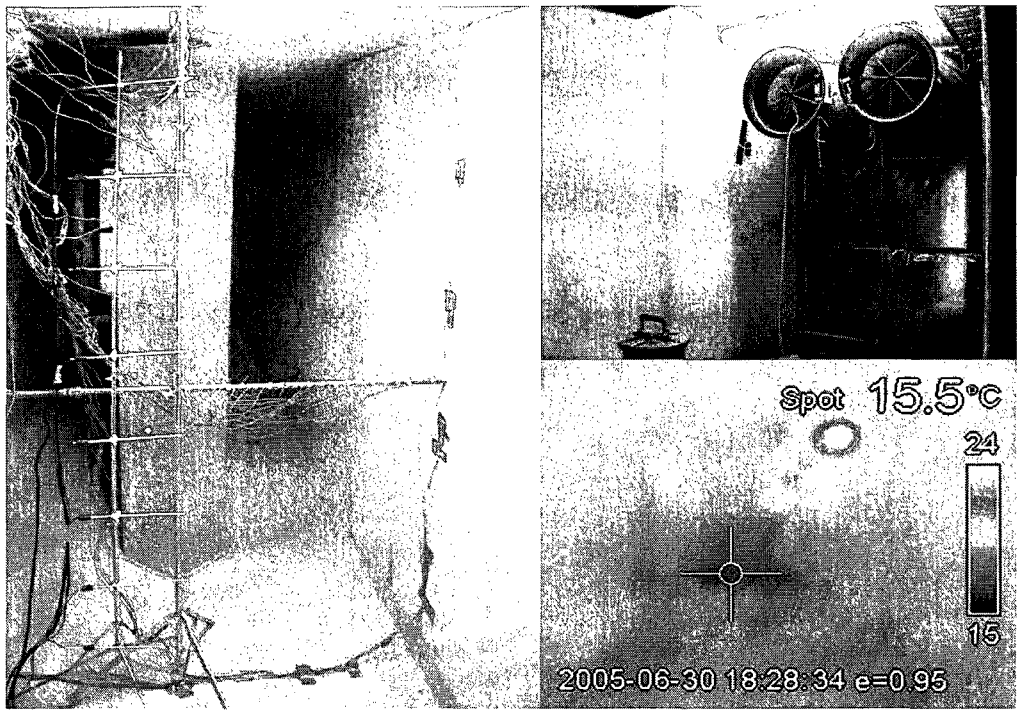

Figure 3.2: Experimental design (left: measurements for surface temperature and air temperature and velocity; upper-right: air capture hoods; lower-right: surface temperatures)

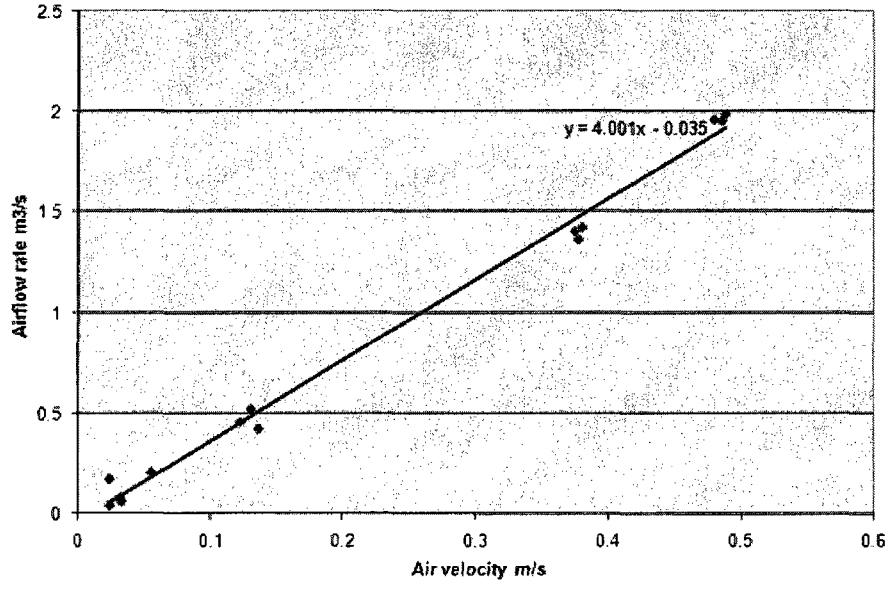

Figure 3.3: Linear relationship between velocity readings from the velocity sensor and airflow rate readings from the air capture hood

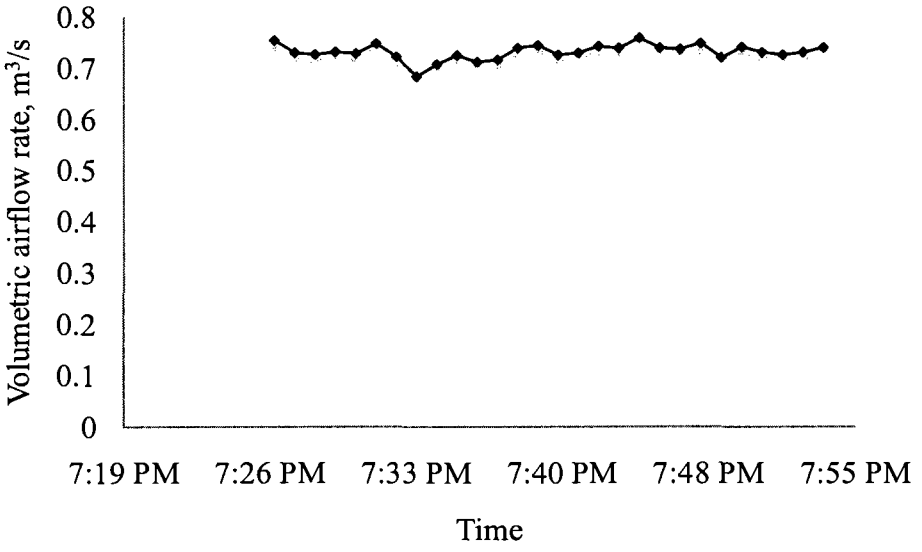

Figure 3.4: Stability of airflow rate measurement when exhaust fan runs at 80%

3.2.4 Derivation of Convective Heat Transfer Coefficients from Measurements

It is very worthwhile to mention previous research conducted on the Mediå School building by Wachenfeldt (2003). He performed an hourly dynamic energy simulation for the building using a software program, i.e. ESP-r, to study the energy performance of the building. In the simulation, the ETAHE was divided into three portions along its length using two fictitious surfaces. Since existing heat convection algorithms were found not suitable for the ETAHE, Wachenfeldt performed some measurements under various system operation conditions. The measured parameters were duct surface temperatures at four locations, airflow rates, and inlet and outlet air temperatures. Using these data, he derived correlation between the Reynolds number and overall convective heat transfer coefficients based on Equation 3.1. Using the same method, the film coefficients based the current measured data were also derived, and they are plotted (see Figure 3.5) together with the Wachenfeldt results and predicted results

from an empirical correlation Equation 3.3 (ASHRAE 2005). Where, h is convective heat transfer coefficient, $\dot{m}$ is the mass flow rate, $c_{p,air}$ is specific heat capacity, T is temperature, A_{ETAHE} is the duct surface area, k is the air thermal conductivity, D_h is the duct hydraulic diameter, Re is the Reynolds number, and Pr is the Prandtl number.

$$h = \frac{\dot{m} \cdot c_{p,air} \cdot (T_{out} - T_{in})}{(T_{surf} - T_{air}) \cdot A_{ETAHE}} \quad 3.1$$

$$h = 0.023 \frac{k}{D_h} Re^{0.8} Pr^{0.33} \quad 3.2$$

Although the current study and Wachenfeldt both used Equation 3.1 to calculate the film coefficients, the results are slightly different. This can be attributed to the different average surface temperature used in the two studies. The T_{surf} in Wachenfeldt's study was averaged from four locations; and in this study, 46 values were used to calculate the average surface temperatures. A thermal picture (see Figure 3.2 lower-right) taken in the ETAHE can explain the variation of the interior surface temperatures. No matter which one is more accurate, it is clear that the average convective heat transfer coefficients were significantly higher than those predicted from the empirical correlation, which should be only suitable for fully developed turbulent flow. This implies that if the existing empirical correlation had been used in the energy simulation, the ETAHE performance would have been significantly underestimated. Therefore, there is a need for development of a prediction algorithm for heat convection in large cross-sectional area ETAHEs; and it is needed for accurate ETAHE design and simulations.

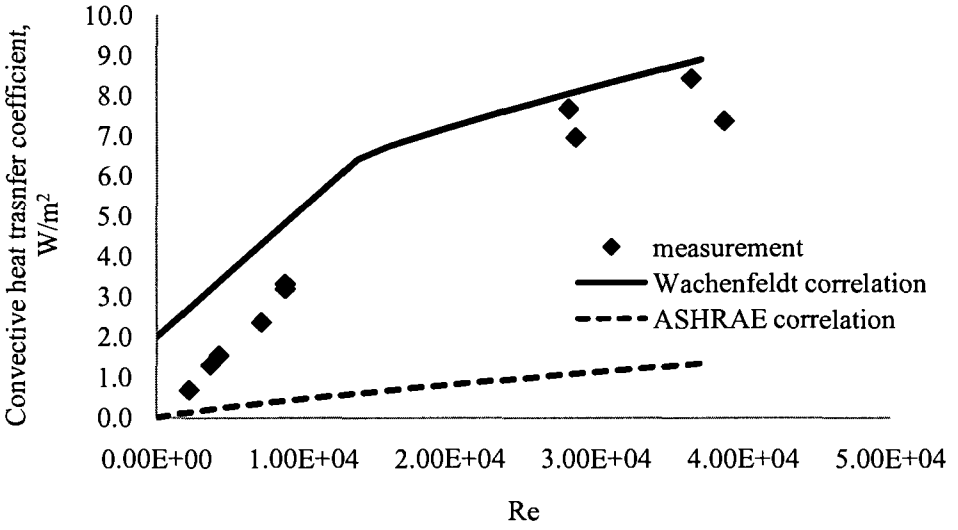

Figure 3.5: Comparison of calculated convective heat transfer coefficients from current measurements, Wachenfeldt's correlation, and ASHRAE correlation

3.3 Preliminary CFD Study of the ETAHE at the Mediå School

Computational Fluid Dynamics (CFD) technique solves conservation equations on every grid of a discretized simulation domain. Airflow in buildings is mostly turbulent and it can be considered as incompressible flow. The governing equations for mass, momentum, and energy in Reynolds-averaged forms can be simplified as Eq. 3.3 - 3.5 using the eddy viscosity concept. The buoyancy force caused by density difference in the fluid is taken into account using the Boussinesq approximation. With recent developments in computer technology, CFD is becoming a more convenient way than traditional experimental methods to study convective heat transfer for indoor airflow due to its flexibility of setting up boundary conditions and extracting results. Successful applications can be found from Zhai and Chen (2004), Hsieh and Lien (2004), and Haghighat et al. (1992). In the current study, it is believed that CFD simulation can be

used to provide more detailed information about the heat transfer and airflow phenomena in the ETAHE than the measurements.

$$\frac{\partial u_i}{\partial x_i} = 0 \tag{3.3}$$

$$\frac{\partial}{\partial x_i}(\rho u_j u_i) = -\frac{\partial p}{\partial x_i} + \frac{\partial}{\partial x_j}\left((\mu_t + \mu)\left(\frac{\partial u_j}{\partial x_i} + \frac{\partial u_i}{\partial x_j}\right)\right) + \rho\beta(T_\infty - T)g_i \tag{3.4}$$

$$\frac{\partial}{\partial x_i}(\rho c_p \mu_t T) = \frac{\partial}{\partial x_i}\left[\left(\lambda + \frac{c_p \mu_t}{Pr_t}\right)\frac{\partial T}{\partial x_i}\right] \tag{3.5}$$

3.3.1 Modeling setup

The configuration of the ETAHE in the Mediå School shown in Figure 3.1 is used as the simulation domain in the CFD. Due to the complex geometry, unstructured mesh was generated with tetrahedral and hexahedral elements using the commercial software "Gambit". The general mesh size was 0.1 m. The buoyancy effect in the flow is simulated using the Boussinesq approximation method. A Standard $k-\varepsilon$ turbulence model with a standard log-law wall function method was used to simulate the turbulence transport. This will be discussed in detail in later sections.

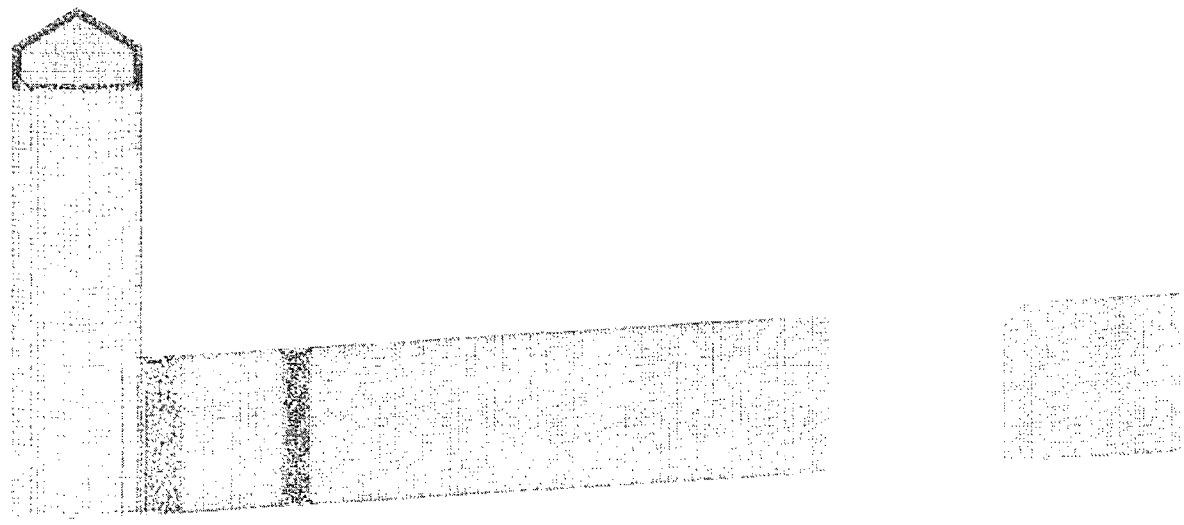

Figure 3.6: Generated mesh for the Mediå School ETAHE at the middle plane

3.3.2 Boundary Conditions

The CFD simulations were performed on various measurement cases, with different airflow rate, and one case is presented in this paper. The measured inlet air temperature was 21.5°C. The exhaust fan was running at full speed, and it created an airflow rate of 0.989 m^3/s. It is assumed that the three inlet openings (on the triangular cross-sectional vertical inlet tower) equally shared this airflow, and uniform velocity normal to each opening surface is used as the inlet boundary condition. Simulations with other inlet velocity directions were also performed but they did not cause noticeable changes to the simulation results in the horizontal ETAHE duct. During the field investigation, temperatures of the ETAHE surfaces on the windward side of the supply fan were not measured. In order define their boundary conditions, two assumptions were be made. 1: the inlet tower's interior surfaces above ground are adiabatic since the duct walls are insulated according to the construction documents; 2: the temperatures of the other duct surfaces (below the ground surface and windward to the supply fan) are a linear function of their depths. The function is obtained from a linear interpolation between the inlet air temperature and the average temperature of the ETAHE duct surfaces on the leeward side of the supply fan. The measured duct surface temperatures at 46 locations were used to provide boundary conditions for the other surfaces of the ETAHE.

3.3.3 Simulation Results

The measured and simulated results of vertical air velocity magnitude profiles, horizontal and vertical air temperature profiles are shown in Figure 3.7 to Figure 3.10. The comparison between the simulation results and measurements shows that the CFD

method can provide acceptable prediction of the airflow and heat transfer. Setting up a field experiment in such a large enclosure requires complicated data logging systems; however, information obtained from such experiment is still very limited. Since the CFD model is verified from its comparison with measurements, it can be used to analyze many details of the physical processes. Figure 3.11 and Figure 3.12 show the simulated air temperature and velocity distributions on the duct middle plane. Two large circulation zones can be observed near the ceiling of the horizontal duct before and after the supply fan. The first one is due to the rectangular turn from inlet tower to the horizontal duct, and the second is caused by the blocking of the fan frame. After the warm air flows through the supply fan frame, the cool duct surfaces gradually cool the air down. Buoyancy force due to the density increase draws the cooler air down to the floor, and the warmer air is pushed up. This process forms obvious air temperature stratification as shown in Figure 3.9. The cooler air keeps accumulating near the duct floor. Although most of it is driven by the main stream to the end of the duct, a small portion is pushed back towards the inlet. Since the velocity transducers in the measurement could only provide the velocity magnitudes, this reverse flow phenomenon can only be clearly identified and interpreted from the CFD simulation.

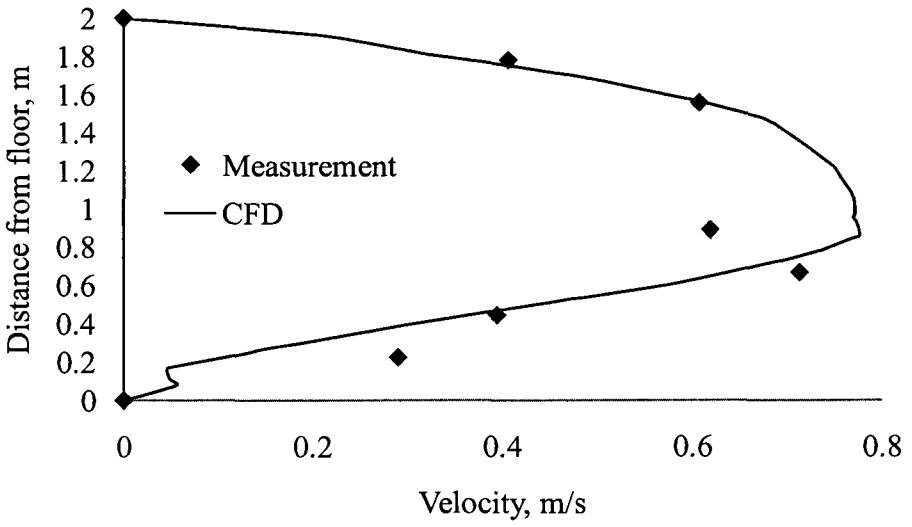

Figure 3.7: Vertical velocity magnitude profile on middle plane at 2.1 m from fan

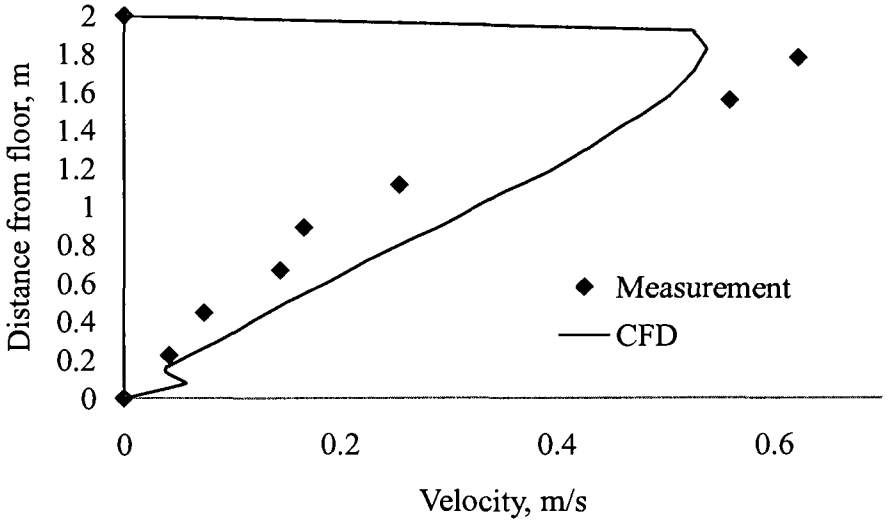

Figure 3.8: Vertical velocity magnitude profile on middle plane at 6.1 m from fan

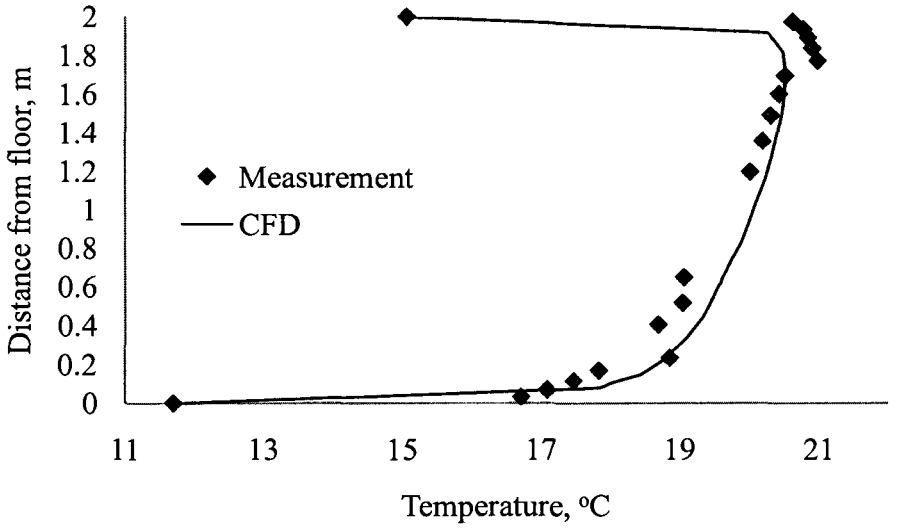

Figure 3.9: Vertical temperature profile on the middle plane at 4.1m from the fan

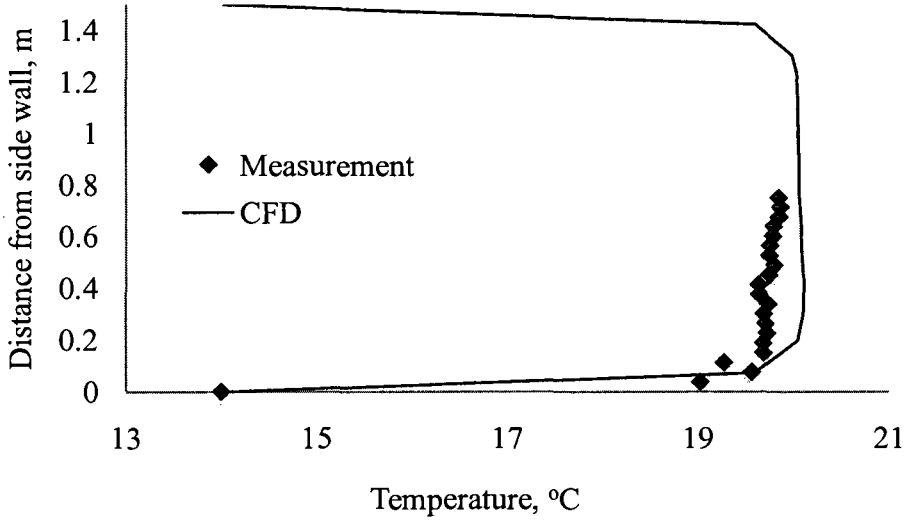

Figure 3.10: Horizontal temperature profile at 1m from the floor and 4.1 m from the fan

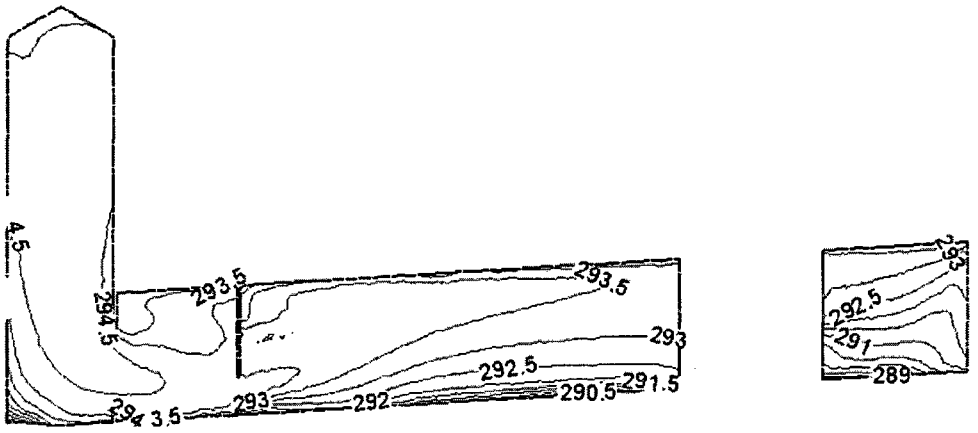

Figure 3.11: Simulated air temperature contour on the Mediå School ETAHE middle plane

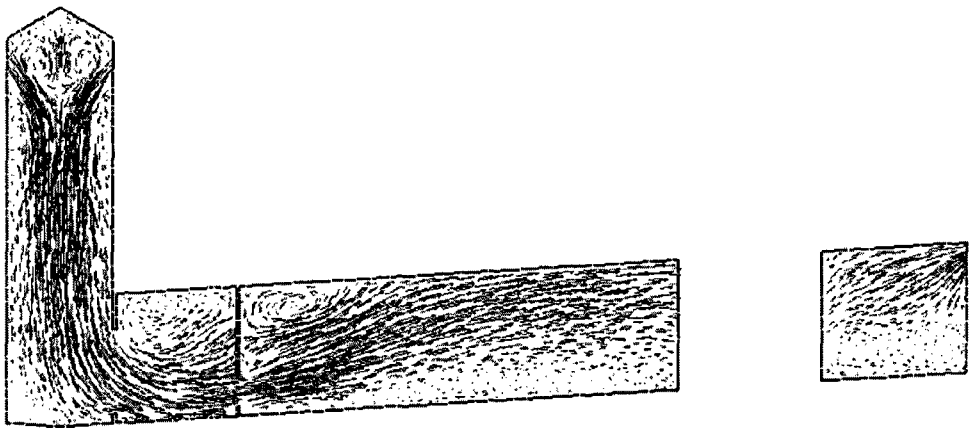

Figure 3.12: Simulated air velocity vector on the Mediå School ETAHE middle plane

3.3.4 Summary of the Preliminary CFD Study

The preliminary CFD simulation has shown very promising results when compared to the field measurements. The simulation accuracy is in a reasonable range and the plotted flow field illustrated much more information than the measurement results. The reversed flow, air temperature and velocity stratification, and surface temperature variation indicate that the flow in such a large cross-sectional area ETAHE was far from fully developed turbulent flow. This is the reason that the empirical

correlation significantly underestimated the intensity of the heat convection. The effects, such as: rapid development of boundary layer at the entrance region of the horizontal duct, the air flushing effect on the duct floor due to the rectangular turn, and the enhancement of heat convection due to buoyancy driven vertical flow, have caused the heat convection in the large cross-sectional area ETAHE to be very complicated. A uniform film coefficient on all the duct surfaces cannot represent the real heat convection in the duct. It would cause significant inaccuracy in energy efficiency analysis when conventional ETAHE simulation models are used for such large duct systems.

3.4 CFD Modeling for Convective Heat Transfer in ETAHEs

The preliminary CFD study of the ETAHE has shown that CFD is a very promising alternative method to the actual experimental methods. Most existing empirical correlations of convective heat transfer coefficients were developed through experimental measurements. The method can generally be summarized as:

- To design an experimental setup, its space size and configuration should be a general representative of the heat convection problem,
- To provide a controlled surface boundary condition, such as constant surface temperature or constant heat flux,
- To maintain the fluid flow conditions in steady states,
- To be able to quantify the heat flux over the surfaces of interest,
- To calculate the film coefficient by dividing the heat flux with a temperature difference between the surface and the fluid at a reference location,
- To repeat the test with various conditions, and

- To generalize the relation between the flow condition and the film coefficient using a mathematical correlation.

CFD method seems to be able to replace all the experimental steps above but as far as the author's knowledge, in the building applications no convective heat transfer coefficient correlation in large enclosures, such as rooms, has been derived based on numerical experiments. The major obstacle was found to be the turbulence modeling. The following subsections describe a CFD model for ETAHEs, and the turbulence modeling issue is discussed.

3.4.1 CFD Model Description

In the current study, an ETAHE is represented by a horizontal duct with an inlet tower, as shown in Figure 3.13. Due to the symmetric geometry, half of the duct is defined as the simulation domain in order to save computational time. The duct surfaces are divided into a number of elements to bring convenience for analyzing the local area-weighted average heat transfer and for assigning different duct surface temperature distributions as boundary conditions. To specify a simulation case, there are few parameters to be specified, i.e. duct length, height, width, inlet width, bulk velocity, inlet air temperature, inlet turbulent intensity, inlet velocity direction, duct surface temperatures, and outlet width. It is assumed that the velocity at the inlet has a uniform profile and the inlet tower walls are adiabatic. The governing equations for mass, momentum and energy are the same as those used in the preliminary CFD study, but the turbulent model needs to be carefully selected.

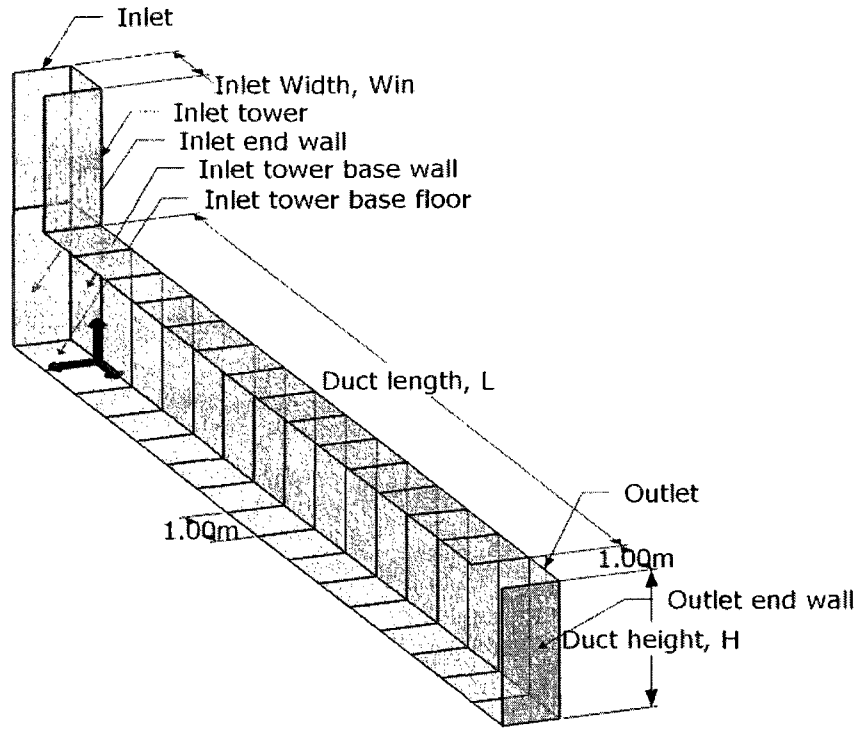

Figure 3.13: Schematic drawing of the ETAHE model

3.4.2 Turbulent Modeling

In a CFD simulation, convective heat flux in turbulent flow is mathematically expressed by Equation 3.6. It indicates that the critical variables affecting the simulated heat flux are the turbulent viscosity and the temperature gradient from the first grid to the surface.

$$q'' = -c_p \left(\frac{\mu}{Pr} + \frac{\mu_t}{Pr_t}\right) \frac{(T_{surf} - T_1)}{D} \qquad 3.6$$

Although many successful studies have been carried out using the Standard $k-\varepsilon$ turbulence model (Launder and Spalding 1974) with log-law wall functions in room airflow applications, the method has been shown deficient in predicting surface convective heat transfer (Zhai and Chen, 2004 and Awbi, 1998). This is because the

model was formulated for fully developed turbulent flows, and it tends to over-predict the eddy viscosity in low flow regions. In addition, the log-law wall functions require the first grid near wall to be out of the viscous sub-layer, within which the temperature gradient has significant effects on the convection simulation (Schild 1997). Low-Reynolds Number turbulence models have been reported to produce improved results (Awbi 1998); however, the computational expenses for full scale simulations are considerably higher. The log-law wall function method is just one of the various wall-functions. The purpose of these functions is to simplify the process of solving differential equations on every fine grid of the viscous affected sub-layer as the Low-Reynolds Number turbulence models usually do (Craft et al. 2006). Two-layer turbulence model is another one of the wall-function approaches. Its principle is to solve main flow regime using two-equation model such as Standard $k-\varepsilon$ model and to solve simplified differential equations on very fine grids across the sub-layer. It takes advantage of the computational efficiency of the Standard $k-\varepsilon$ turbulence model and the accuracy of the Low-Reynolds Number turbulence model at the near-wall region.. Xu et al. (1998) developed a Two-lay turbulence model to solve near-wall natural convection. Good prediction results were obtained for main flow and turbulence for natural convection with Ra around 5.4×10^5. Development of a recent two-layer turbulence model was reported by Gant (2002) and Craft et al. (2006). It has also shown good performance for flow with strong streamline curvature. All turbulence models have their own ranges of applicability, and verification or validation is the most trustable way for selecting suitable turbulence model. This study selected a two-layer turbulence model, which solves a one-equation $k-l$ model (Wolfshtein 1969) in the near-wall region and applies the Standard $k-\varepsilon$

model (Launder and Spalding 1974) in the outer region. The demarcation of the two regions is determined by a critical turbulent Reynolds number, Re_y, defined by Equation 3.7. The flow in outer region, $Re_y > 200$, is assumed to be fully developed turbulent. The viscous-effected near-wall region is defined by $Re_y < 200$. In the $k - l$ model, the momentum equations and the k equation are retained the same as in the Standard $k - \varepsilon$ model, and the turbulent viscosity, μ_t, is computed using Equation 3.8, in which the turbulent length scale, l_μ, is defined by Equation 3.9 (Chen and Patel 1988). To smoothly blend the two regions, an enhanced wall treatment method is adopted and the detail formulation can be found in Fluent (2003).

$$Re_y = \frac{\rho y \sqrt{k}}{\mu} \tag{3.7}$$

$$\mu_t = \rho C_\mu l_\mu \sqrt{k} \tag{3.8}$$

$$l_\mu = y c_l \left(1 - e^{Re_y / A_\mu}\right) \tag{3.9}$$

3.4.3 Mesh Development

The two-layer turbulence model can resolve detailed flow information in the viscous-effected near-wall region, which determines the prediction of convective heat flux. A very fine mesh is required to obtain sufficiently accurate solutions of the flow variables, but this takes a great amount of computational time for each simulation. In the current study, the computational domain is discretized into two smoothly adjacent regions, i.e. the boundary layer with a fine grid and the outer region with a relatively coarse one. Hexahedral elements were generated throughout the computational domain. From the duct surfaces, the element sizes proportionally grow away based on a properly

selected first grid size and a growth factor. In the outer region, the grid is developed based on a uniform characteristic length.

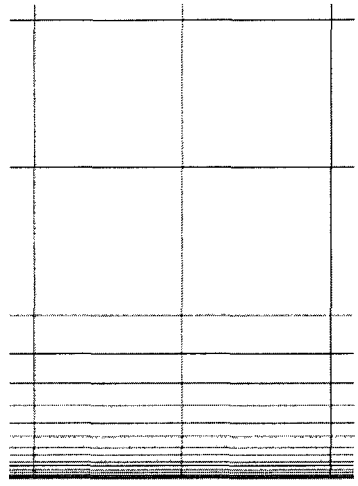

Figure 3.14: An example of the generated mesh

3.4.4 Boundary Conditions

The wall surfaces of the inlet tower are set to be adiabatic since they are normally insulated to protect them from freezing. No-slip conditions for velocity and steady temperatures are applied at the duct surfaces. Zero diffusion flux of all flow variables in the direction normal to the outlet is used. At the inlet, uniform velocity is used and the direction is normal to the opening. Turbulence parameters at the inlet are defined using turbulence intensity (assuming 5%) and inlet characteristic length (hydraulic diameter) method, as shown in Equations 3.10 and 3.11.

$$k = \frac{3}{2}(u_{\mathrm{m}} I)^2 \qquad 3.10$$

$$\varepsilon = C_{\mu}^{3/4} \frac{k^{3/2}}{l} \qquad 3.11$$

3.4.5 Solving Technique

This study used a fully-unstructured finite-volume CFD solver, Fluent 6.2, for the simulation. The SIMPLE algorithm is applied to the pressure-velocity coupling in the segregated solver. A second-order upwind scheme is adopted for the discretization of the governing equations. The convergence criteria for all variables were set to be 10^{-4}, except for energy, which was set to be 10^{-6}.

3.4.6 Model Verification

In the preliminary CFD study, the CFD simulation was roughly verified by comparing its air velocity and temperature profiles with the measurements. However as addressed before, to derive accurate convective heat transfer coefficients, the modeling method has to be verified against measured convective heat flux and this could not be obtained from the field investigation in Mediå School. Therefore, measurement results of a room size chamber published by Spitler (1990) and Fisher (1995) were selected. The similarity of the two applications exists in their cavity sizes, boundary conditions, and flow regimes. Comparisons of the two cases on their characteristic parameter ranges are listed in Table 3.2.

The chamber was designed to measure the area-weighted average heat flux over the ceiling, floor, and three adjacent levels of wall surfaces, which were all controlled at a steady temperature of 30°C. Constant supply airflow rates and temperatures were kept for each experiment and they range from 6 to 100 Air Changes per Hour (ACH) and from 10 to 25°C for various cases. This covered both forced and mixed convection regimes. The significance of grid generation on the simulation results was addressed earlier. Therefore, a grid independence exam was firstly performed to determine proper mesh generation

criteria. The quality of the mesh in the boundary layer and outer region was separately analyzed. Firstly, the boundary layer mesh was fixed and the characteristic length of the grid in the outer region was set to be 0.05, 0.075, 0.1, 0.15, and 0.2 m. The five meshes were tested on an experimental case with an airflow rate of 50 ACH and inlet air temperature of 16°C. The simulated temperature and x-velocity profiles at a vertical line in the chamber are shown in Figure 3.16 and Figure 3.17. They indicate that when the grid sizes are smaller than 100 mm, the results become independent of the sizes. Secondly, the same case with different first grid sizes in the boundary layer mesh was simulated, i.e. 0.2, 0.4, 0.8, and 1.2 mm. Figure 3.18 plots the simulated area-weighted average heat flux over the five surfaces versus the area-weighted average y^+ value of the mesh. In order to show the comparison, the measurement results are plotted at $y^+ = 0$ axis. The deviation of between the simulated results to the measurement is between 7% and 30% except for the ceiling, at which very low heat flux were measured. The important finding from the figure is that the predicted results are independent of the first grid size. Therefore, the following criteria were selected for the mesh development in this research: first grid size of 0.2 mm; 15 grids in the boundary layer with a growth factor of 1.3; and grids with characteristic length of 75 mm in the outer region. Based on these criteria, the calculation domain in Figure 3.15 was discretized into 129924 control elements. Four experimental cases from the literature were simulated, and the computations took up-to 48 hours with a 3.06 gigahertz CPU and 3 gigabyte memory. The results are shown in Figure 3.19. The difference between the simulation results an the measurements ranges from 3% to 27%, and the largest deviation, 27%, occurs for the ceiling case, which has relatively a small heat flux. According to Spitler (1990) and Fisher (1995), the accuracy

of their measurements was about 20%. Therefore, the simulation results are considered satisfactory.

Table 3.2: Characteristic parameters of the experimental chamber case and an ETAHE

Characteristic Parameters	*name*	*unit*	*Spitler 1990 and Fisher 1995*		*ETAHE*	
			Low	*High*	*Low*	*High*
$L_{en} = \sqrt[3]{V_{en}}, L_{en} = D_h$	*Char. length*	*m*	*3.25*		*0.2*	*3*
$U = Q/A_{in}, or\ Q/A_c$	*Velocity*	*m/s*	*0.08*	*2.65*	*0.1*	*4*
$\Delta T = T_{surf} - T_{in}$	*Temp. diff.*	*°C*	*20*		*5*	*30*
$Re = UL_{en}/\nu$	*Re*		*1.6E+04*	*5.5E+05*	*6.4E+03*	*7.6E+05*
$Gr = g\beta\Delta TL_{en}^3/\nu^2$	*Gr*		*9.3E+10*		*5.4E+06*	*1.1E+11*
$Ra = g\beta\Delta TL_{en}^3/(\nu\alpha_{air})$	*Ra*		*6.6E+10*		*3.9E+06*	*7.8E+10*
$Ri = Gr/Re^2$	*Ri*		*0.3*	*344.5*		

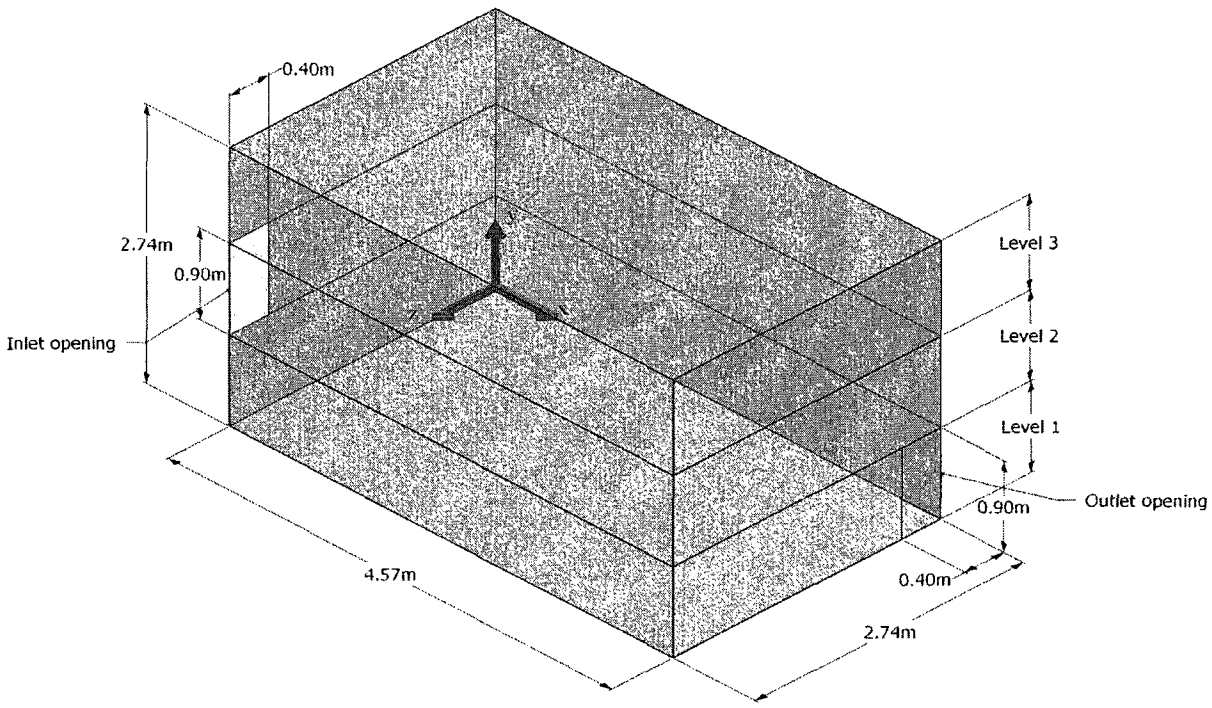

Figure 3.15: Configuration of the experimental chamber

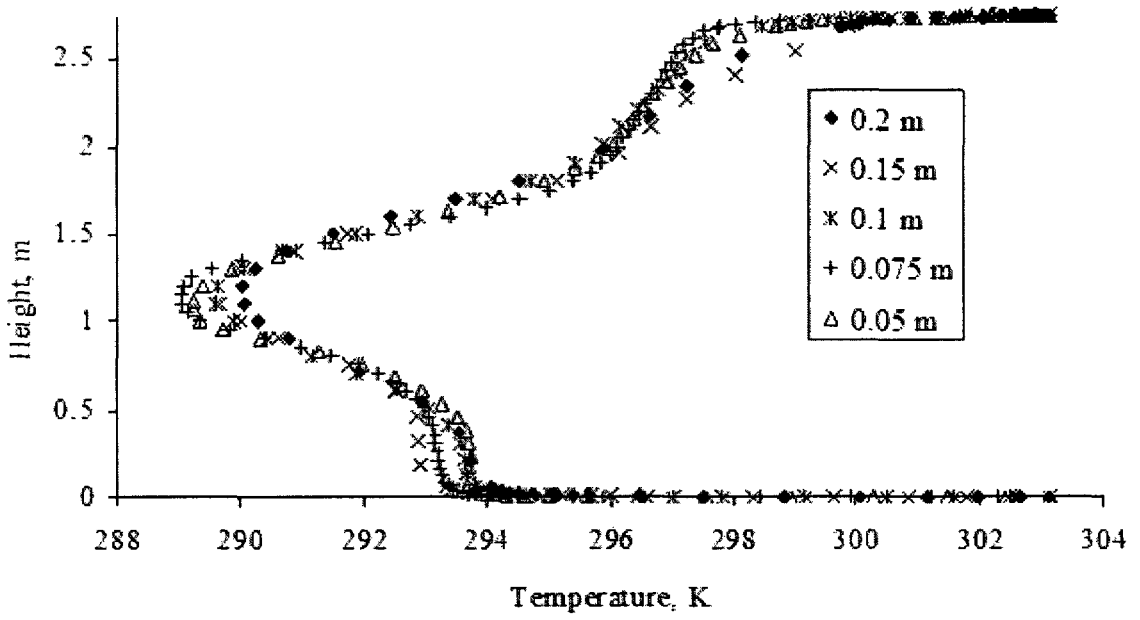

Figure 3.16: Comparison of air temperature profiles along a vertical axis in the chamber with various characteristic grid lengths in the outer region

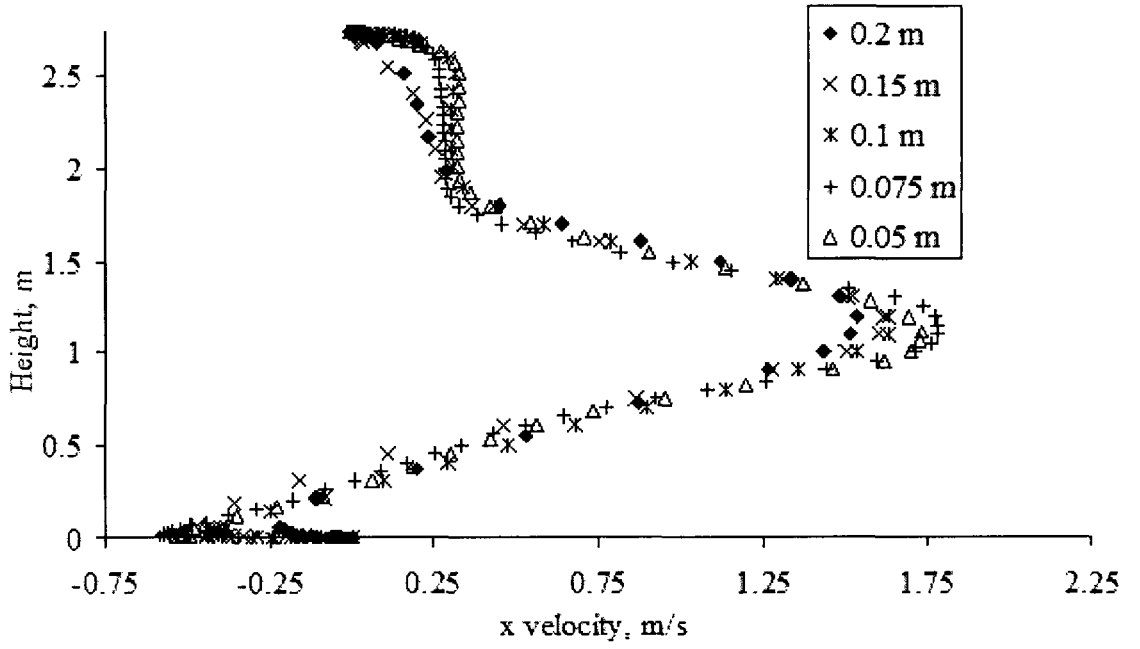

Figure 3.17: Comparison of air x-velocity profiles along a vertical axis in the chamber with various characteristic grid lengths in the outer region

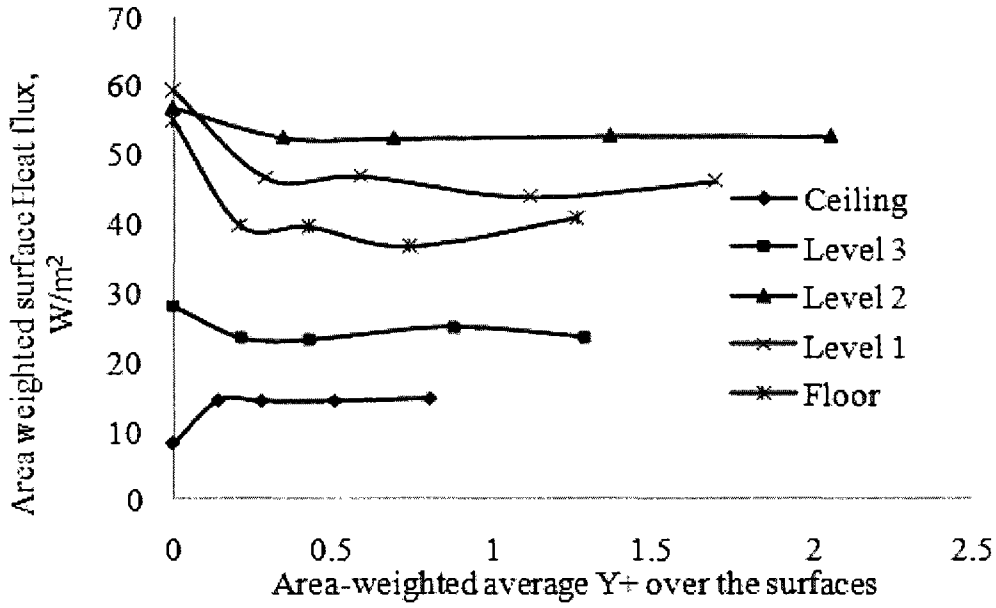

Figure 3.18: Comparison of area-weighted average surface heat flux with various y^+ with measurements

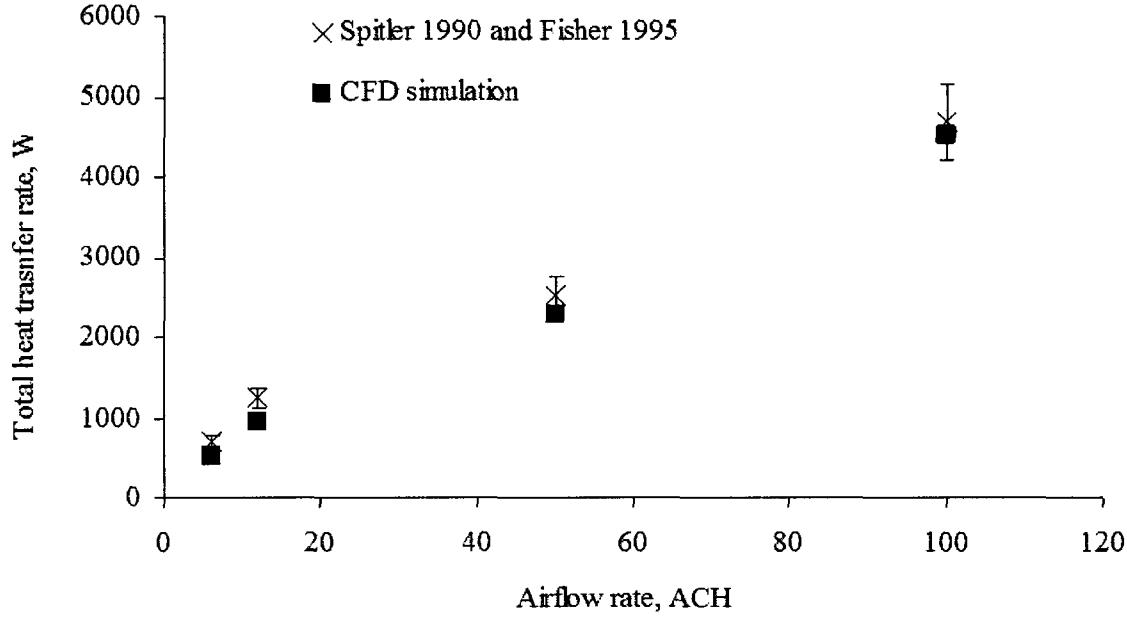

Figure 3.19: Comparison of total heat transfer rate results between the simulations and the experiments

3.4.7 CFD Simulation Results of Nusselt Numbers

After the CFD modeling method is verified, it can be used with confidence to calculate the convective heat transfer in ETAHEs. Figure 3.13 is the basic ETAHE design setup as a general representation of a large cross-sectional area ETAHE. To conduct a simulation, specific dimensions and boundary conditions need to be decided. In the first sample simulation case, the following parameters were used: duct length (L) = 14 m, height (H) = 1 m, width (W) = 1.5 m, inlet width (W_{in}) = 1 m, bulk velocity (U) = 0.67 m/s, inlet air temperature (T_{in}) = -10°C, inlet turbulent intensity (I_{in}) = 5%, inlet velocity vector ($\vec{V}$) = (0, -1, 0), duct surface temperature (T_{surf}) = 10°C, outlet width (W_{out}) = 1 m. Given these conditions, the ETAHE case was simulated and the area-weighted local average Nusselt numbers calculated based on Equation 3.12 are plotted in Figure 3.20.

$$Nu_{avg} = \frac{D_h}{k} \frac{\sum \dot{q}_{\text{element}}}{(T_{surf} - T_{in}) \cdot \sum A_{\text{element}}} \qquad 3.12$$

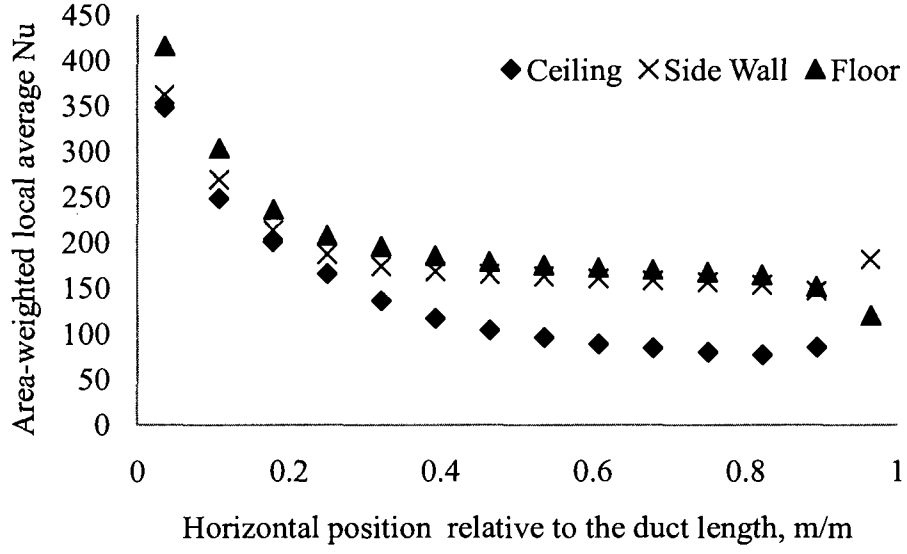

Figure 3.20: Simulated area-weighted average Nusselt numbers at different locations of the ETAHE duct

From Figure 3.20, one can note that the predicted Nu numbers decrease along the duct length for all three surfaces, i.e. ceiling, wall, and floor. This should be attributed to the entrance effects. In addition, the differences between of the Nu numbers at the same cross section with different heights are very large. This could be due to the buoyancy effect and/or the flushing effect from the 90° turn from the duct inlet tower to the horizontal part.

3.5 Summary

The results of a field study on a large cross-sectional area ETAHE in a hybrid ventilation system was presented. It was found that the interior surface temperatures of the duct may differ at various locations by a few degrees. The measured data was used to calculate an overall convective heat transfer coefficient of the duct surfaces, and the results showed that the empirical correlation for fully developed turbulent heat convection significantly underestimates heat transfer intensity.

A preliminary CFD simulation for the ETAHE was conducted. Some phenomena, such as air temperature stratification, air velocity stratification, and buoyancy driven secondary flow, indicate that the heat transfer in the large duct is far from fully developed. Since the CFD method was found to be able to predict the heat convection with good accuracy, it was further improved by modifying the turbulent model from standard $k-\varepsilon$ model with log-law wall function to a Two-layer turbulent model. It uses a one equation $k-l$ model in the near wall region and a standard $k-\varepsilon$ model in the outer region. An appropriate grid generation guide was also developed based on careful grid independence examination. The improved model has shown to be able to predict

convective heat transfer rate with satisfactory accuracy when comparing its results with experimental results from the literature.

Finally, a standard ETAHE configuration was determined to be a general representative of the large cross-sectional area ETAHEs. Such an ETAHE with specific configurations and boundary conditions was simulated using the developed CFD model. Local area-weighted Nusselt numbers of the ETAHE were predicted. The results indicate that entrance effect and the buoyancy effect caused a significant non-uniform distribution of convective heat transfer rate on the ETAHE duct surfaces. Therefore there is need to develop a new convective heat transfer algorithm for ETAHEs.

Chapter 4 Development of Convective Heat Transfer Algorithm

4.1 Introduction

The need for investigation of airflow and convective heat transfer in ETAHEs was clearly shown in the previous chapter. To this end, this chapter will first identify parameters influencing the heat convection in ETAHEs and then conduct a large number of numerical experiments using the developed and verified CFD model.

4.2 Sensitivity Study of the Design Parameters

The efficiency of an ETAHE is based on the energy exchange between the airflow through the duct and the duct surfaces. Similar to indoor airflow, the heat convection in a large cross-sectional ETAHE duct is affected by various design factors. Therefore, a sensitivity study was conducted to identify the influential variables so that minimum number of parameters would be included as the inputs for predicting the heat convection. Several parameters can be identified using common engineering experience, for example the duct length, duct height, duct width, and bulk velocity. The sensitivity of the heat convection to several other parameters needs to be individually tested.

4.2.1 Sensitivity of ETAHE Heat Convection to Design Parameters

When air flows in a buried duct, the temperature difference between the air and the duct may cause surface temperature variations along the flow direction. The differences in surface depths also result in such variations along the vertical direction. To evaluate the effects of the surface temperature difference on heat convection, the sample ETAHE case in Section 3.4.7 is selected as a comparative reference, and another numerical case with a staircase change in the surface temperatures from the inlet to the outlet and from the ceiling to the floor was simulated. The difference between any two

adjacent surface elements is 0.25°C, which ensures an overall average surface temperature of 10°C. The resulted largest temperature difference among the surfaces is 4.5°C. Figure 4.1 shows the predicted area-weighted local average Nusselt numbers at the ceiling and the floor of the duct for the two cases. It indicates that the effects of the surface temperature variation on the convective heat transfer rate are negligible. Therefore, the isothermal surface condition of 10°C was used in all further studies, and the impact of weather was reflected by controlling the inlet air temperature.

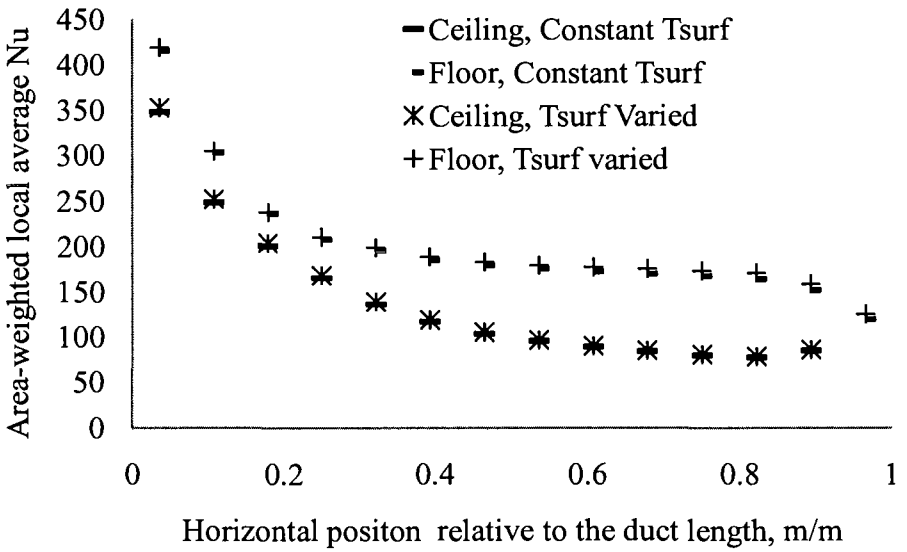

Figure 4.1: Effects of surface temperature distribution on the heat convection

It is inconvenient to quantitatively evaluate the difference between two cases based on their local Nusselt numbers. Therefore, it was decided to use the three average Nusselt numbers of the duct ceiling, wall, and floor, i.e. $Nu_{avg,c}$, $Nu_{avg,w}$, and $Nu_{avg,f}$, to represent the characteristics of the heat transfer process. The effects of another four parameters were evaluated based on a reference case: duct length L = 13.5 m, height H = 1.5 m, width W = 1.5 m, inlet width W_{in} = 1.5 m, bulk velocity U = 1.33 m/s, inlet air

temperature T_{in} = -10°C, inlet turbulent intensity I_{in} = 5%, inlet velocity vector $\vec{V}$ = (0, -1, 0), duct surface temperature T_{surf} = 10°C, outlet width W_{out} = 1 m. The selected parameters are inlet turbulence intensity I_{in}, outlet size W_{out}, inlet velocity vector $\vec{V}$, and inlet air temperature T_{in}. The cases were set up by changing one parameter at a time from the reference to an extreme value. The simulation results are listed in Table 4.1.

Table 4.1: The effect of four parameters on the surface heat convection

Evaluated factors, variation from reference case	*Ceiling Nu*		*Wall Nu*		*Floor Nu*	
	results	*variation*	*results*	*variation*	*results*	*variatio*
Reference case	*336*	*N/A*	*415*	*N/A*	*462*	*N/A*
I_{in}, from 5% to 20%	*335*	*-0.3%*	*415*	*0.1%*	*464*	*0.4%*
W_{out},, from 1 m to 0.5 m	*330*	*-1.8%*	*444*	*7.0%*	*461*	*-0.3%*
$\vec{V}$, from (0, -1 ,0) to (1, -1, 0)	*303*	*-9.9%*	*411*	*-0.9%*	*488*	*5.6%*
T_{in} from -10 to 30°C	*361*	*7.3%*	*368*	*-11.2%*	*338*	*-26.9%*

The turbulent intensity, I_{in}, and outlet width, W_{out}, as shown in Table 4.1 have marginal effects on the heat convection. When the inlet velocity vector, $\vec{V}$, was changed from normal to the opening (0, -1, 0) to 45° to the x axis (1, -1, 0), the airflow momentum in the x direction was increased even though the bulk velocity U remained the same. The 90° angle turn from the inlet tower to the horizontal duct causes the x-velocity component to accelerate at the lower level of the duct and decelerate at the upper level. Therefore, the $Nu_{avg,f}$ was increased, and $Nu_{avg,c}$ was decreased when compared to the reference case. This phenomenon may happen when the inlet tower is designed to take advantage of wind. In reality, the wind may come from different directions, and the extent of its effects may be moderated by opening size, orientation, inlet dumpers, filters, and inlet tower geometry, etc. Therefore, in the current research study, the inlet velocity

direction was not selected as an influential parameter when developing the later algorithm for predicting heat convection. According to Table 4.1, changing the inlet air temperature from -10°C to 30°C (i.e. ΔT was changed from 20°C to -20°C) resulted in significant changes in the simulated Nu numbers. Figure 4.2 gives a clear comparison between the two cases on their area-weighted local average Nu numbers. The only difference between the two cases is their inlet air temperatures, which represent winter heating and summer cooling conditions. The temperature differences between the surfaces and the air are the same for both cases. Therefore, the Nu number differences shown in Figure 4.2 are only attributed to the buoyancy effect. This indicates that the buoyancy force played an important role, which is normally expected in the mixed convection situation.

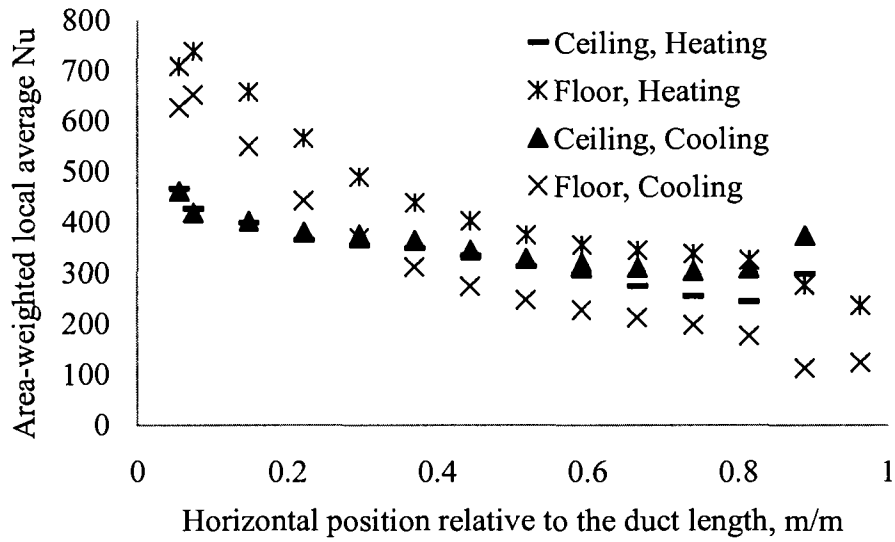

Figure 4.2: Effects of buoyancy force on the heat convection

Based on the sensitivity study, six influential design parameters are identified, and they are bulk velocity (U), duct geometry (L, H, W, and W_{in}), and temperature difference (ΔT) between duct surfaces and inlet air. In fact, since predicting local convective heat transfer rate is one of the major objectives of this research, the surface location relative to

the duct length is also one crucial parameter determining the heat transfer intensity. The initial plan was: to group these influential parameters into dimensionless numbers, such as Re_{D_h} and Gr_{D_h}, to use them as independent variables to derive correlations between the dimensionless groups and local Nu numbers. However, according to their definitions by Equations 4.1 and 5.3, a characteristic length of the heat convection problem has to be determined. This length should represent the thermal boundary layer developments not only along duct length direction (forced convection due to main flow) but also along the duct height direction (natural convection due to buoyancy effect). In addition, local values of Nu numbers are the great interest of this research. Therefore, the six physical influential parameters are chosen as the independent variables for the heat convection. Later sections will also address how to predict local Nu numbers.

$$Re_{D_h} = \frac{U \cdot D_h}{\nu} \tag{4.1}$$

$$Gr_{D_h} = \frac{g\beta\Delta T D_h^3}{\nu^2} \tag{4.2}$$

4.3 Development of an Artificial Neural Network Model for Predicting Discrete Area-weighted Local Average Nu Numbers

According to the complexity of a physical problem, methods for identifying the relation between its independent variables and dependent variables are different. In conventional convective heat transfer analysis, empirical correlations of Nu numbers are usually derived by fitting experimental results using regression analysis methods. One of the simplest methods is linear regression, which fits a straight line to a set of experimental values (Walpole 2007). More complex problems need multivariate non-linear regression analysis. The challenge of using regression analysis is that the form of

the mathematical function must be specified (Berthouex and Brown 2002). As addressed in Section 4.2.1, for the current problem, although the six influential parameters are identified, their impacts on the heat convection cannot be expressed as fixed forms of mathematical terms.

Artificial Neural Networks are known as an effective method for approximating nonlinear model functions and for finding relationships between the functions input and output pairs. As in nature, neural network functions are determined by the neural connections. By adjusting the values of the connections (weights) between neurons based on given pairs of inputs and outputs, an Artificial Neural Network model can be trained. Trained neural networks work as mathematical functions to approximate outputs of other input sets, and their performance is dependent on the network structures and the training processes. Successful applications have been reported to use ANNs to predict convective heat transfer coefficients (Scalabrin and Piazza 2003 and Scalabrin et al. 2003) and indoor thermal comfort (Zhou and Haghighat 2007). Since the relation between the ETAHE design parameters and local Nu numbers are highly non-linear, the ANN method is believed to be an efficient way to find the relation. The first step of developing an ANN model is to prepare a case data base for training.

4.3.1 Preparation of ANN Training Cases Using Numerical Experiments

Proper training can enable an ANN to provide fast and accurate approximation for a system and for a given range of variables. Proper training means that a sufficient number of cases should be used, and the influential parameters in these cases should be well distributed to cover a reasonable range for each of the parameters. Table 4.2 lists the parameters studied as well as their lower and upper bounds. An ANN model should be

trained for a given search space, and it requires a limited number of sample cases to represent the whole search space. To this end, a Latin Hypercube Sampling (LHS) method was adopted to prepare the design of the numerical experiments. LHS is known as a proper method to generate a reasonable distribution for a group of parameter values. It generates random samples which are ensured to be relatively uniformly distributed over each dimension (Mathworks 2005). Using this method, thirty numerical experiment design cases of ETAHEs were generated. Before planning for this method, the author had also conducted 52 simulation cases based on a fractional factorial design of the six parameters. Therefore, eighty two cases in total are used for ANN training and verification purposes, and their setups are listed in Appendix A.

Table 4.2: Design parameters and their lower and upper bounds

	ΔT	U	L	H	W	W_{in}
max	*39.5*	*4.7*	*41*	*3*	*3*	*3*
min	*-45.8*	*0.5*	*10*	*0.2*	*0.2*	*0.2*

4.3.2 ANN Structure

As seen in Figure 3.13, to properly track the heat convection variation along the duct length, the horizontal portion of the ETAHE is divided into multiple surfaces with one meter distance in the x direction. Therefore, the number of area-weighted average Nu numbers from CFD simulations is dependent on the duct length. For example, the simulation results for a 40-meter ETAHE would include one Nu number from its inlet end wall, one from its inlet tower base wall, one from its inlet tower base floor, one from its outlet end wall, 40 from its side wall, 40 from its floor, and 39 from its ceiling. The names, such as inlet end wall, are referred in Figure 3.13. To build an ANN model, the number of its outputs from the training cases has to be the same. Therefore, to train

ANNs using the simulation results, a post-processing treatment for changing CFD results to a fixed number of Nu numbers was performed. Firstly, the Nu numbers were categorized to four groups: ceiling, side wall, floor and four individual surfaces (inlet end wall, inlet tower base wall, inlet tower base floor, and outlet end wall). For each ceiling, side wall, and floor group, the multiple Nu numbers and their corresponding normalized position (x/L) relative to duct lengths were fitted to a polynomial curve. After that, ten Nusselt numbers corresponding to x/L = 0.1, 0.2 ... and 1.0 were obtained from each curve. Therefore, four Artificial Neural Network models were constructed for the four groups. Each of the three ANN models (for ceiling, floor, and wall) has 10 outputs; and the fourth network (for the four discrete surfaces) has four outputs. All the four networks are made of three layers, and they all have one hidden layer with 40 nodes. A sample of the network structures for the duct ceiling is shown in Figure 4.3.

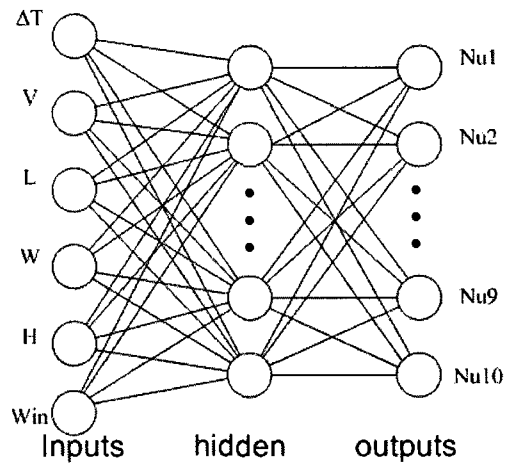

Figure 4.3: The structure of the neural network for ETAHE ceiling

4.3.3 ANN Training and Results

In the present study, the networks were trained using a kind of backpropagation training algorithm, Resilient Backpropagation, implemented in Matlab 7.1 (Mathworks

2005). After the training, another group of CFD simulation results with different setups than the training cases were used for verification of the ANN model. The output results from ANN against the target results from CFD simulation are plotted in Figure 4.4. It can be seen that the ANN model predicted very accurate results when compared to the CFD simulations.

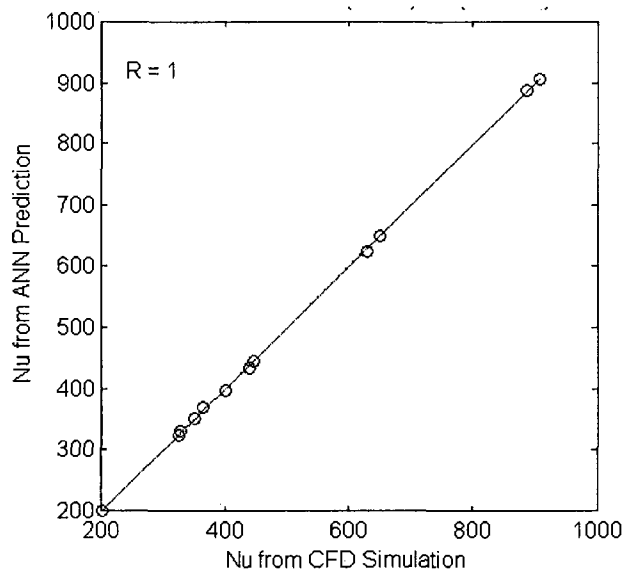

Figure 4.4 Comparison of Nusselt numbers from ANN prediction with CFD simulations

4.4 Development of an ANN-based Heat Convection Algorithm

The areas of the four individual surfaces (inlet end wall, inlet tower base wall, inlet tower base floor, and outlet end wall) are relatively small comparing to the total duct surface area, it is reasonable to assign one area-weighted average Nu number to each of them using the fourth ANN model. The other three ANN models can be used as mathematical functions in a form like Equation 5.3. When a set of six design parameters are provided, 10 Nu numbers can be calculated from each of the three ANN models. Although these discrete Nu numbers provide a profile of the heat convection variation,

the local heat convection information is still limited. For example, if an ETAHE is 40-meter long, the three ANN models can only provide one area-weighted local Nu number for every 4-meter duct portion. It is favored to have an algorithm to provide continuous local Nu numbers as a function of the surface location, especially along the airflow direction. In addition, this algorithm should be able to take two time-dependent parameters, ΔT and U, as independent variables. A proper heat convection algorithm should be able to predict transient and local Nu numbers on the duct surface. With these features, thermal modeling of ETAHEs will be able to obtain correct heat convection boundary conditions on duct surfaces, and the ETAHEs' performance would be properly predicted. To this end, an ANN-based Heat Convection (ANN-HC) algorithm is developed, and its work flow cart is shown in Figure 4.5.

$$Nu|_{\frac{x}{L}=0.1,0.2,\ldots 1.0} = f(\Delta T, U, L, H, W, W_{in}) \qquad 4.3$$

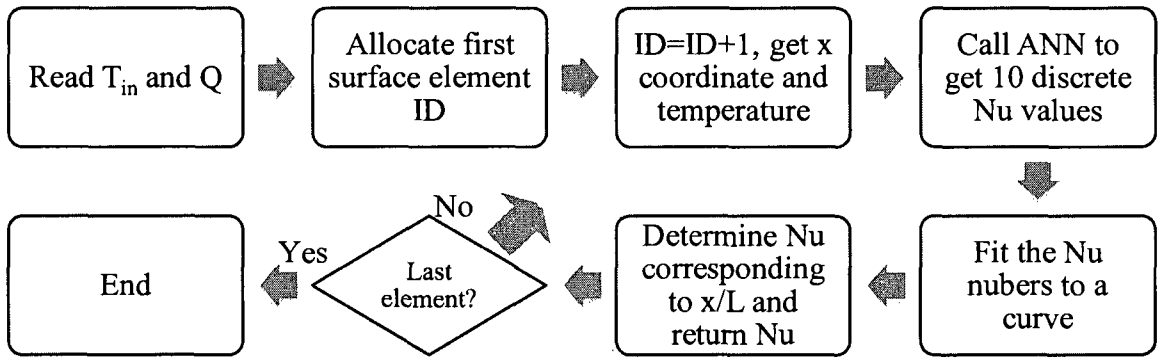

Figure 4.5: Flow chart of the ANN-based Heat Convection (ANN-HC) algorithm

Imagine a thermal simulation for an ETAHE is in process, and it is waiting for convective heat transfer boundary conditions on the ETAHE surfaces. The thermal simulation model contains information, such as ETAHE configurations, inlet air temperatures, and airflow rates. As addressed before, heat convection in large cross-

sectional area ETAHEs is not uniform. The Nu numbers should be a function of the surface location and the six design parameters. The developed ANN-HC algorithm is programmed for this purpose. It is coupled with the thermal simulation program. It gets the coordinates and the surface temperature of a specific surface element. At this point, all six parameters are known, so the trained three neural networks can be called to predict ten discrete Nu numbers on each ceiling, duct wall, and floor. A polynomial curve fitting function is called using a least square curve fitting method to graphically fit the ten Nu numbers with their corresponding x/L locations (0.1, 0.2, ... 1.0) to a curve. Then, the algorithm can determine the local Nu numbers corresponding to the specific surface element coordinates, and it can return the Nu numbers to the thermal simulation model. The same procedure is then continued to the next surface element until the last element is assigned a local Nu number. This ANN-based Heat Convection Algorithm is implemented as a Fluent User Defined Function using C Language programming (see Appendix B), and its function will be demonstrated in the next chapter.

Chapter 5 Development of a Thermal Simulation Model for ETAHEs

5.1 Introduction

This thesis' literature review of the existing ETAHE simulation models has shown that they cannot simulate the performance of large cross-sectional area ETAHEs because their assumptions concerning heat convection in ETAHE ducts are inappropriate. With the ANN-based Heat Convection Algorithm developed in Section 4.4, a new thermal simulation model is proposed in this chapter.

5.2 Model Description

Heat transfer in the ground surrounding ETAHEs is a three-dimensional and mainly conduction process. In order to simplify the problem, the heat flow due to moisture transfer is not simulated in this model. Its effects can be taken into consideration by using effective properties of the ground. The governing equation for three-dimensional heat conduction in the ground is given by Equation 5.3. When an ETAHE is designed as shown in Figure 5.1, the ground surrounding the ETAHE is defined as the simulation domain, and this domain should be divided into many control volumes.

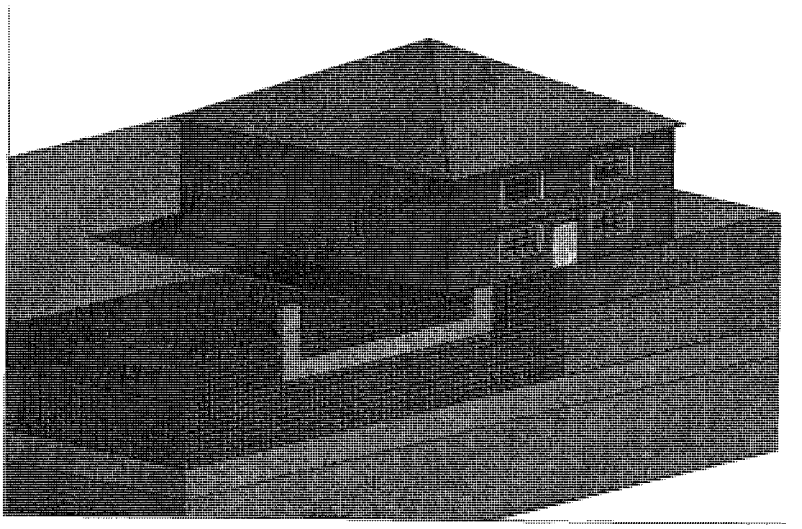

Figure 5.1: An example of an ETAHE design

$$\frac{\partial}{\partial x}(\rho_s c_{p,s} T) = \frac{\partial}{\partial x}\left(k_s \frac{\partial T}{\partial x}\right) + \frac{\partial}{\partial y}\left(k_s \frac{\partial T}{\partial y}\right) + \frac{\partial}{\partial z}\left(k_s \frac{\partial T}{\partial z}\right) \quad 5.1$$

5.3 Boundary Conditions

As shown in Figure 5.1, the simulation domain in the current model includes a large volume of ground from the ground surface to the water table or to deep ground boundary depth. When the duct is partially under building construction, indoor temperature can be used as the boundary condition. At the lower boundary where the underground water table is met, the water temperature can be used as the boundary conditions. At vertical boundaries far away from the ETAHE, adiabatic surface conditions can be assumed. A study conducted by the IEA BESTEST (Neymark and Judkoff 2008) on ground coupled heat transfer related to slab-on-grade construction showed that the deep ground boundary depth and far field distance (heat flux negligible) can be taken at 20 meters with an accuracy of 0.16% and at 10 meters with an accuracy of 2.34%.

As addressed in Section 2.4, heat transfer at the duct surfaces takes place through heat convection, inter-surface long-wave radiation, and latent heat exchange due to condensation or evaporation. The largest surface temperature difference among the duct surface is in a magnitude of 5°C and the coolest and warmest surface locations are usually at the two ends of the duct. Therefore, the heat transfer due to radiation is small comparing to the convection, and it is neglected in the current model. The impact of latent heat exchange has also been analyzed in Section 2.4, and heat convection is concluded as the focus of this research. Therefore, the boundary conditions at the duct surfaces can be obtained by coupling this thermal model with the ANN-based Heat Convection Algorithm. When a local Nu number, Nu_x, is obtained for a surface element

i, the convective heat transfer rate, $\dot{q}_{element}$, can be calculated using Equation 5.2. As such, the ETAHE's outlet air temperature can be calculated using Equation 5.3. Meanwhile, the ETAHE's energy efficiency, i.e. total heat transfer rate, can be predicted as $\sum \dot{q}_{element}$.

$$\dot{q}_{element} = A_{element} \frac{\mathrm{k}}{D_h} Nu_x (T_{surf} - T_{in}) \tag{5.2}$$

$$T_{out} = T_{in} + \frac{\sum \dot{q}_{element}}{c_{p,air} \cdot \dot{\mathrm{m}}} \tag{5.3}$$

For most locations, ground surface temperature data are not available. In such case, a sol-air temperature can be used as a convective heat transfer boundary condition using Equation 5.4. It is defined as the outdoor air temperature that in the absence of all radiation changes gives the same rate of heat entry into the surface as would the combination of incident solar radiation, radiant energy exchange with the sky and other outdoor surroundings, and convective heat exchange with outdoor air. Therefore the rate of heat transfer at the ground surface can be expressed as Equation 5.5.

$$T_e = T_{air} + \frac{\alpha \cdot I_t}{h_0} - \frac{\varepsilon \cdot \Delta R}{h_0} \tag{5.4}$$

$$q'' = h_0 (T_e - T_{surf}) \tag{5.5}$$

Where

q'' is the heat flux, $\mathrm{W/m^2}$

h_0 is the coefficient of heat transfer by long-wave radiation and convection, $\mathrm{W/(m^2 \cdot °C)}$

T_e is the sol-air temperature, °C

T_{surf} is the surface temperature, °C

T_{air} is the air temperature, °C

α is the surface absorptance for solar radiation

I_t is the total solar radiation incident on a surface, W/m^2

ε is the hemispherical emittance of surface, and

ΔR is the difference between long-wave radiation incident on surface from sky and surroundings and radiation emitted by blackbody at outdoor air temperature, W/m^2.

5.4 Thermal Simulation of ETAHEs Using the New Model

The simulation procedure of an ETAHE can be divided into several steps as shown in Figure 5.2. A case study is used to illustrate the procedure in the next section.

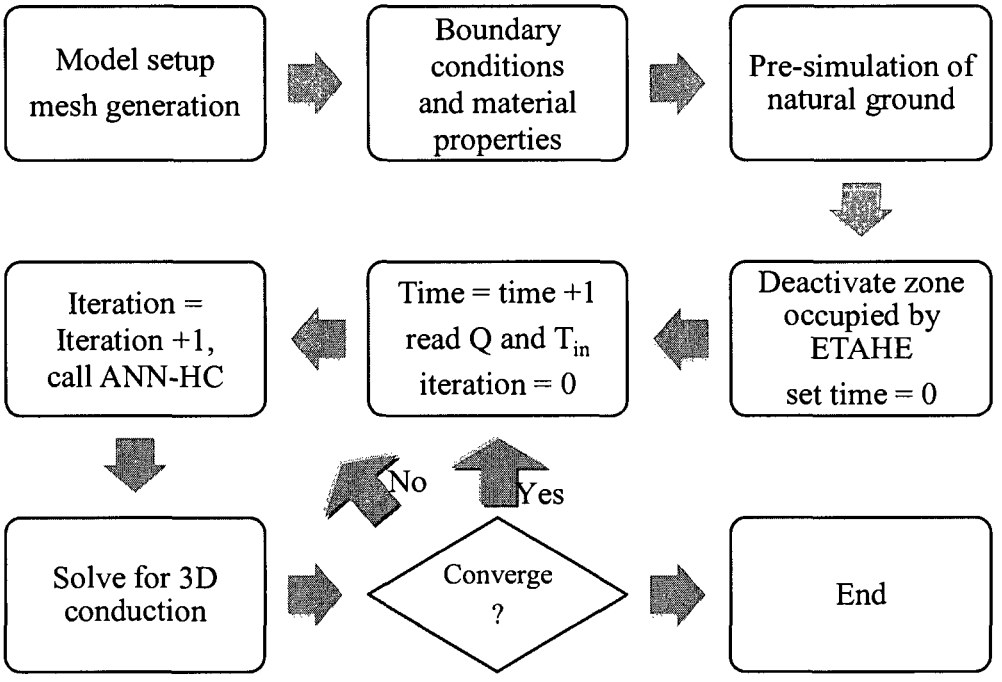

Figure 5.2: Flow chart of the new thermal simulation model of ETAHEs

5.5 Demonstration of the Thermal Simulation Model Using a Case Study

5.5.1 System Description

It is assumed that an ETAHE will be constructed in Ottawa, Ontario, Canada, and its operation will start on June 15. The ETAHE is designed to have a length of 15 m,

width of 1.5 m, height of 2.0 m, depth of 2.0 m, and an inlet width of 1.0 m. The hourly ambient air temperature variation throughout one year is plotted in Figure 5.3. The airflow through the ETAHE is controlled as an on/off operation mode. From 7AM to 7PM the airflow rate is 1.8 m^3/s, and its ventilation is shut off for the rest of the time (see Figure 5.4).

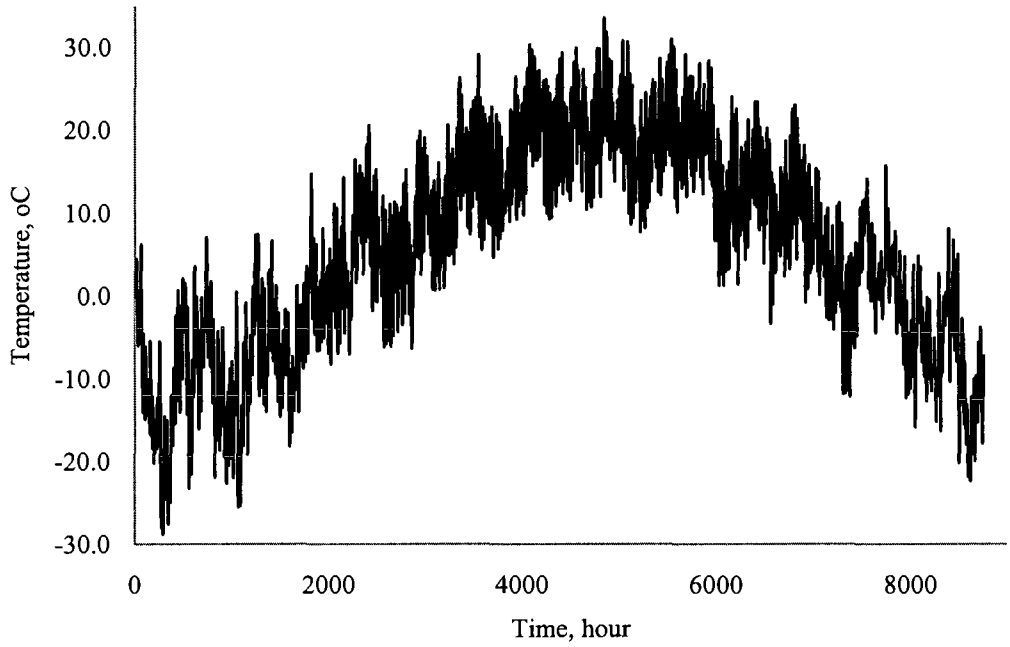

Figure 5.3: Hourly ambient air temperature variation of Ottawa, Canada (exported from TRNSYS program's weather data) (2007)

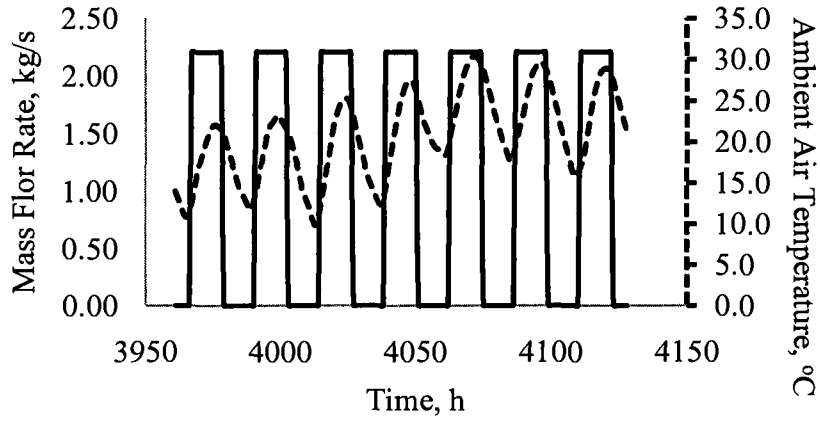

Figure 5.4: Ventilation rate and ambient air temperature from June 15 to June 21

Table 5.1: Soil properties

Property	***Unit***	***Value***
Density	*kg/m3*	*500*
Specific heat capacity	*j/kg-k*	*2160*
Thermal conductivity	*w/m-k*	*1.6*

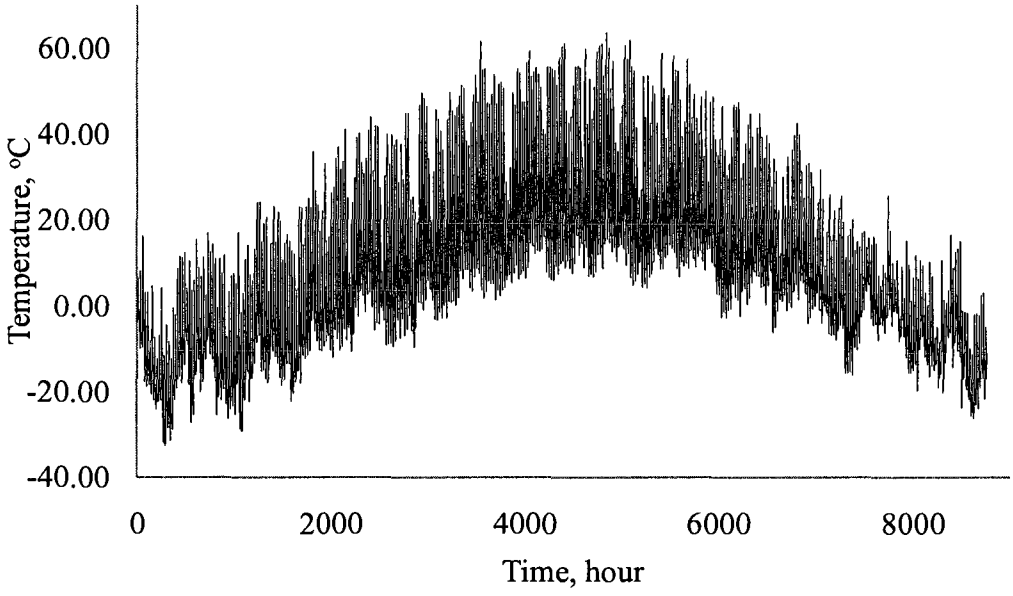

Figure 5.5: Sol-air temperature over one year in Ottawa

5.5.2 Model Setup and Mesh Generation

As shown in Figure 5.2, the first step is to select the calculation domain and generate the mesh. The geometry of the ETAHE is given, and a distance of 10 m from the duct surface is assumed to be the far field where the ground temperatures are not affected by the operation of the ETAHE. At this step, the ETAHE zone is occupied by soil as if the ETAHE has not been constructed. The mesh was generated using commercial

software "Gambit" with hexahedral elements. The grids near the duct surfaces and ground surface were chosen to be as small as 0.05 m and the size proportionally grows as the distance from the surfaces increases. The total number of mesh volumes was 92088.

5.5.3 Defining Boundary Conditions and Material Properties

The sol-air temperature (see Figure 5.5) and coefficient of heat transfer by long-wave radiation and convection $h_0 = 17\,\mathrm{W/(m^2 \cdot °C)}$ is used (ASHRAE 2005). At the lower boundary of the ground domain, an adiabatic condition and undisturbed ground temperature condition were both tested. The simulated temperature profiles in the ground from the two boundary conditions are almost the same; therefore the adiabatic condition was used. The model can assign the ground with different composition and different properties. Since the detailed information is known, dry soil property was used for the entire ground domain as listed in Table 5.1. Soil properties are highly dependent on its composition, moisture contents, location, etc. The values in Table 5.1 are just used for demonstration of the model.

5.5.4 Preparation of Initial Conditions for ETAHE Thermal Simulation

Heat transfer in the ground is a dynamic and transient process. In order to obtain a realistic initial conditions for ETAHE simulation, the natural ground was pre-simulated for more than three years until June 14th midnight. At this step, the soil zone, which is supposed to be occupied by the ETAHE, is removed from the simulation domain. The duct surfaces are assigned with new boundary conditions by coupling the simulation program with the ANN-based Heat Convection algorithm. Appendix B only provides a sample of the ANN-HC algorithm code for the duct ceiling.

5.5.5 Solving Process

From the simulation time of June 15th, ground temperature starts being affected by the operation of the ETAHE. From 1AM to 6AM, since airflow rate through the ETAHE is zero, all duct surfaces are assigned with a Nu number of zero by the ANN-HC algorithm. From 7AM, the ANN-HC algorithm for duct ceiling, side wall, and floor is called to provide local Nu numbers for each finite surface element. For instance, on the duct ceiling, a surface element i with x coordinate of x_i is waiting for a Nu number. The temperature difference between i and the inlet air, bulk velocity, and the duct configuration (length, height, width, and inlet width) provides a set of six inputs to the ANN-HC algorithm. The ANN produces 10 Nu numbers as shown in Figure 5.6. In the ANN-HC algorithm, a function is then called to fit the Nu numbers and their corresponding x/L to a curve. After that, the coordinate x_i can help to precisely locate a Nu number, and the algorithm returns it to the thermal simulation. The thermal simulation model would solve the 3D heat conduction equation at this time step. If the solution satisfies the convergence criteria, the simulation moves to the next time step. If not, more iteration is called and the ANN-HC algorithm will be called again in order to ensure that accurate local convective heat flux is calculated based on the transient duct surface temperature conditions.

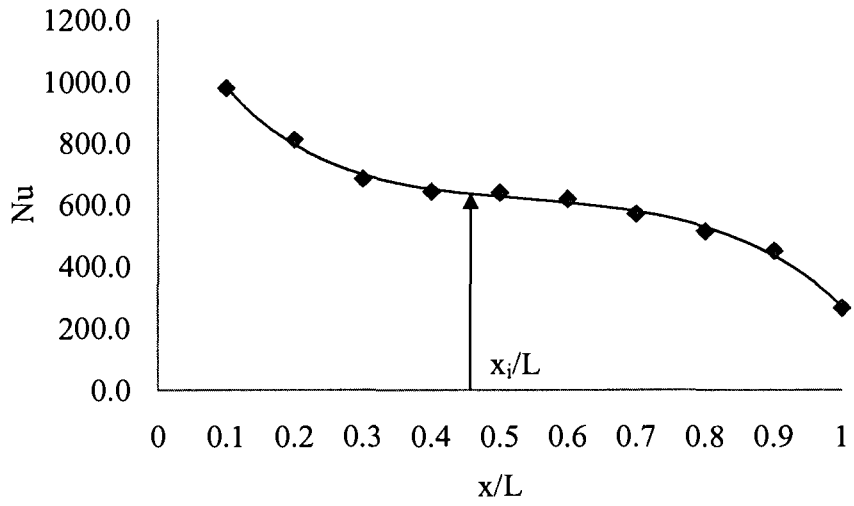

Figure 5.6: Demonstration of the coupling process between the thermal simulation model and the ANN-based Heat Convection Algorithm

5.5.6 Simulation Results

In order to demonstrate the difference between the new ETAHE thermal model and the existing models, an empirical heat convection correlation from ASHRAE is also used to provide heat convection boundary conditions to the same problem in another simulation. The results from the two simulations are compared in Figure 5.7 to Figure 5.9. Figure 5.7 shows the predicted outlet air temperatures from the two methods in comparison with the inlet air temperatures. It is noted that the maximum temperature reduction of 4.2°C is predicted using the ANN-HC algorithm. The maximum temperature reduction from the simulation using the ASHRAE correlation is 2.9°C. The difference is more significant when the total heat transfer from the two simulations is plotted. Figure 5.8 shows that when the empirical correlation for fully developed turbulent flow is used in thermal simulation, the system energy performance is significantly underestimated. Figure 5.9 shows the difference of the simulated ground temperature along the duct

middle plane from the two simulations. Since the ASHRAE correlation can only give one Nu number to all the surfaces of the ETAHE duct, the simulated ground temperature is symmetric between the inlet and the outlet. This is not realistic because in the summer the warm air should transfer more heat to the inlet side of the duct than the outlet side. Nevertheless, the new thermal model with the ANN-based Heat Convection algorithm provides accurate local Nu numbers during the calculation. It is dynamically calculated based on the flow condition and temperature difference between the air and the local surface element. Due to the initial momentum of the airflow, the warmer air flushes the duct floor near the inlet, therefore, it can be seen that that part of the ground has warmer temperatures than other locations. Since the warmer air tends to stay on the upper zone of the duct and the cooled air is drawn to the ground, the temperature differences between the air and wall are larger near the ceiling than the floor. Therefore, on the outlet side of the duct, the temperature of the ceiling is significantly warmer than that of the floor.

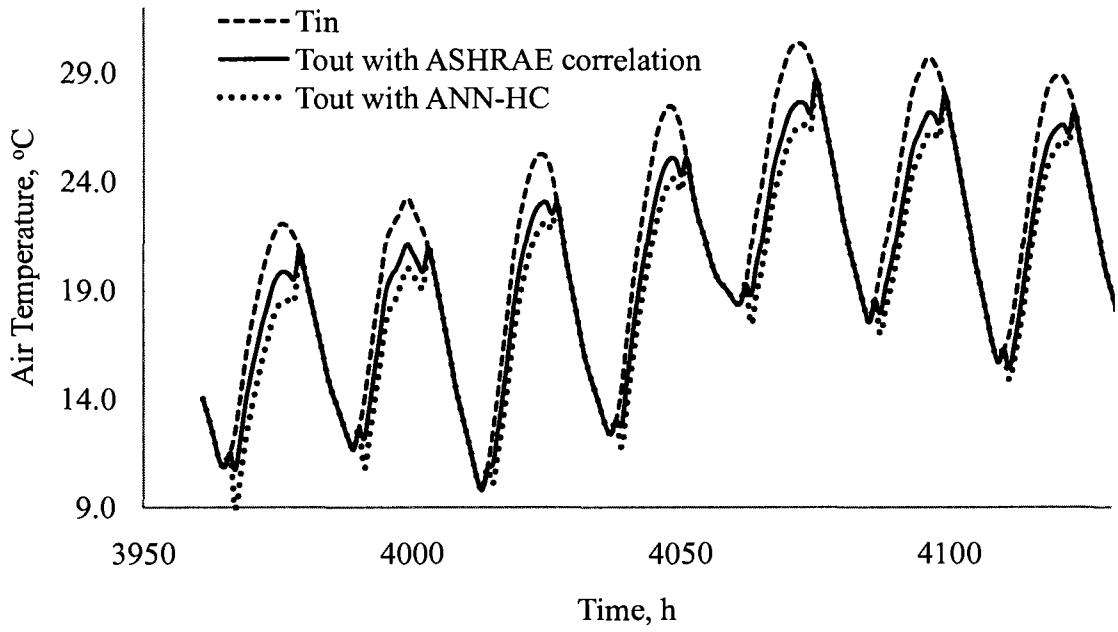

Figure 5.7: Comparison of predicted outlet air temperatures by ANN-HC and ASHRAE

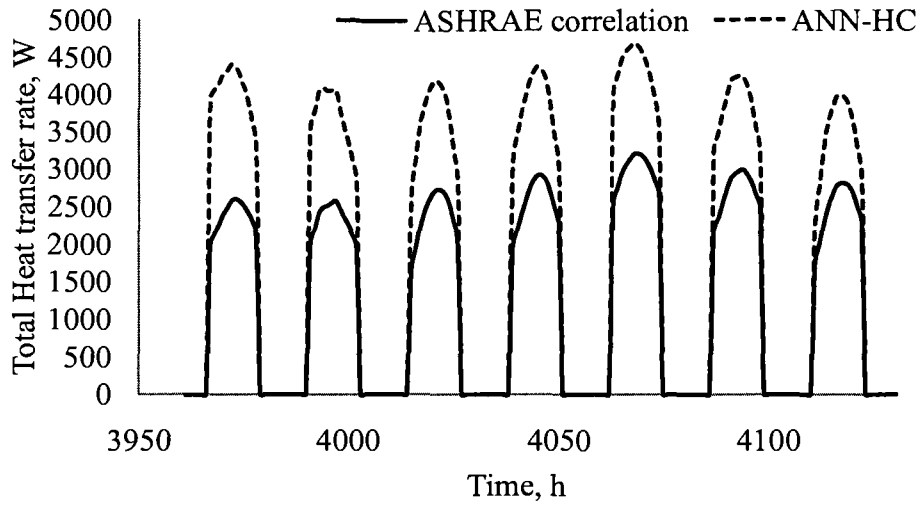

Figure 5.8: Comparison of predicted ETAHE efficiency from the ANN-HC algorithm and ASHRAE correlation

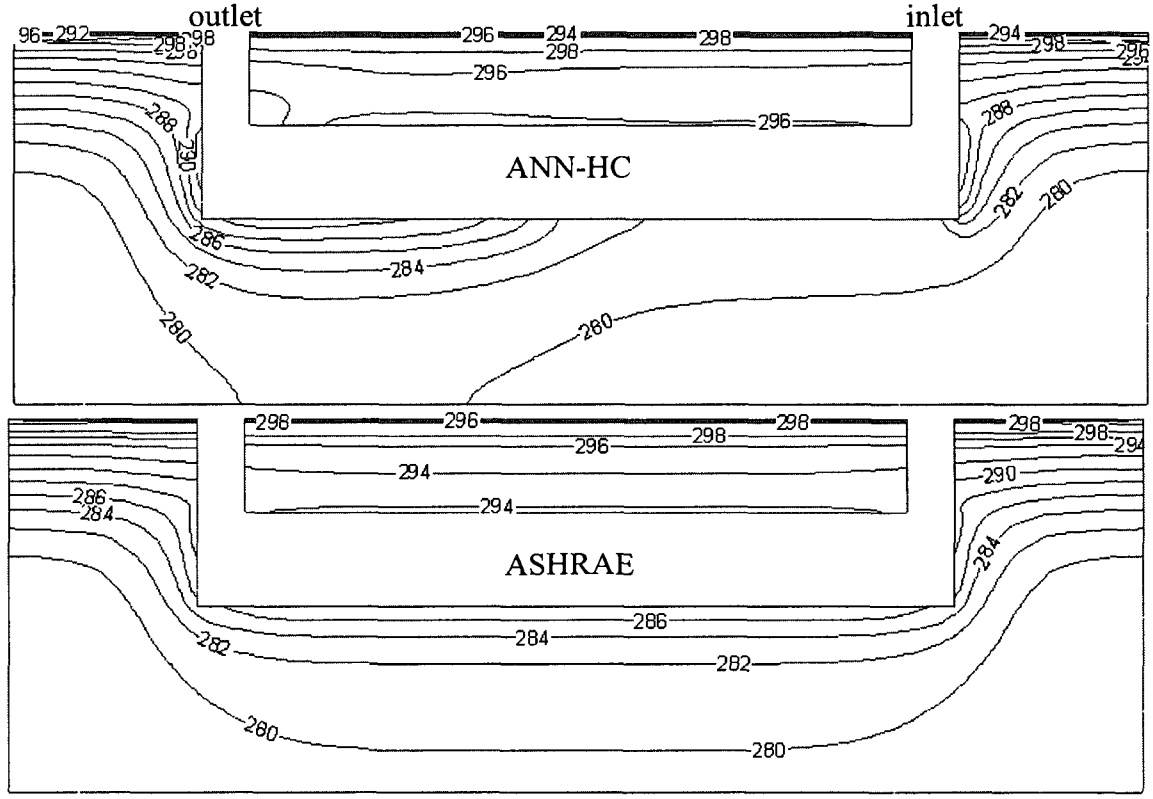

Figure 5.9: Comparison of the predicted ground temperature distribution from ANN-HC algorithm (upper) and ASHRAE correlation (lower)

Chapter 6 Conclusions and Suggestions for Future Work

6.1 Summary of Findings

The state-of-the art review has shown that an ETAHE is an Environmentally Responsive Element, which actively uses ground thermal storage to save energy for conditioning ventilation air. ETAHEs can be used in various types of buildings and wide range of climate conditions. Many hybrid ventilation buildings have integrated ETAHEs as a free pre-cooling and/or preheating component. Although successful applications have demonstrated the benefits of this integration, current design practice is lacking reliable analytical tools and simulation models to promote it. Especially, the large cross-sectional area ETAHE's performance is significantly dependent on its interactions with its environment, such as the status of ground thermal storage capacity, outdoor air temperature variations, ventilation requirements, and the source of the airflow driving forces. A proper ETAHE design relies on the designers' understanding of all those interactions, and that determines the control strategy. Computer simulation tools are regarded as the most convenient way to analyze and predict the performance of ETAHEs. Although many simulation studies have shown success when predicting conventional ETAHEs in mechanical ventilation systems, they were found to be not applicable to large cross-sectional area ETAHEs. The reason is that their assumptions concerning heat convection in convectional systems are not valid in the large cross-sectional area ETAHEs, and this non-applicability was proven by the measurement results from the field investigation of the Mediå School's ETAHE. The preliminary CFD simulation for that ETAHE provided more evidence for the incapability of the existing models. The investigations clearly indicated that heat convection in the ETAHE was complicated due

to the non-uniform surface temperature distribution, entrance effect, and buoyancy effects. It is shown that the intensity of the heat convection in the ETAHE was much higher than that predicted by empirical correlations, which are only suitable for fully developed flow heat convection in pipes. Lessons learnt from the field investigation are the following:

- Performing detailed airflow and heat transfer measurements for the quantification of interior surface heat convection requires a large number of simultaneous monitoring data for surface temperatures, air temperatures, and airflow rates, and from these one can only obtain overall average convective heat transfer rates.
- It was difficult to quantify the airflow rate in the system without making some temporary modifications to the system.
- Only results under quasi-steady states could be obtained.

The preliminary CFD simulation for the Mediå School ETAHE showed that CFD is a very promising tool for analysis of the heat convection in ETAHEs. Therefore, the model was further improved using a Two-Layer turbulence model, which can provide satisfactory flow information in the viscous affected near-wall region without significantly increasing the computational cost. Based on the mesh independence tests, proper mesh generation criteria were established.

Using the CFD model as a numerical experimental tool, the sensitivity analysis of five design parameters was conducted. The six parameters, i.e. temperature differences between duct surfaces and inlet air, bulk velocity, duct length, height, width, and inlet width, were identified as the influential parameters determining the intensity and distribution of local convective heat transfer in ETAHEs. Since the objective was to seek

prediction methods for local convective heat transfer, dimensionless group numbers, such as Re, Ra, and Gr, were not selected to develop conventional form of heat convection correlations. It is believed that they are unable to capture the local heat convection information for three reasons:

1. The natural convection acts on the vertical direction while the forced convection acts on the horizontal direction,

2. It is difficult to find a mutual characteristic length that can represent the boundary layer developments of both natural and forced convection.

3. It is difficult to correlate the dimensionless groups to predict local convective heat transfer, which is considered as necessary boundary condition for accurate thermal modeling for heat transfer in the ground.

Therefore an Artificial Neural Network method was adapted to establish mathematical relationships between the design parameters and area-weighted local average Nusselt numbers. The trained ANN models were found to be able to predict accurate area-weighted local average Nusselt numbers when compared to those results from CFD simulations. Based on these ANNs, and ANN-based Heat Convection algorithm was developed to supply dynamic and local Nusselt numbers when it is coupled thermal simulation model.

6.2 Research Contributions

- The state-of-the-art review of ETAHEs was documented as a guide for designers, building owners, and researchers who are interested in using ETAHEs for indoor space conditioning. It is going to be accessible to the design, industry and research communities through the IEA-ECBCS Annex 44 project.

- The field measurements at the Mediå School were the first detailed field investigation on a large cross-sectional area ETAHE. It showed that heat convection in ETAHEs is significantly dominated by entrance and buoyancy effects. The results proved that the empirical correlation of fully developed turbulent flow may significantly underestimate heat convection, and simulation models using such correlations are not suitable for large cross-sectional area ETAHEs.
- The CFD modeling method using the Two-Layer turbulence model was identified as an appropriate technique to analyze local convective heat transfer in ETAHEs. In the future, this method and its corresponding mesh generation criteria can be used in other heat convection analysis problems, especially in large enclosures and indoor spaces.
- The ANN-based Heat Convection algorithm was developed to provide local Nu numbers as boundary conditions to the coupled thermal simulation model. It stands out against other correlations in four ways:
    1. It can provide local Nu numbers while most correlations can only provide an average value for overall surfaces.
    2. It gives dynamic Nu numbers which are not only a function of the flow regime but also a function of the surface temperature. This feature is particularly important when the flow is highly affected by buoyancy force.
    3. It can be coupled with the thermal model, which needs dynamic boundary conditions for its iterative solving technique.

4. The capacity of the algorithm is expandable to wider ranges of the design parameters by extending the training database.

- The conventional way of developing convective heat transfer correlations is to conduct experiments and to correlate the flow condition and the average rate of convection over surfaces. This thesis developed an alternative methodology, which is to use numerical experiments, i.e. CFD, to replace laboratory experiments, and to use Artificial Neural Networks to generalize the highly non-linear relation between the physical design variables and the local convective heat transfer coefficients. This method can be used to develop correlations for many other heat convection problems.
- Using the ANN-HC algorithm, a new thermal model of ETAHEs was developed. It can be used as a design and analysis tool to predict the performance of ETAHEs. The interaction between the ETAHEs and its environment is better simulated than other existing models. It will be very helpful for optimal system design and determination of proper control strategies.

6.3 Recommendations for Future Work

Using the new thermal model of ETAHEs, the calculation for sensible heat exchange between the ventilation air and the ETAHE surface is shown to be more accurate than other existing models. However, latent heat exchange and long-wave radiation heat transfer at the duct surfaces were not included in the model development since they were not the focus of the current research. It is recommended to include those functions in the future so that the model will represent more realistic process.

The CFD cases used for the ANN training covered finite ranges of the design variables. The lower bound of the bulk velocity range was selected to be around 0.5 m/s. Because of the nature of the ANN method, the ANN-HC algorithm cannot predict heat convection in ETAHEs with lower velocity. To solve this issue, more CFD simulation cases are suggested for the ANN training. However, the limitation of CFD simulations for the natural convection dominated mixed convection problem should be overcome first. Difficulties for getting simulation convergence were incurred during the research when low airflow rate cases were simulated.

The developed thermal model of ETAHE simplifies heat transfer in the ground as a transient three-dimensional heat conduction process. To improve the accuracy of the model, one may include moisture transfer in the simulation model in the future.

LIST OF REFERENCES

Al-Ajmi, F., Loveday, D.L., and Hanby, V.I. (2006). The Cooling Potential of Earth-Air Heat Exchangers for Domestic Buildings in a Desert Climate. Building and Environment, 41(3), 235-244.

Arzano, L., and Goswami, D.Y. (1996). Performance Analysis of a Closed Loop Underground Air Tunnel for Residential Housing in a Hot and Humid Climate.

ASHRAE. (2005). ASHRAE Handbook of Fundamentals, Atlanta, GA.

Athienitis, A.K., Roy, M., and Zhao, M. (2005). Design and Simulation of a Hybrid Ventilation System with Earth-Air Heat Exchanger. Ninth International IBPSA Conference, Building Simulation 2005, Montreal, Canada, 1, 27-32, Aug. 15-18, 2005.

Awbi, H.B. (1998). Calculation of Convective Heat Transfer Coefficients of Room Surfaces for Natural Convection. Energy and Buildings, 28(2), 219-227.

Bahadori, M.C. (1978). Passive Cooling Systems in Iranian Architecture. Scientific American, 238(2), 144-154.

Bansal, N.K., Sodha, M.S., and Bharadwaj, S.S. (1983). Performance of Earth Air Tunnels. International Journal of Energy Research, 7(4), 333-345.

Beisel, S. (1999). Vermessung, Modellierung Und Bewertung Des Erdreichwärmeübertragers Beim Passiv-Solarhaus Cölbe, PhD Thesis, Philipps-Universität Marburg, Marburg.

Benkert, S., and Heidt, F.D. (1998). Designing Earth Heat Exchangers with GAEA. Proceedings EuroSun '98, Volume IV, IV.2.2-1...7, Sept. 14th-17th, 1998.

Benkert, S., Heidt, F.D., and Scholer, D. (1997). Calculation Tool for Earth Heat Exchangers Gaea. Proceeding of Building Simulation, Fifth International IBPSA Conference, Prague, Vol. 2, PP 9-16, Sep. 8-10.

Berthouex, P.M., and Brown, L.C. (2002). Statistics for Environmental Engineers, Lewis Publishers, Boca Raton.

Boelter, L.M.K., Young, G., and Iversen, H.W. (1948). An Investigation of Aircraft Heaters Xxvii: Distribution of Heat-Transfer Rate in the Entrance Section of a Circular Tube. Report Number: NACA-TN-1451.

Bojic, M., Papadakis, G., and Kyritsis, S. (1999). Energy from a Two-Pipe, Earth-to-Air Heat Exchanger. Energy (Oxford), 24(6), 519-523.

Bojic, M., Trifunovic, N., Papadakis, G., and Kyritsis, S. (1997). Numerical Simulation, Technical and Economic Evaluation of Air-to-Earth Heat Exchanger Coupled to a Building. Energy, 22(12), 1151-1158.

Burmeister, L.C. (1993). Convective Heat Transfer, John Wiley and Sons, INC.

Burton, S. (2004). Coolhouse Final Technical Report. Energie Demonstration Project NNE5 –1999 -193 FaberMaunsell Ltd, London.

Chen, H.C., and Patel, V.C. (1988). Near-Wall Turbulence Models for Complex Flows Including Separation. AIAA Journal, 26(6), 641-648.

Craft, T.J., Gant, S.E., Gerasimov, A.V., Iacovides, H., and Launder, B.E. (2006). Development and Application of Wall-Function Treatments for Turbulent Forced and Mixed Convection Flows. Fluid Dynamics Research, 38(2-3), 127-144.

Craft, T.J., Gant, S.E., Rides, H.L., and Launder, B.E. (2004). A New Wall Function Strategy for Complex Turbulent Flows. Numerical Heat Transfer: Part B – Fundamentals.

De Paepe, M., and Janssens, A. (2003). Thermo-Hydraulic Design of Earth-Air Heat Exchangers. Energy and Buildings, 35(4), 389-397.

Deissler, R.G. (1953). Analysis of Turbulent Heat Transfer and Flow in the Entrance Regions of Smooth Passages. NACA TN 3016.

Fink, C., Blümel, E., Kouba, R., and Heimrath, R. (2002). Passive Kühlkonzepte Für Büro- Und Verwaltungsgebäude Mittels Luft- Bzw. Wasserdurchströmten Erdreichwärmetauschern (Passive Cooling Concepts for Office and Administrative Buildings Using Earth-to-Air and Earth-to-Fluid Heat Exchangers).

Fisher, D.E. (1995). An Experimental Investigation of Mixed Convection Heat Transfer in a Rectangular Enclosure. Ph.D. Thesis, University of Illinois, USA.

Fluent-Inc. (2003). Fluent 6.1 User'S Guide.

Ghosal, M.K., Tiwari, G.N., and Srivastava, N.S.L. (2004). Thermal Modeling of a Greenhouse with an Integrated Earth to Air Heat Exchanger: An Experimental Validation. Energy and Buildings, 36(3), 219-227.

Goswami, D.Y., and Dhaliwal, A.S. (1985). Heat Transfer Analysis in Environmental Control Using an Underground Air Tunnel. Journal of Solar Energy Engineering, Transactions of the ASME, 107(2), 141-145.

Goswami, D.Y., and Ileslamlou, S. (1990). Performance Analysis of a Closed-Loop Climate Control System Using Underground Air Tunnel. Journal of Solar Energy Engineering, Transactions of the ASME, 112(May), 76-81.

Gant, S.E. (2002). Development and Application of a New Wall Function for Complex Turbulent Flows, UMIST, Manchester.

Haghighat, F., Jiang, J., Wang, J.C.Y., and Allard, F. (1992). Air Movement in Buildings Using Computational Fluid Dynamics. Transactions of the ASAE ; Vol/Issue: 114, Pages: 84-92.

Heidt, F.D., and Benkert, S. (2000). Designing Earth Exchangers-Validation of the Software GAEA. Proceedings World Renewable Energy Congress VI, Brighton, UK, pp. 1818-1821, 01.-07.07.2000.

Heiselberg, P. (2004). Building Integrated Ventilation Systems - Modelling and Design Challenges. CIB 2004 World Building Congress, Toronto, Canada.

Heiselberg, P. ed. (2002). Principle of Hybrid Ventilation, Aarhus University Center, Denmark.

Hollmuller, P. (2002). Utilisation Des changeurs Air/Sol Pour Le Chauffage Et Le Rafraîchissement Des Bâtiments Mesures in Situ, Modélisation Analytique, Simulation Numérique Et Analyse Systémique, PhD Thesis, Université de Genève, Genève.

Hollmuller, P., and Lachal, B. (1998). TRNSYS Compatible Moist Air Hypocaust Model - Final Report. 19507, Centre universitaire d'étude des problèmes de l'énergie, University de Geneve.

Hsieh, K.J., and Lien, F.S. (2004). Numerical Modeling of Buoyancy-Driven Turbulent Flows in Enclosures. International Journal of Heat and Fluid Flow, 25(4), 659-670.

IEA-ECBCS. (2002). IEA ECBCS Strategic Plan 2002-2007, FaberMaunsell Ltd.

Jacovides, C.P., and Mihalakakou, G. (1995). Underground Pipe System as an Energy Source for Cooling/Heating Purposes. Renewable Energy, 6(8), 893-900.

Jeong, Y., and Haghighat, F. (2002). Modelling of a Hybrid-Ventilated Building - Using ESP-r. International Journal of Ventilation, 1(2), 127-139.

Krarti, M., and Kreider, J.F. (1996). Analytical Model for Heat Transfer in an Underground Air Tunnel. Energy Conversion and Management, 37(10), 1561-1574.

Kumar, R., Ramesh, S., and Kaushik, S.C. (2003a). Performance Evaluation and Energy Conservation Potential of Earth-Air-Tunnel System Coupled with Non-Air-Conditioned Building. Building and Environment, 38(6), 807-813.

Kumar, R., Srikonda, A.R., and Kaushik, S.C. (2003b). Cooling and Heating Potential of Earth-Air Tunnel Heat Exchanger (Eathe) for Non-Air-Conditioned Building. International Journal of Global Energy Issues, 19(4), 373-386.

Labs, K. (1979). Underground Building Climate. Solar Age, 4(10), 44-50.

Launder, B.E., and Spalding, D.B. (1974). The Numerical Computation of Turbulent Flows. Computer Methods in Applied Mechanics and Engineering, 3(2), 269-289.

Liddament, M.W. (2000). IEA ECBCS Annex 28 Low Energy Cooling, Technical Synthesis Report.

Lienhard, J.I., and Lienhard, J.V. (2005). A Heat Transfer Textbook, Phlogiston Press, Cambridge, Massachusetts, U.S.A.

Mathworks. (2005). Matlab Help (V7.1 R14), Mathworks, Cambridge MA.

Mihalakakou, G. (2003). On the Heating Potential of a Single Buried Pipe Using Deterministic and Intelligent Techniques. Renewable Energy, 28(6), 917-927.

Mihalakakou, G., Lewis, J.O., and Santamouris, M. (1996a). The Influence of Different Ground Covers on the Heating Potential of Earth-to-Air Heat Exchangers. Renewable Energy, 7(1), 33-46.

Mihalakakou, G., Santamouris, M., and Asimakopoulos, D. (1994a). Modelling the Thermal Performance of Earth-to-Air Heat Exchangers. Solar Energy, 53(3), 301-305.

Mihalakakou, G., Santamouris, M., and Asimakopoulos, D. (1994b). Use of the Ground for Heat Dissipation. Energy (Oxford), 19(1), 17-25.

Mills, A.F. (1962). Experimental Investigation of Turbulent Heat Transfer in the Entrance Region of Circular Conduit. J. Mech. Engng. Sci., 4, 63-77. Mu, L. (1982). Underground Tunnel Cooling, China Architecture and Building Press, Beijing.

Neymark, J., and Judkoff, R. (2008). In-Depth Diagnostic Cases for Ground Coupled Heat Transfer Related to Slab-on-Grade Construction. NREL/TP-550-43388, International Energy Agency Building Energy Simulation Test and Diagnostic Method (IEA BESTEST) National Renewable Energy Laboratory, Golden, Colorado.

Pfafferott, J. (2003). Evaluation of Earth-to-Air Heat Exchangers with a Standardised Method to Calculate Energy Efficiency. Energy and Buildings, 35(10), 971-983.

Reise, C. (2001). Planning Tool for Earth-to-Air Heat Exchangers. EU-Contract JOR3-CT98-7041.

Santamouris, M., and Asimakopoulos, D.N. (1996). Passive Cooling of Buildings, James & James, London.

Sawhney, R.L., and Mahajan, U. (1994). Heating and Cooling Potential of an Underground Air-Pipe System. International Journal of Energy Research, 18(5), 509-524.

Scalabrin, G., and Piazza, L. (2003). Analysis of Forced Convection Heat Transfer to Supercritical Carbon Dioxide inside Tubes Using Neural Networks. International Journal of Heat and Mass Transfer, 46(7), 1139-1154.

Scalabrin, G., Piazza, L., and Condosta, M. (2003). Convective Cooling of Supercritical Carbon Dioxide inside Tubes: Heat Transfer Analysis through Neural Networks. International Journal of Heat and Mass Transfer, 46(23), 4413-4425.

Schild, P.G. (2001). An Overview of Norwegian Buildings with Hybrid Ventilation. HybVent Forum '01 Delft University of Technology, The Netherlands.

Schild, P.G. (1997). Accurate Prediction of Indoor Climate in Glazed Enclosures, PhD Thesis, Norwegian University of Science and Technology, Trondheim Norway.

Schild, P.G. (2002). Jaer School. IEA ECBCS Annex-35 (HybVent) Technical Report, Nesodden Municipality, Norway.

Singh, S.P. (1994). Optimization of Earth-Air Tunnel System for Space Cooling. Energy Conversion and Management, 35(8), 721-725.

Sleicher, C.A., and Tribus, M. (1956). Proceedings of Heat Transfer and Fluid Mechanics Institute. P. 56. Department of Mechanical Engineering, Stanford University.

Sodha, M.S., Mahajan, U., and Sawhney, R.L. (1994a). Thermal Performance of a Parallel Earth Air-Pipes System. International Journal of Energy Research, 18(4), 437-447.

Spitler, J.D. (1990). An Experimental Investigation of Air Flow and Convective Heat Transfer in Enclosures Having Large Ventilative Flow Rates, PhD thesis, University of Illinois at Urbana-Champaign.

Tjelflaat, P.O. (2000a). Pilot Study Report - Mediå School. IEA ECBCS Annex-35 (HybVent) Technical Report.

Tjelflaat, P.O. (2000b). The Grong School in Norway the Hybrid Ventilation System. IEA ECBCS Annex-35 (HybVent) Technical Report.

Tzaferis, A., Liparakis, D., Santamouris, M., and Argiriou, A. (1992). Analysis of the Accuracy and Sensitivity of Eight Models to Predict the Performance of Earth-to-Air Heat Exchangers. Energy and Buildings, 18(1), 35-43.

Wachenfeldt, B.J. (2003). Natural Ventilation in Buildings Detailed Prediction of Energy Performance, PhD Thesis, Norwegian University of Science and Technology.

Wagner, R., Beisel, S., Spieler, A., and Vajen, K. (2000a). Measurement, Modeling and Simulation of an Earth-to-Air Heat Exchanger in Marburg (Germany). 4. ISES Europe Solar Congress, Copenhagen, Denmark.

Walpole, R.E. (2007). Probability & Statistics for Engineers & Scientists, Pearson Prentice Hall, Upper Saddle River, NJ.

Wolfshtein, M. (1969). The Velocity and Temperature Distribution in One-Dimensional Flow with Turbulence Augmentation and Pressure Gradient. International Journal of Heat and Mass Transfer, 12(3), 301-318.

Xu, W., Chen, Q., and Nieuwstadt, F.T.M. (1998). A New Turbulence Model for near-Wall Natural Convection. International Journal of Heat and Mass Transfer, 41(21), 3161-3176.

Zhai, Z., and (Yan) Chen, Q. (2004). Numerical Determination and Treatment of Convective Heat Transfer Coefficient in the Coupled Building Energy and CFD Simulation. Building and Environment, 39(8), 1001-1009.

Zhou, L., and Haghighat, F. (2009). Optimization of Ventilation System Design and Operation in Office Environment, Part I: Methodology. Building and Environment, 44(4), 651-656.

Zimmermann, M. (1995). Ground Cooling with Air, IEA-ECBCS Annex 28 Low Energy Cooling, Subtask 1 Report, Review of Low Energy Cooling Technologies.

Zimmermann, M., and Remund, S. (2001). IEA-ECBCS Annex 28 Subtask 2 Report 2, Chapter F Ground Coupled Air Systems. Low Energy Cooling - Technology Selection and Early Design Guidance, N. Barnard and D. Jaunzens, eds., Construction Research Communications Ltd, pp 95-109.

APPENDICES

Appendix A. Design Cases for ANN Training and Testing

ΔT	U	L	H	W	W_{in}
33.296	1.3376	10	2.6	0.6	2.2
39.5238	3.9977	14	3	2.4	1.8
18.4582	1.7591	15	2.8	0.4	2.4
27.8839	3.6843	17	2	0.8	0.8
25.6412	3.486	20	1.6	2.6	1.4
9.6182	0.5194	23	0.4	1.4	0.4
23.3019	1.1365	28	1.2	1.6	1.2
4.7785	3.0203	31	0.6	1.2	2
36.6989	1.6532	32	1.8	0.2	1.6
29.3827	3.1103	34	2.4	3	1
11.1367	2.7869	36	1.4	1	2.6
5.9497	2.3817	39	2.2	2.2	0.2
1.1859	2.3343	41	1	1.8	2.8
10	0.666667	14	1	1.5	1
20	0.666667	14	1	1.5	1
10	2	14	1	1.5	1
10	3.333333	14	1	1.5	1
20	3.333333	14	1	1.5	1
10	4.666667	14	1	1.5	1
20	4.666667	14	1	1.5	1
10	1.333333	13.5	1.5	1.5	1.5
20	1.333333	13.5	1.5	1.5	1.5
10	2.222222	13.5	1.5	1.5	1.5
20	2.222222	13.5	1.5	1.5	1.5
10	3.111111	13.5	1.5	1.5	1.5
20	3.111111	13.5	1.5	1.5	1.5
10	1	13	2	1.5	2
20	1	13	2	1.5	2
10	1.666667	13	2	1.5	2
20	1.666667	13	2	1.5	2
10	3.333333	24	1	1.5	1
20	3.333333	24	1	1.5	1
10	2.333333	13	2	1.5	2
20	2.333333	13	2	1.5	2
10	4.666667	24	1	1.5	1
20	4.666667	24	1	1.5	1
10	1.666667	23	2	1.5	2
20	1.666667	23	2	1.5	2
-33.296	1.3376	10	2.6	0.6	2.2

-39.5238	3.9977	14	3	2.4	1.8
-18.4582	1.7591	15	2.8	0.4	2.4
-45.7678	3.6843	17	2	0.8	0.8
-25.6412	3.486	20	1.6	2.6	1.4
-9.6182	0.5194	23	0.4	1.4	0.4
-21.0435	1.9248	25	0.2	2.8	0.6
-23.3019	1.1365	28	1.2	1.6	1.2
-4.7785	3.0203	31	0.6	1.2	2
-36.6989	1.6532	32	1.8	0.2	1.6
-29.3827	3.1103	34	2.4	3	1
-11.1367	2.7869	36	1.4	1	2.6
-5.9497	2.3817	39	2.2	2.2	0.2
-1.1859	2.3343	41	1	1.8	2.8
-20	0.666667	14	1	1.5	1
-10	0.666667	14	1	1.5	1
-20	2	14	1	1.5	1
-10	2	14	1	1.5	1
-20	3.333333	14	1	1.5	1
-10	3.333333	14	1	1.5	1
-20	4.666667	14	1	1.5	1
-10	4.666667	14	1	1.5	1
-20	1.333333	13.5	1.5	1.5	1.5
-10	1.333333	13.5	1.5	1.5	1.5
-20	2.222222	13.5	1.5	1.5	1.5
-10	2.222222	13.5	1.5	1.5	1.5
-20	3.111111	13.5	1.5	1.5	1.5
-10	3.111111	13.5	1.5	1.5	1.5
-20	1	13	2	1.5	2
-10	1	13	2	1.5	2
-20	1.666667	13	2	1.5	2
-10	1.666667	13	2	1.5	2
-20	2.333333	13	2	1.5	2
-10	2.333333	13	2	1.5	2
-10	0.666667	24	1	1.5	1
-10	2	24	1	1.5	1
-20	3.333333	24	1	1.5	1
-10	3.333333	24	1	1.5	1
-20	4.666667	24	1	1.5	1
-10	4.666667	24	1	1.5	1
-20	1.666667	23	2	1.5	2
-10	1.666667	23	2	1.5	2
-20	2.333333	23	2	1.5	2
-10	2.333333	23	2	1.5	2

Appendix B. ANN-Based Heat Convection Algorithm Implemented as a Fluent User Defined Function

```
#include "udf.h"
#include "stdio.h"
/* material property */
#define conductivity 0.0242 /* thermal conductivity in W/mK */
#define viscosity 0.0000179 /* viscosity in kg/ms */
#define density 1.225  /* density in kg/m3 */
#define specific_heat 1005 /* specific heat capacity in J/KgK */
#define input_size 6
#define hidden_size 30
#define output_size 9
/* duct demension */
#define duct_length 15 /* duct length*/
#define duct_height 1.5 /* duct height*/
#define duct_width 1.5 /* duct width*/
#define duct_inlet_width 1.0 /* duct */
#define hydraulic_diameter 1.5 /* duct hydraulic diameter in meter */
#define day 86400
#define hour 3600
/* constant coefficient */
#define pai 3.1415926535 /* pi */
#define node 9
```

```
#define t_ave_annual 279.04
#define t_amplitude_annual 25.0
double d_val[54];
double e1_val[6];//first derivative
double e2_val[36];//
double re_val[36];//reverse matrix;
double bulk_velocity;
int current_time;
double det(double *a,int  n);
double rem(double *a,int  i,int  j,int  n);
void  inv(double *a,double*  b,  int  n);
void matrconver(double *a);
void matrrevconver(double *a);
void myxnext(double *a);
double mytime(double a,int n);
void myfun(double *f,double *a,double *b,double *c);
double mynorm(double *f);
void myderive(double *b);
void myed1(double *f);
void myed2();
void leastsquare(double *z,double *x, double *y);
void velocity_control();
```

```
void velocity_control()
{
        current_time=CURRENT_TIME;
        if((current_time%day < 25200)||(current_time%day > 64800))
bulk_velocity = 0.52;
        else bulk_velocity = 0.8;
}

void myfun(double *f,double *a,double *b,double *c)
{
        int i;
  for(i=0;i<node;i++)
  {
          *f=*c-pow((*b),5)*(*a)-pow((*b),4)*(*(a+1))-pow((*b),3)*(*(a+2))-
pow((*b),2)*(*(a+3))-(*b)*(*(a+4))-(*(a+5));
     f=f+1;
        c=c+1;
        b=b+1;
  }
}
double mynorm(double *f)
{
        int i;
```

```
        double m=0;
  for(i=0;i<node;i++)
  {
          m=m+(*f)*(*f);
          f=f+1;
  }
  return m;
}
void myderive(double *b)
{
        int i, j;
  for(i=0;i<9;i++)
  {
          for(j=0;j<6;j++)
          {
                  d_val[i*6+j]=-pow(*(b+i),5-j);
          }
  }
}
void myed1(double *f)
{
        double temp;
        int i, j;
```

```
   for (i=0;i<6;i++)
        {
                temp=0.0;
                for(j=0;j<9;j++)
                {
                        temp=temp+(*(f+j))*d_val[(j*6+i)];
                }
      e1_val[i]=temp*2;
        }
}
void myed2()
{
        double temp;
        int i, j, k;
   for (i=0;i<6;i++)
        {
                for (j=0;j<6;j++)
                {
                   temp=0.0;
              for(k=0;k<9;k++)
                        {
                          temp=temp+d_val[k*6+i]*d_val[k*6+j];
                        }
```

```
            e2_val[i*6+j]=temp*2;
                    }
            }
        }
        double  det(double*  a,int  n)
         {
            int j;
            double sum;
         if(n==1)  return  a[0];
          sum= 0.0;
         for(j=0;j<n;j++)  sum+=a[0*n+j]*rem(a,0,j,n);
         return  sum;
         }
        double  rem(double*  a,int  i,int  j,int  n)
         {
         int  k,m;
         double    *pTemp=(double *) malloc((sizeof(double))*(n-1)*(n-1));      // new
double[(n-1)*(n-1)];
         double dResult;
         for(k=0;k<i;k++)
         {
         for(m=0;m<j;m++) pTemp[k*(n-1)+m]=a[k*n+m];
         for(m=j;m<n-1;m++)  pTemp[k*(n-1)+m]=a[k*n+m+1];
```

```
}
for(k=i;k<n-1;k++)
{
for(m=0;m<j;m++) pTemp[k*(n-1)+m]=a[(k+1)*n+m];
for(m=j;m<n-1;m++)  pTemp[k*(n-1)+m]=a[(k+1)*n+m+1];
}
if ((i+j)%2==1)
        dResult = -1 * det(pTemp,n-1);
      else
            dResult = 1 * det(pTemp,n-1);
free(pTemp);
return  dResult;
}
void  inv(double* a,double*  b,  int  n)
{
        int i, j;
double  deta=det(a,n);
for(i=0;i<n;i++)
for(j=0;j<n;j++)
b[i*n+j]=rem(a,j,i,n)/deta;
}
void myxnext(double *a)
{
```

```
        int i, j;
        double temp;
        inv(e2_val, re_val, 6);
        for (i=0;i<6;i++)
        {
                temp=0;
                for (j=0;j<6;j++)
                {
                        temp=temp+re_val[i*6+j]*e1_val[j];
                }
    *(a+i)=*(a+i)-temp;
        }
}

void leastsquare(double *z,double *x, double *y)
{
double f_val[9];
double m_val;
int i;
int iteration =0;
while(iteration<4)
{
        myfun(f_val,x,y,z);
```

```
    m_val=mynorm(f_val);
    myderive(y);
    myed1(f_val);
        myed2();
    myxnext(x);
        iteration++;
}
}
/*      ////////////////////////////////////////////////////////////////////////////      */
/*      ///                    htc_ceil                    ///      */
/*      ////////////////////////////////////////////////////////////////////////////      */
DEFINE_PROFILE(htc_ceil, thread, position) /* Define the heat transfer coefficient. */
{
        int x,y,i,j;
        double max_input[6]= {39.5238,    4.666666667, 41,    3,    3,
2.8};  /* max original input */
        double min_input[6]={-45.7678,    0.5194,      10,    0.2,  0.2,
0.2}; /* min original input */
        double max_output[9]= {3318.3, 2434.8, 1658.7, 1254.1, 1272.3, 1413.5,
1450.7, 1592.7, 2786.2};      /* max original output */
        double min_output[9]={16.9, 23.6, 16.5, 15.1, 15.8, 14, 9.9, 7.5, 9};
/* min original output */
```

```
        double
corresponding_x_coordinate[9]={0.1,0.2,0.3,0.4,0.5,0.6,0.7,0.8,0.9};
        double second_layer[30];
        double output_layer[9];
        double input[6];
        double output[9];
        double original_input[6];  /* original input */
        double original_output[9];
        double flw[6][30];
    double slw[30][9];
        double temp;
        double hidden[hidden_size];
        double temperature_inlet;
        double temperature_surface;
        double temperature_difference;
        double coefficient[6] = {1.0, 1.0, 1.0, 1.0, 1.0, 1.0};
        Domain *domain;
        int zone_ID;
        face_t f, f_ground_surface;
        Thread *ground_surface_thread;
        double NV_VEC(area);
        double coordinate[ND_ND]; /* this will hold the position vector */
        double x_coordinate;
```

```
double total_area, total_temperature, average_temperature, htc_correlated;
double flw_array_input[180] = {-4.336686105232195,
1.669444171374169, 0.00536104668375, -1.034279963481168, -
0.55018947003971, 1.350741719210272,
0.103825605964073, 1.554902136098054, 0.273066015986045,
0.38500210424064, -1.916806754592613, -1.410928996707511,
1.376643870710998, -1.70930113795331, -0.692786588234052,
1.626826267567731, 1.18084299146012, 0.790945192662832,
0.027602175339339, -1.596627860555559, -0.289199059550631, -
1.193944298178872, 0.401449799577874, -0.312512329116053,
0.057780307094332, -0.660956675480718, 0.927241405182404, -
0.169071931710247, 0.482366952068776, -0.27428535683813,
-2.845353852396373, 3.103118215246837, 1.460816601157492, -
0.422116176199107, -0.816027965775518, -1.685983206811947,
0.145083246029087, -0.260876939606809, 0.714947038851879, -
1.772726930099388, -0.412875767170131, -0.730119596902702,
-0.089402843585367, 0.172535070398858, 1.05278644327779,
0.296350628599385, -0.882556575767749, -1.081010286353823,
0.704418531703641, -1.556836907340937, 0.730928724105471,
0.722306147590413, -0.420891124226316, 1.144479853246785,
1.439168896773304, 2.248988157425231, -0.131201962001624, -
0.191140764430699, -0.532787685088898, -0.527898887550679,
```

-0.129847172202221, 0.949327653162649, 0.190780552436071,

1.365891675428434, 0.285256869266365, -0.946406997456607,

0.694758342896553, 0.464508881900077, -0.28144695021447, -

1.174723174940064, 1.186827837094111, -0.578574647072141,

-1.527431446766192, 1.59320087054909, 0.786916361707078, -

0.793027055593379, -0.063491090925028, -0.585818903990924,

0.740689753956832, 0.227046419258449, -0.277055002898879,

0.771343875301753, 0.099997339978125, -0.970909873302873,

-0.119224168193306, 0.567281509014378, -1.420954563612154,

0.567398433531765, 0.492038707316781, 0.706269689640353,

-0.510066016430278, -1.325721533226124, -0.129317813046695, -

0.897408670972072, 0.632016799439658, 0.875845395226184,

-1.771221809628693, -2.107784904795706, -0.049564306155701,

0.001540238959374, -0.391098228089392, 2.209016628604565,

-0.849052913641308, 1.189656451121288, 0.24147637557002,

0.868415991105927, 0.19162135821212, 1.191845757013548,

3.155082570739259, -1.271389421334052, 0.124573088155254,

0.101848875719405, 1.199825201375557, -0.224343249303002,

-0.007389815522349, -0.090431201383587, 0.004597099841324, -

0.147261261006322, -1.585395636490085, -0.107633678049332,

-1.538685441696116, 0.447608811824665, 0.914202143565128, -

0.45218654179294, -2.060769803638046, -0.49406981914079,

2.369406809302736, 1.64608332397359, -0.016069689363924, -0.269059661236209, -1.074674315827059, -1.618707140711426,
2.337653374659831, -0.954047662564853, -0.21984543817654,
0.182094187731435, -1.167936430389292, 0.047558925023477,
2.001448020291083, -1.191112735199521, 0.391706643078568, -0.541653269976504, 2.134445496542223, 0.703985888178901,
1.275250743500282, 0.793897938394273, 0.025140693852906,
1.682748691852502, -0.781059662217848, -0.741768376598167,
0.343920743723787, -1.556497914520537, -0.973937261704589,
0.299923034377567, 2.472842954809956, 0.22359125188891,
-0.101266661957498, -1.226879491543921, 0.251919944253295,
0.890029414092124, 1.723378798028704, 1.270452458698384,
-0.042824833359125, 2.472925506438198, 0.117335612812808,
0.844186452722638, -0.664710099666627, 1.896746197046915,
0.817510568628976, -1.654426882835849, 0.263914539284543,
0.516729061750656, 0.919404566755412, 0.367988203879245,
0.94955565672204, -0.195831196761131, 0.534584366782707,
1.046046543377418, 0.397904912803601, 0.75998314332655} ;

double slw_array_input[270] = {0.32599721645331,
0.673721207146537, -0.159635635778728, -0.090025806611723,
0.716767367286555, -0.090974915500456, 0.047135446338036, -1.0740044695838, 0.282518141130464, 0.011033713104401, 1.137894480459881,
0.256718486877442, 0.088877098893256, -0.107882630432304, -

0.557809220343709, -0.327837440951554, 0.026907266429137, 0.063620465184559,
0.664546496733215, -0.145651363879699, 0.169372781299589, -
0.034609893296795, 0.06910343122299, -0.427815259459499, -0.014253295402018,
0.091496591231802, 0.342140601256293, -0.116505365499194,
0.02444524373347, -0.379003840499321,
0.292320147520567, 0.488109373560195, -0.038845456346555,
0.397089675969096, 0.481981696334466, -0.25311823781111, -
0.179215208249175, -0.593525683772534, -0.25878362961924, 0.12764630345259,
0.567041423488426, -0.02392338594149, 0.467524768844387, -
0.536893842820889, -0.012211888090849, -0.277973510482499, -0.216141754356543,
0.042925818760296, 0.546549951567418, -0.350833850372836,
0.188103534554026, -0.242047504698434, 0.23216210839879, -
0.525231343870121, 0.292141163762079, 0.085256691993853, 0.147646996066635,
0.12898299606174, 0.466759177429883, 0.030167888321897,
0.260410746014946, 0.12880280954242, 0.161052135141322,
0.252778505468486, -0.011560309658196, -0.525291296008555, -
0.300005153778312, 0.059457065139722, -0.854980337942528, 0.389411593182337,
-0.253680132113614, -0.19620627014166, 1.056738097980828, -
0.883748731744312, 0.505203713357497, 0.139073160343108, -0.527053459828049,
0.025550481913831, 0.449586202116834, -0.245170358736223,
0.109190802267494, -0.469622696890204, 0.346094251559882, -
0.648808248943076, 0.566072897644836, 0.035494256527638, 0.039572511001674,
0.013259970690263, 0.989437078232311, 0.436310533910711,

0.291415803132411, -0.00079387323505, 0.336431028364888, -0.563022979368731, -0.304063048256809, -0.727110151261796, -0.306476313809018, 0.373848513249328, -0.860123059484095, 0.697307052572626, -0.342804295668586, -0.126209263390635, 1.451986573761557, -0.560931947206285, 0.720152951458858, 0.983244202185577, -0.621421240685898, 0.017212964190563, 0.549930462102431, -0.119532299799633, -0.073611281468041, -0.498267514362196, 0.277933140956032, -0.751386560166492, 0.438800729867067, -0.124475139719205, 0.008275868795522, -0.399451758520095, 1.116878591650354, 0.444350987409795, 0.371116551350796, 0.271348604866955, 0.277741083483707, -0.716647457034886, -0.03180984715529, -0.584695012190185, -0.286743028157898, 0.111246244700552, -0.260126155636334, 0.686917467740102, 0.274087714614376, 0.125392259428444, 1.126747557044683, 0.198960133327193, 0.547382037094045, 1.280723644294477, -0.377756865547138, 0.076948965501696, 0.80034000308394, -0.077253865862608, -0.197539465979961, -0.272975735298074, 0.027676414485327, -0.702303567917724, 0.048852187470092, -0.263258638362004, 0.154787880023612, -0.418494253328903, 0.58033292023463, 0.073637174005384, 0.457392807949091, 0.597710463575222, 0.10324704128945, 0.144340814988996, 0.379470076817968, -0.335265171584365, -0.355170867337038, -0.198656880918176, 0.129792069193919, 0.467243359522195, 0.582955475839236, 0.29585086973682, 0.612402532570939, 0.582665679820911, 0.381424212396241, 0.857731415938024, -

0.158344903502273, 0.185090799393061, 1.026838595481541, -0.046334698618608, -0.199170621736086, -0.099983575745811, -0.164553642298627, -0.624725078210829, -0.11375567961449, -0.297118541000549, 0.405086513495037, 0.0506577000917, 0.04585943274071, -0.164011603384421, 0.545538214873752, 0.838634899570349, -0.053336833301752, 1.170585429442732, 0.659447827069022, -0.155632033462521, -0.459557582746946, -0.37064005274755, 0.268466207769099, 0.251694690946643, 0.553828682756148, 0.386459838399939, 0.254964594215964, 0.656055634991376, 0.318749725861689, 0.28877094176801, -0.048577285222807, 0.282570852158172, 1.211539411907858, -0.019989284852572, -0.162558503547807, -0.026533656712198, -0.258656652974112, -0.587912086894579, -0.113364002719694, -0.286289409571849, 0.63753831556278, 0.572718638347908, -0.268777834728459, -0.255380853861036, 0.54707622902876, 0.822617051371675, -0.174753885398087, 1.408996018261045, 0.722774220159521, -0.017418658495496, -0.427444097145036, -0.462810108730971, 0.369744916352323, 0.04311991274677, 0.51484976830215, 0.435365582199954, -0.01609115649839, 0.497094329417276, 0.382132105285141, -0.168599969500771, 0.042751291893548, 0.26464033236472, 1.180251750217874, -0.038987426645833, -0.076096815513849, 0.03538141492668, -0.230716169111473, -0.500625732343884, -0.086371292795922, -0.148781147157613, 0.62982454945432, 0.712369002638582, -0.424382625031758, -0.326686387958306,

0.341058386946118, 0.277067744714221, -0.239559984195371,

0.782283409048759, 0.51100497546741, 0.109027813760606, -

0.212723174121494, -0.325823448441628, 0.21321661292487, -0.168497523783253,

0.296375832155904, 0.366225306968309, -0.238617216597977, -

0.092309651728195, 0.765631083015808, -0.556808460827459, 0.059064332102261,

0.116298128706326, 0.722885790014748, 0.055619098894851,

0.10057425565255, 0.053662403194093, -0.071547618304196, -

0.304457483879069, 0.12958889333812, 0.208459572730027, 0.302356705720116,

0.435716012257561, -0.36868881634233, -0.195305756873518} ;

double bias[39] = {0.874944538547172, 0.755980939163675,

0.79231283981969, -0.645781629335304, 0.213441144168911, 0.779415193189605, -

0.841146476303419, 0.518524154280577, -0.770334457237034, -0.855189672690136, -

1.531047770165061, 1.044878592964863, 0.246378653128207, 0.758301410214918, -

2.195593067807193, 0.16026165000737, -1.024969288238974, -0.003773447893342, -

0.549935971723807, -0.511762651456107, 0.468008570093182, 0.223402910422953, -

0.602600662004151, -0.193166940599609, 1.051314431629637, 0.082824250694331, -

0.23690369188036, 0.680639219562979, -0.718348931992718, -0.641679521148696, -

0.206485972431025, 0.096899561483154, 0.166505671790581, 0.109378403069235, -

0.077014998215932, -0.25511576853311, -0.391666791209314, -0.352439088172034,

0.000039935271451} ;

begin_f_loop(f, thread)

{

if PRINCIPAL_FACE_P(f,thread)

```
        {
                F_AREA(area,f,thread);
                total_area += NV_MAG(area);
                total_temperature += NV_MAG(area)*F_T(f,thread);
        }
}
end_f_loop(f, thread)
total_area = PRF_GRSUM1(total_area);
total_temperature = PRF_GRSUM1(total_temperature);
average_temperature = total_temperature / total_area;
domain = Get_Domain(1);
zone_ID = 48;
ground_surface_thread = Lookup_Thread(domain, zone_ID);
temperature_inlet = F_T(f_ground_surface, ground_surface_thread);
temperature_difference = temperature_inlet - average_temperature;
velocity_control();
original_input[ 0 ] = temperature_difference ;
original_input[ 1 ] = bulk_velocity;
original_input[ 2 ] = duct_length;
original_input[ 3 ] = duct_height;
original_input[ 4 ] = duct_width;
original_input[ 5 ] = duct_inlet_width;
for(i=0; i<input_size; i++)
```

```
                {
                        input[i]=2      *       (original_input[i]-min_input[i])        /
(max_input[i]-min_input[i]) - 1;        /* scale the original input down to 0-1 */
                }
                temp = 0.0;
        /*              inPUT -> HIDDEN */
                for(y=0; y<hidden_size; y++)
                {
                        for(x=0; x<input_size; x++)
                                {
                                        temp  =  flw_array_input[y*input_size+x]  *
input [x] + temp;
                }
                        hidden[y] = -1 + 2 / (1 + exp(-2 * (temp + bias[y])));
                temp = 0.0;
                }
        /*              HIDDEN -> OUTPUT */
                for(y=0; y<output_size; y++)
                {
                        for(x=0; x<hidden_size; x++)
                                {
                                        temp  =  slw_array_input[y  *  hidden_size  +
x] * hidden[x]+ temp;
```

```
                }
                output[y] =temp +bias[y+hidden_size];
                temp = 0.0;
                original_output[y] = 0.5*(output[y]+1) * (max_output[y]-
min_output[y]) + min_output[y];
            }
        leastsquare(original_output,coefficient, corresponding_x_coordinate);
        current_time = CURRENT_TIME;
        if((current_time%day < 25200)||(current_time%day > 64800))
            begin_f_loop(f, thread)
              {
                    F_PROFILE(f, thread, position) = 0.0;
                }
            end_f_loop(f, thread)
        else
        begin_f_loop(f, thread)
          {
                F_CENTROID(coordinate,f,thread);
                x_coordinate = coordinate[0]/duct_length;
                htc_correlated = conductivity / hydraulic_diameter *
(coefficient[0]* pow(x_coordinate, 5) + coefficient[1]* pow (x_coordinate, 4) +
coefficient[2]* pow (x_coordinate, 3) + coefficient[3]* pow (x_coordinate, 2) +
coefficient[4]* x_coordinate + coefficient[5]);
```

```
                if (htc_correlated > 0.0)
                        F_PROFILE(f, thread, position) = htc_correlated;
                else
                        F_PROFILE(f, thread, position) = 0.0;
        }
    end_f_loop(f, thread)
}
```